# Dynamics of resonant X-ray and Auger scattering.

Faris Gel'mukhanov[1,2,3,4], Michael Odelius [5], Sergey P. Polyutov[3,4], Alexander Föhlisch[2,6], and Victor Kimberg[1,3]

[1]*Department of Theoretical Chemistry and Biology,*

*KTH Royal Institute of Technology,*

*10691 Stockholm, Sweden*

[2]*Institute for Methods and Instrumentation in Synchrotron Radiation Research,*

*Helmholtz-Zentrum Berlin für Materialien und Energie Albert-Einstein-Strasse 15,*

*12489 Berlin, Germany*

[3]*International Research Center of Spectroscopy*

*and Quantum Chemistry - IRC SQC,*

*Siberian Federal University,*

*660041 Krasnoyarsk, Russia*

[4]*Kirensky Institute of Physics,*

*Federal Research Center KSC SB RAS,*

*660036 Krasnoyarsk, Russia*

[5]*Department of Physics,*

*AlbaNova University Center,*

*Stockholm University,*

*SE-106 91 Stockholm, Sweden*

[6]*Institut für Physik und Astronomie,*

*Universität Potsdam,*

*Karl-Liebknecht-Strasse 24-25,*

*14476 Potsdam,*

*Germany*

# Abstract

We present an overview of both experimental and theoretical results in the field of resonant scattering of tunable soft and hard X-ray radiation, with a main focus on the closely related processes of resonant inelastic X-ray scattering (RIXS) and resonant Auger scattering (RAS). The review starts with an overview of fundamental dynamical aspects of RIXS illustrated for different systems. We give a detailed analysis of case studies with increasing complexity, considering both gas phase and condensed matter (liquids and solids) applications. In the review, we outline the most important achievements in investigations of coupled electron-nuclear dynamics and structural aspects in studies of liquids and solids over the last two decades. To give a perspective on the insights from RIXS and RAS, we briefly discuss the X-ray results against the background of complementary experimental techniques like vibrational infrared absorption and Raman spectroscopy, as well as small-angle X-ray and neutron scattering. Finally, recent achievements in time-resolved studies based on X-ray free-electron lasers (XFEL) are described briefly.

**CONTENTS**

2

## I. INTRODUCTION

Scattering of photons, electrons, and neutrons are utilized in many experimental probes for investigation of the structure of matter and of dynamical processes (Sivia, 2011). The interaction with photons has the undeniable advantage of the simplicity of the matrix element of interaction with atoms and molecules. The absorption of X-rays by matter involves the interaction of photons with electrons in atomic levels, the energies of which are specific for each element. This makes X-ray spectroscopy a unique, element-specific probe (Svanberg, 2001). Elemental selectivity, greatly simplifying the spectrum (compared to optical and ultraviolet spectroscopy), gives detailed information about the local electronic structure in complex systems, since conceptually an atom projected contribution to the electronic states can be determined. X-ray spectroscopy includes X-ray absorption spectroscopy (XAS), X-ray photoelectron spectroscopy (XPS), non-resonant X-ray emission spectroscopy (XES), time-of-flight mass spectroscopy (TOF), coincidence spectroscopy, Auger spectroscopy, Compton spectroscopy (Hämäläinen and Manninen, 2001; Kane, 1992), etc. Since the creation of X-ray Free-Electron Lasers (XFEL) (Pellegrini *et al.*, 2016) and High-Harmonic Generation (HHG) light sources, research has begun in the field of nonlinear spectroscopy and pump-probe field spectroscopy. In this review, we focus on two spectroscopic techniques, initially enabled by the appearance of X-ray synchrotron radiation light sources. We refer to resonant inelastic X-ray scattering (RIXS) and resonant Auger scattering (RAS), known also as Resonant X-ray Raman Scattering and Resonant Photoemission (RPE), respectively. Apart from the review by (van den Brink, 2016; Nordgren and Rubensson, 2013; Schmitt *et al.*, 2014; Simon and Schmitt, 2013; van Veenendaal, 2015) and the more recent review of RIXS in the hard X-ray region (Piancastelli *et al.*, 2020), the preceding monography (Schülke, 2007) and review articles (Ament *et al.*, 2011; Brühwiler *et al.*, 2002; Gel'mukhanov and Ågren, 1999; Glatzel and Bergmann, 2005; de Groot, 2001; Kotani and Shin, 2001), which to some extent cover these areas of research, were published about decade ago. RIXS investi-

gations of electronic structure and excitations in liquids and solids under high pressure were summarized in review the (Rueff and Shukla, 2010) and in the recent article (Rossi *et al.*, 2019b). There are also recent reviews devoted to theoretical aspects of X-ray spectroscopy (Bokarev and Kühn, 2020; van den Brink, 2016; Norman and Dreuw, 2018; van Veenendaal, 2015), to RIXS of transition metal complexes(Lundberg and Wernet, 2019), and to XFEL based time-resolved RIXS studies (Wernet, 2019). One should mention also linear-response time-dependent density functional theory of RIXS of complex systems (Vaz da Cruz *et al.*, 2021).

The main emphasis in our review is on processes that are most pronounced in molecules and solids. Nevertheless, we give an overview also of investigations of liquids, for which significant progress has recently been observed. We discuss also the most important results obtained using XFEL.

## II. SOURCES OF X-RAY RADIATION AND SPECTRAL INSTRUMENTATION

A detailed overview of experimental methods is beyond our review. For this, we recommend extensive analysis of RIXS instrumentation in Refs.(Ament *et al.*, 2011; Ismail *et al.*, 2020; Jaeschke *et al.*, 2020; Piancastelli *et al.*, 2020; Wollenweber *et al.*, 2021) and RAS measurements in Refs. (Lindblad *et al.*, 2013; Liu *et al.*, 2013). The analysis of experimental techniques used in time-resolved XFEL based RIXS, can be found in Refs.(Jaeschke *et al.*, 2020; Lundberg and Wernet, 2019; Wernet, 2019).

Presently two contemporary sources of polarized intense X-ray radiation are used (Ishikawa, 2018). The first category is third-generation synchrotron radiation sources with the storage rings optimized for the use of undulator radiation while the second category is X-ray free-electron lasers (XFEL). XFELs are in turn subdivided into XFELs based on self-amplified spontaneous emission (SASE) (Ishikawa, 2018; Rossbach *et al.*, 2019), seeded-XFELs in which an external laser is used to initiate the emission process (Amann *et al.*, 2012; Petrillo *et al.*, 2020) and self-seeded XFELs (Kumar *et al.*, 2020).

One should notice that there are two types of X-ray spectrometers used in polarization resolved RIXS, namely with (Brookes *et al.*, 2018; Gao *et al.*, 2016; Ishii *et al.*, 2013; Kim *et al.*, 2018; Lindle *et al.*, 1991; Sala *et al.*, 2018; Southworth, 1994) and without (Brookes *et al.*, 2018; Schmitt *et al.*, 2013) polarization resolution for the scattered photon (see Sec. IV).
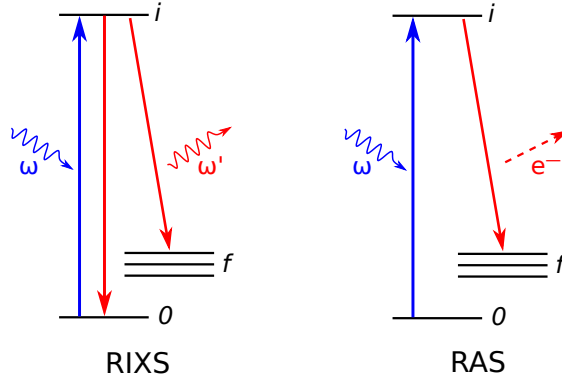
FIG. 1 Illustration of resonant elastic and inelastic X-ray scattering (photon-in/photon-out) and resonant Auger (photon-in/electron-out) scattering; 0, $i$, and $f$ refer to the ground, intermediate core-excited, and final electronic states, respectively.

The spectral resolution is very different in soft and hard X-ray regions. The spectral resolution is usually about 5-10 meV (see below) for hard X-ray wavelength matched the distance between successive lattice planes (Ament *et al.*, 2011). Ultrahigh resolution 0.1 meV was obtained in hard X-ray spectrometer with the multi-crystal multi-reflection optics as dispersing element (Chubar *et al.*, 2016; Shvyd'ko *et al.*, 2013). This scheme does not work for soft X-rays, where the long wavelengths prohibit the use of crystal optics. Instead artificial periodic structures, diffraction gratings, are used. In soft X-ray region the best resolution is about 30-100 meV (or even better (Jarrige *et al.*, 2018)) which depends on spectrometer design and quality of the grating (Brookes *et al.*, 2018; Chaix *et al.*, 2017; Couto *et al.*, 2017; Schmitt *et al.*, 2014).

## III. FINGERPRINTS OF RIXS AND RAS

Resonant X-ray scattering occurs when the incoming X-ray photon $\gamma$ triggers a resonant electronic transition in a target $A$ (atoms, molecules, liquids and solids). The excited state decays via emission of a photon $\gamma'$ with the frequency $\omega'$ or an Auger electron $e^-$ with the kinetic energy $E$ (see Fig. 1), giving rise to the radiative (RIXS) and resonant Auger (RAS) scattering channels, respectively

$$\gamma + A \rightarrow A_i \rightarrow A_f + \begin{cases} \gamma' \\ e^- \end{cases} \tag{1}$$

**RIXS cross section**. The Kramers-Heisenberg (KH) equation

$$\sigma(\omega', \omega) = r_\circ^2 \sum_f |F_f|^2 \Delta(\omega' + \omega_{f0} - \omega, \Gamma_f), \tag{2}$$

$$F_f = F_f^T + \sum_i \frac{\omega\omega'}{\omega - \omega_{i0} + \imath\Gamma}$$

$$\times \langle f| \sum (\mathbf{e}' \cdot \mathbf{d}) e^{\imath(\mathbf{k}' \cdot \mathbf{r})} |i\rangle \langle i| \sum (\mathbf{e} \cdot \mathbf{d}) e^{-\imath(\mathbf{k} \cdot \mathbf{r})} |0\rangle,$$

$$F_f^T = (\mathbf{e} \cdot \mathbf{e}') \langle f|\rho_\mathbf{q}|0\rangle, \quad \rho_\mathbf{q} = \sum e^{\imath\mathbf{q} \cdot \mathbf{r}}$$

for the photon scattering cross section was obtained in 1925 before the discovery of quantum mechanics (Kramers and Heisenberg, 1925). Two years later, Dirac provided a quantum derivation of this formula (Dirac, 1927). Here, the first term $F_f^T$ in the scattering amplitude $F_f$ describes the Thomson scattering, for which the contribution to the cross section is determined by the dynamic structural factor $S(\mathbf{q}, \omega - \omega') = |\langle f|\rho_\mathbf{q}|0\rangle|^2 \Delta(\omega' + \omega_{f0} - \omega, \Gamma_f)$, $r_\circ = \alpha^2 \approx 2.83 \times 10^{-13} cm$ - the classic electron radius, $\mathbf{q} = \mathbf{k}' - \mathbf{k}$ - the momentum transfer, $\alpha = 1/137$ - the fine-structure constant, $\omega_{ij} = E_i - E_j$ - the spacing between the levels of the quantum system, $\mathbf{k}$, $\mathbf{e}$, $\mathbf{k}'$, $\mathbf{e}'$ - momentum and polarization vectors of the initial and scattered photons, $\sum$ denotes a sum over the electrons, $\mathbf{r}$ is radius-vector of electron, $\Delta(\Omega, \Gamma) = \Gamma/\pi(\Omega^2 + \Gamma^2)$. Throughout the article, we will adhere to the atomic system of units.

In RIXS studies of magnetic materials spin-flip scattering channels are important (Das *et al.*, 2018; Elnaggar *et al.*, 2019; Nag *et al.*, 2020). To describe this process one must add the small relativistic correction to the Thomson term (Blume, 1985)

$$\rho_\mathbf{q} \to \rho_\mathbf{q} - \imath\omega\alpha^2 \sum e^{\imath\mathbf{q} \cdot \mathbf{r}} \left( \imath \frac{\mathbf{p} \times \mathbf{q}}{k^2} \cdot \mathbf{A} + \mathbf{s} \cdot \mathbf{B} \right) \tag{3}$$

where $\mathbf{A} = \mathbf{e}' \times \mathbf{e}$, $\mathbf{B} = \mathbf{e}' \times \mathbf{e} + (\hat{\mathbf{k}}' \times \mathbf{e}')(\hat{\mathbf{k}}' \cdot \mathbf{e}) - (\hat{\mathbf{k}} \times \mathbf{e})(\hat{\mathbf{k}} \cdot \mathbf{e}') - (\hat{\mathbf{k}}' \times \mathbf{e}')(\hat{\mathbf{k}} \times \mathbf{e})$, $\hat{\mathbf{k}} = \mathbf{k}/k$, $\mathbf{p} = -\imath\partial/\partial\mathbf{r}$ is the momentum of electron, and $\mathbf{s} = \boldsymbol{\sigma}/2$ is the spin operator comprises Pauli matrices $\boldsymbol{\sigma}$. At the same time, magnetic terms can be neglected in the resonant scattering channel where the dipole approximation (Eq. (2)) is good enough to describe the spin-flip transitions (Ament *et al.*, 2011; Såthe *et al.*, 2006). This is because magnetic scattering is usually studied for RIXS channels with non-zero orbital momentum of the core-hole. In this case the magnetic spin-flip transitions occur because of the spin-orbital (SO) mixing of spin and orbital momentum in core-excited state (de Groot *et al.*, 1998; Såthe *et al.*, 2006). However, modern RIXS with super-high resolution resolves low-energy ($\lesssim 100$ meV) spin-flip

peaks caused by SO interaction in the valence shell (Das *et al.*, 2018; Elnaggar *et al.*, 2019; Nag *et al.*, 2020) (see Sec.XIII.D).

**RAS cross section**. The structure of the RAS amplitude and cross section is very similar to the KH Eq. (2)

$$F_f = (\mathbf{e} \cdot \mathbf{d_{p0}}) + \sum_i \frac{Q_{fi}(\mathbf{e} \cdot \mathbf{d}_{i0})}{\omega - \omega_{i0} + \imath \Gamma},$$

$$\sigma(E, \omega) = \sum_f |F_f|^2 \Delta(E + \omega_{f0} - \omega, \Gamma_f), \tag{4}$$

where the first non-resonant term in the scattering amplitude describes the direct photoionization of an electron with kinetic energy $E = p^2/2$, while the second term gives the amplitude of resonant Auger scattering through the intermediate state $|i\rangle$ of a target. The only difference in the second term between RIXS and RAS is that the dipole operator in RIXS is replaced by the interelectronic Coulomb interaction $Q$, which describes the Auger decay in RAS. This makes the scattering anisotropy of RAS and RIXS very different.

Usually, spectral broadening $\Gamma_f$ of the final valence excited state is much smaller than the natural width $\Gamma$ of the X-ray excited state

$$\Gamma_f \ll \Gamma. \tag{5}$$

For this reason, RIXS and RAS spectroscopy can be measured with superhigh resolution, which is limited only by the degree of monochromatization of the initial X-ray beam and spectral resolution of the instrument. An important distinguishing feature of RIXS and RAS is the Raman dispersion law

$$\omega' = \omega - \omega_{f0}, \quad E = \omega - \omega_{f0}, \tag{6}$$

which is described by Lorentzian $\Delta(\Omega, \Gamma)$ in Eqs. (2,4) and which is nothing else but the energy conservation law of the scattering process. Since fraction of fluorescence yield is on the order of $10^{-4}$ for the first row molecules, intensity of the Auger signal is higher, resulting in much better statistics in RAS measurements and as a result in a better spectral resolution of RAS as compared to RIXS. In the soft X-ray range contrary to the hard X-ray range, the Auger contribution to the width $\Gamma$ exceeds that of the radiative transitions. It was found recently that $\Gamma$ can be controlled in an X-ray cavity which modifies the spontaneous emission rate (Huang *et al.*, 2021).

Due to lack of selection rules for the $Q$ operator, the RAS spectral profile usually contains many overlapping lines which makes its interpretation more difficult, as compared to RIXS spectra. One should notice that the nuclear dynamics in intermediate state strongly violated the Raman dispersion (Eq. (6)) (Gel'mukhanov and Ågren, 1996a; Hikosaka $et$ $al.$, 2008; Liu $et$ $al.$, 2011a; Velkov $et$ $al.$, 2009; Weinhardt $et$ $al.$, 2011).

A special attention will be paid below to the factor $\exp(\imath(\mathbf{q} \cdot \mathbf{R}))$, which is responsible for the recoil effect, namely, the momentum exchange between photons, electrons, and nuclei with nuclear coordinate $\mathbf{R}$. For example, in the soft X-ray region $qR \ll 1$ and Thomson scattering, described by the first term in Eq. (2) $F_f^T \propto \delta_{f,0}$, is an elastic process. Increase of the X-ray photon energy ($qR \gtrsim 1$) opens an inelastic (Compton) scattering channel (Hämäläinen and Manninen, 2001; Kane, 1992; Spielberger $et$ $al.$, 1995). A similar factor in the RAS $\exp(\imath(\mathbf{p} \cdot \mathbf{R}))$, which describes the Doppler and recoil effects, leads to a number of interesting phenomena already in the soft X-ray range, due to the large magnitude of the Auger electron momentum $\mathbf{p}$ (see Sec. V).

## IV. POLARIZATION-RESOLVED RIXS

The polarization anisotropy of RIXS from disordered systems and crystals (Braicovich $et$ $al.$, 2014; Brookes $et$ $al.$, 2018) (Sec. XII) allows to gain information on the symmetry of the excitations and therefore on their nature. The polarization filters overlapping energy states of different symmetry (Braicovich $et$ $al.$, 2014) and allows to reduce the non-resonant contributions. In studies of magnetic circular dichroism (MCD) we need circular polarized light (Sec.XII). The first impression is that the scattering by randomly oriented molecules in a gas or liquid must be isotropic. However, this is not the case (Gel'mukhanov and Ågren, 1994; Gel'mukhanov and Mazalov, 1977).

### A. Scattering anisotropy by randomly oriented molecules

Anisotropy of RIXS from randomly oriented samples was confirmed already in the first measurements on polarization dependence (Lindle $et$ $al.$, 1991). Moreover, the scattering anisotropy is different for different molecular orbitals involved in the RIXS (Gel'mukhanov and Ågren, 1994; Gel'mukhanov and Mazalov, 1977). The physical reason for the scattering

anisotropy is that RIXS is a two-step process. At the absorption stage, $\propto (\mathbf{e} \cdot \mathbf{d}_{i0})^2$, mainly molecules with a dipole transition moment $\mathbf{d}_{i0}$ predominantly aligned along $\mathbf{e}$ are excited. Thus, even in an isotropic ensemble, the excited molecules are not randomly oriented. Taking into account that the emission of the final photon comes from an ensemble of partially aligned molecules, it is possible to see that the scattering will be anisotropic with the scattering anisotropy $R_{fi}$, depending on the relative orientation of the dipole moments of the emission and absorption of $(\mathbf{d}_{fi} \cdot \mathbf{d}_{i0})$ (Gel'mukhanov and Ågren, 1994; Gel'mukhanov and Mazalov, 1977)

$$\sigma_{fi}(\omega', \omega, \theta) = \sigma_{fi}[1 + R_{fi}(3\cos^2\theta - 1)], \tag{7}$$
$$R_{fi} = \frac{1}{5}(3(\hat{\mathbf{d}}_{fi} \cdot \hat{\mathbf{d}}_{i0})^2 - 1).$$

This expression is obtained by averaging over molecular orientations of the resonance contribution to the cross section (Eq. (2)) with one intermediate state $i$. Here $\sigma_{fi} \equiv \sigma_{fi}(\omega', \omega)$ is the isotropic part of the cross section and $\theta = \angle(\mathbf{e}', \mathbf{e})$ . The anisotropy parameter in the experiment is defined as $R_{fi} = [\sigma_{fi}(0) - \sigma_{fi}(90°)]/[\sigma_{fi}(0) + 2\sigma_{fi}(90°)]$. The RIXS anisotropy of Eq. (7) can be measured using instruments with polarization resolution for the scattered photons.

In experiments without polarization resolution for the scattered photons, the spectrometer "sums" all final polarizations (Gel'mukhanov and Ågren, 1994; Gunnelin $et$ $al.$, 1998; Vaz da Cruz $et$ $al.$, 2019b). Therefore, the RIXS cross section (Eq. (7)) should be averaged over the orientations $\mathbf{e}'$ around the direction of departure $\mathbf{k}'$ of the scattered photon using

$$e_i' e_j' \rightarrow \frac{1}{2}(\delta_{ij} - \hat{\mathbf{k}}_i' \hat{\mathbf{k}}_j'). \tag{8}$$

Here and below, a hat denotes the unit vector, $\hat{\mathbf{k}} = \mathbf{k}/k$. After the averaging the cross section depends on the angle $\chi = \angle(\mathbf{k}', \mathbf{e})$ between the polarization vector of the initial and the direction of the scattered photons

$$\sigma_{fi}(\omega', \omega, \chi) = \sigma_{fi}[1 + \mathcal{R}_{fi}(3\cos^2\chi - 1)]. \tag{9}$$

Since we kept the same structure of Eq. (9) as in Eq. (7), the expression for the scattering anisotropy changed: $\mathcal{R}_{fi} = -R_{fi}/2$. The anisotropy parameter decreased by a factor of two due to additional averaging over the orientations of $\mathbf{e}'$. Let us illustrate the large magnitude of the RIXS anisotropy effect using the case of $1s \rightarrow \sigma^*$ absorption transition in a diatomic

molecule with subsequent emission transitions from occupied $\sigma$ and $\pi$ molecular orbitals: $R_{\sigma\sigma^*} = 2/\ 5$, $R_{\pi\sigma^*} = -1/5$. This example clearly shows that polarization measurements can extract information about the spatial orientation of molecular orbitals, which has been repeatedly confirmed in experiments. The scattering anisotropy in RIXS has been studied for many systems $CH_3Cl$ (Lindle *et al.*, 1991, 1998), $CF_3Cl$ (Lindle *et al.*, 1991; Southworth *et al.*, 1991), $H_2S$ (Mayer *et al.*, 1991), $CF_2Cl_2$, $CFCl_2$ (Lindle *et al.*, 1991), $SF_6$ (Ekholm *et al.*, 2020), $C_{60}$ (Luo *et al.*, 1995), $C_{70}$ (Guo *et al.*, 1995), $CO_2$ (Gunnelin *et al.*, 1998), liquid water (Forsberg *et al.*, 2009; Odelius, 2009a), etc. A spherical tensor technique for the RIXS cross-section allows to study general properties of the scattering anisotropy beyond the dipole approximation (Juhin *et al.*, 2014).

## B. Scattering anisotropy due to molecular field splitting of the core shell

The molecular field can break the spherical symmetry of the core shells (Ertan *et al.*, 2020; Gel'mukhanov *et al.*, 1996b; Svensson *et al.*, 1994), slightly ($\sim 100$ meV) splitting the spin-orbit sublevels of deep core electrons. This occurs, for example, in the $L_{II,III}$ shell of the sulfur atom of the $H_2S$ molecule or chlorine atom in the HCl and $CF_3Cl$ molecules. The spin-orbit components split by the molecular field acquire a certain spatial orientation (Gel'mukhanov *et al.*, 1996b; Svensson *et al.*, 1994), thereby making the intensity distribution dependent on the relative orientation of the core and valence molecular orbitals (Gel'mukhanov *et al.*, 1996b; Svensson *et al.*, 1994). This introduces a specific scattering anisotropy in RIXS (Carniato *et al.*, 2009; Guillemin *et al.*, 2008; Puglisi *et al.*, 2020).

## V. INTERFERENCE OF SCATTERING CHANNELS

Quite often, there are several intermediate core-excited states that are closely spaced in energy. Obviously, channel interference should be expected for RIXS through these states.

## A. YDSE interference of scattering channels in symmetric molecules and selection rules

One of the most striking manifestations of interference in RIXS is the interference of resonant scattering channels through intermediate states with core hole localized at different atoms. It can manifest in symmetrical molecules, as $N_2$, $O_2$, $Cl_2$ (Gel'mukhanov and Ågren, 1994, 1999; Gel'mukhanov $et$ $al.$, 1976), or in the crystals (Gel'mukhanov $et$ $al.$, 1977b). This effect is in close analogy with wave scattering by two slits (Young's double-slit experiment (YDSE)) (Gel'mukhanov and Ågren, 1999; Gel'mukhanov $et$ $al.$, 1998c; Liu $et$ $al.$, 2015). YDSE interference in symmetrical molecules has been repeatedly studied in XPS (Argenti $et$ $al.$, 2012; Canton $et$ $al.$, 2011; Gel'mukhanov $et$ $al.$, 2007; Liu $et$ $al.$, 2006; Ueda $et$ $al.$, 2006) where it is named the Cohen-Fano effect after the seminal article by Cohen and Fano, 1966. YDSE interference in RAS of molecular oxygen gives a unique realization of the Einstein-Bohr recoiling double-slit gedanken experiment at the molecular level (Liu $et$ $al.$, 2015) (see Sec. VII.B).

To clarify the physical picture of the phenomenon, we consider RIXS by a homonuclear diatomic molecule in the gerade ($g$) ground state. The initial photon ($\omega$, $\mathbf{e}$, $\mathbf{k}$) excites the $1s$ electron of one of the atoms to the unoccupied $\sigma$ molecular orbital (MO) $\psi_\nu$. Then the electron from the occupied $\sigma$ MO $\psi_j$ fills the vacancy at the $1s$ level and a scattered photon is emitted ($\omega'$, $\mathbf{e}'$, $\mathbf{k}'$). For definiteness, we will assume that both molecular orbitals have $\sigma$ symmetry. Obviously, both scattering channels must be taken into account.

$$\omega + A_2 \rightarrow \left\{ \begin{array}{c} A^*A \\ AA^* \end{array} \right\} \rightarrow [A_2]_f + \omega'. \tag{10}$$

An asterisk marks an atom with a $1s$ hole. Having placed the origin at the center of symmetry and neglecting an insignificant constant prefactor, we write the total scattering amplitude as the sum of the amplitudes of both channels

$$F_f = (\mathbf{e} \cdot \mathbf{n})(\mathbf{e}' \cdot \mathbf{n}) \left( e^{\imath(\mathbf{q} \cdot \mathbf{R})/2} + \mathcal{P}_f e^{-\imath(\mathbf{q} \cdot \mathbf{R})/2} \right), \tag{11}$$

where $\mathbf{n} = \mathbf{R}/R$, $\mathbf{R}$ - interatomic radius-vector, $\mathcal{P}_f = 1$ or -1 when $f = g$ or $u$, respectively. The parity $\mathcal{P}_f$ of the final state $|f\rangle = |\psi_j^{-1}\psi_\nu^1\rangle$ is defined by the parity of the product $\psi_j\psi_\nu$. First, let us write the expression for the scattering cross section of a molecule oriented in
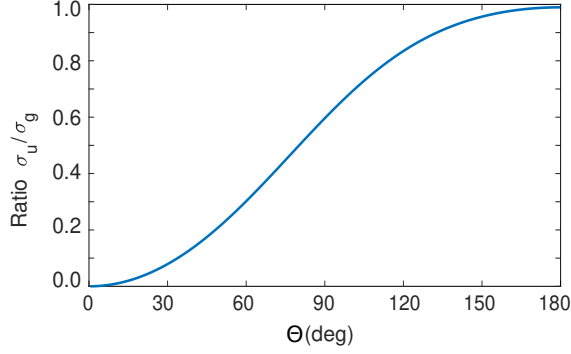
FIG. 2 Ratio $\sigma_u/\sigma_g = 15j_2(qR)/(qR)^2$ (Eq. (13)) for the Cl 1s RIXS of the $Cl_2$ molecule vs the scattering angle $\Theta$. $\mathbf{e}' \parallel \mathbf{e}$.

space

$$
\begin{aligned}
\sigma_f &= |F_f|^2 = 2a^2(1 + \mathcal{P}_f \cos(\mathbf{q} \cdot \mathbf{R})) \\
&\times \frac{\Delta(\omega' - \omega + \omega_{f0}, \Gamma_f)}{(\omega - \omega_{i0})^2 + \Gamma^2}, \\
a &= (\mathbf{e} \cdot \mathbf{n})^2 (\mathbf{e}' \cdot \mathbf{n})^2, \quad q \approx 2k \sin\frac{\Theta}{2}.
\end{aligned}
\tag{12}
$$

Here $\Theta = \angle(\mathbf{k}', \mathbf{k})$ is the scattering angle. In obtaining the expression for $q$, we have used the fact that the energy of the valence electron is small in comparison to the photon energy $\omega$. As expected, the selection rules for the scattering cross section, $\sigma_u = 0$, are satisfied in the region of soft X-ray radiation or small-angle scattering $qR \ll 1$. However, the selection rules are violated when moving into the hard X-ray regime $qR > 1$, where the scattering channel to the ungerade final state opens, $\sigma_u \neq 0$.

In a real experimental situation, the molecules are randomly oriented and the scattering cross section must be averaged over all orientations, following the theoretical work (Gel'mukhanov and Ågren, 1994; Gel'mukhanov *et al.*, 1998c, 1976). Due to our interest in selection rules, we write down the ratio of the peak intensities of the forbidden and allowed scattering channels (Fig. 2)

$$
\frac{\sigma_u(\omega', \omega)}{\sigma_g(\omega', \omega)} = \frac{1 - \varrho}{1 + \varrho} = \begin{cases} 0, & qR \ll 1, \\ 1, & qR \gg 1. \end{cases}
\tag{13}
$$

where the interference factor $\varrho = \overline{a \cos(\mathbf{q} \cdot \mathbf{R})}/\bar{a}$ (Gel'mukhanov and Ågren, 1994; Gel'mukhanov *et al.*, 1998c, 1976)
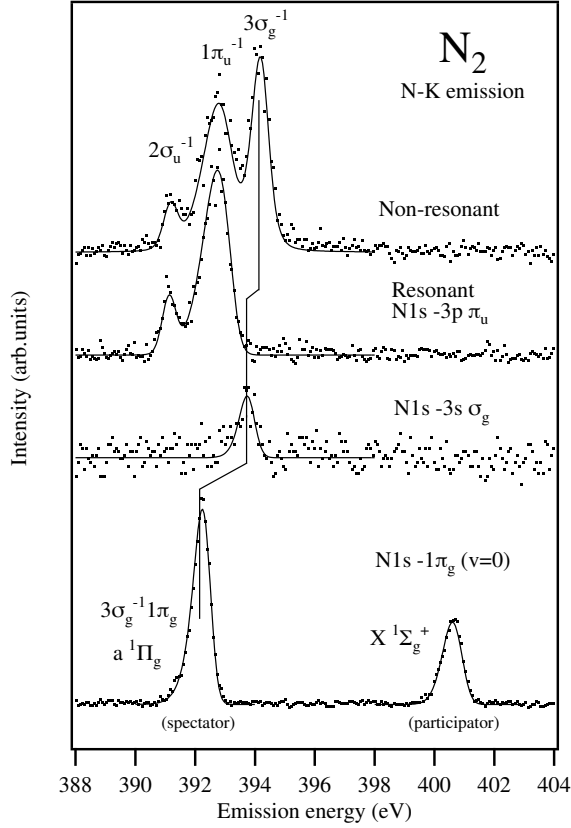
FIG. 3 Soft X-ray RIXS spectra of the $N_2$ $(1\sigma_g^2, 1\sigma_u^2, 2\sigma_g^2, 2\sigma_u^2, 1\pi_u^4, 3\sigma_g^2)$ molecule shows that the scattering to ungerade final states $3\sigma_g^{-1}3p\pi_u^1$, $(1\pi_u^{-1}3s\sigma_g^1, 2\sigma_u^{-1}3s\sigma_g^1)$ and $(1\pi_u^{-1}1\pi_g^1, 2\sigma_u^{-1}1\pi_g^1)$ are forbidden under core-excitation to ungerade core-excited states $1\sigma_g^{-1}3p\pi_u^1$, $1\sigma_u^{-1}3s\sigma_g^1$ and $1\sigma_u^{-1}1\pi_g^1$, respectively. These selection rules are absent for non-resonant X-ray emission due to degeneracy of the final continuum states with opposite parities (Gel'mukhanov and Ågren, 1994). Circles and solid lines show experimental and theoretical spectra, respectively. Reprinted from Glans *et al.*, 1996b with permission from Elsevier.

$$\varrho = 15 \left[ \frac{j_2(qR)}{(qR)^2} - \frac{j_3(qR)}{4qR\sin^2\frac{\Theta}{2}} \frac{(\mathbf{e}' \cdot \hat{\mathbf{k}})^2}{(1 + 2(\mathbf{e}' \cdot \mathbf{e})^2)} \right]. \tag{14}$$

tends to unity for soft X-ray radiation or small angle scattering, $qR \ll 1$. In the opposite limit of the hard X-ray regime, $qR \gg 1$, the interference factor tends to zero $\varrho \sim 1/(qR)^2$. Here $j_\ell(x)$ is the Bessel spherical function, and the overline refers to averaging over the molecular orientations. To avoid cumbersome expressions, Eq. (14) is written for the typical geometry of the experiment, where $\mathbf{k}' \perp \mathbf{e}$ (Lindle *et al.*, 1991).

Eq. (13) shows that the selection rules are fulfilled only for soft X-ray radiation or small-
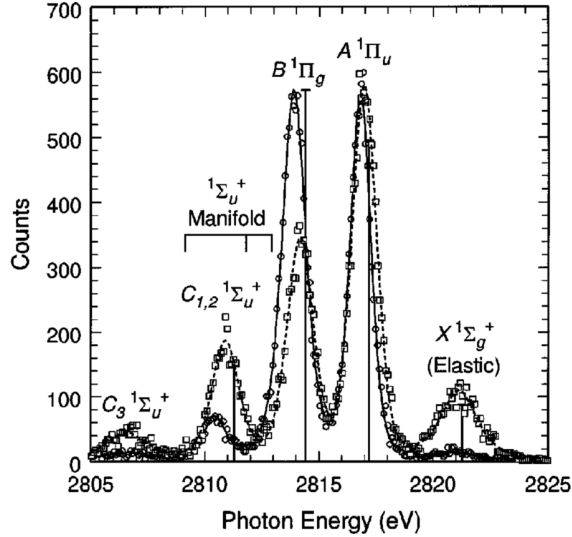
FIG. 4 RIXS in the hard X-ray region of the $Cl_2$ molecule shows the symmetry forbidden resonances $C^1_{1,2}\Sigma^+_u$ and $A^1\Pi_u$ ($\varrho < 1$, see Eq. (13)). The experiment was performed for $\angle(\mathbf{k'}, \mathbf{k}) = 90°$ and two orientations of polarizations of initial and scattered photons, $\angle(\mathbf{e'}, \mathbf{e}) = 90°$ (squares) and $0°$ (circles). From Mills $et\ al.$, 1997.

angle scattering ($\varrho \approx 1$), which was nicely confirmed in experiments with the $N_2$ (Glans $et\ al.$, 1996b) molecule (see Fig. 3) and $O_2$ (Glans $et\ al.$, 1996a). The same selection rules hold under core-excitation above core-ionization threshold in the region of shape resonances (Gel'mukhanov and Ågren, 1996c; Glans $et\ al.$, 1996c).

The interference of scattering channels in the hard X-ray range ($\varrho < 1$) violates the parity ban and opens the scattering channel from a gerade initial to a ungerade final state. This effect, previously predicted by (Gel'mukhanov and Ågren, 1994; Gel'mukhanov $et\ al.$, 1998c, 1976), was experimentally confirmed in a study (Mills $et\ al.$, 1997) of the $Cl_2$ molecule (see Fig. 4).

The interference structure (Eq. 12) for oriented diatomic molecules is reduced in the gas phase (Fig. 2) due to orientational disorder (Eq. 14). In the $Ba_3CeIr_2O_9$ crystal, which contain quasi-molecular orbitals localized on ordered dimers, a distinct interference structure (Eq. 12) was observed (Revelli $et\ al.$, 2019).

The selection rules in RIXS deserve a special comment (see also Sec.VIII). The dipole selection rules can be violated in the hard X-ray region. For example, the importance of quadrupole transitions was demonstrated in $1s2p$ RIXS of titanium oxide ($\omega \approx 4970$ eV) (Bagger $et\ al.$, 2017). The role of higher multipoles in RIXS was analysed in Refs. (Ament

*et al.*, 2011; Juhin *et al.*, 2014; van Veenendaal, 2015). The violation of selection rules due to YDSE interference (Eq. (12)) is defined by the molecular size $R$ instead of much the smaller size of the localized core hole $a_{1s}$. This remarkable fact is related to the size of delocalized core-hole $1\sigma_{g,u} = (1s_1 \pm 1s_2)/\sqrt{2}$ which is equal to $R$ (Gel'mukhanov and Ågren, 1994, 1998a, 1999; Gel'mukhanov *et al.*, 1998b; Mills *et al.*, 1997). Thus, the YDSE breakdown of selection rules gives raise to a strong non-dipolar effect defined by parameter $qR$, instead of $qa_{1s}$. The selection rules can be also broken due to vibronic coupling (VC) or electron-phonon interaction (Köuppel *et al.*, 2007; Miedema *et al.*, 2014; Skytt *et al.*, 1996) (Sec. VIII). The internal spin symmetry of molecular oxygen leads to new selectional rules in RIXS (Sun *et al.*, 2011b). The selection rules can be broken also because the core-electron and excited electron can swap parity in RIXS (Sun *et al.*, 2013, 2011b). There are also special selection rules for Franck-Condon (FC) amplitudes (Couto *et al.*, 2017; Vaz da Cruz *et al.*, 2018).

### B. Interference of scattering channels in crystals. Conservation of momentum

The interference considered above should also occur in crystals with a periodic arrangement of identical atoms. The initial photon in the crystal excites a $1s_n$ electron localized on the $n$ th atom to the conduction band: $1s_n \rightarrow \psi_{c\mathbf{p}}$. Then the valence electron fills the vacancy in the $1s_n$ level, $\psi_{v\mathbf{p}'} \rightarrow 1s_n$, and photon $\omega'$ is emitted. In the RIXS amplitude, we must sum over all intermediate core-hole states, similar to the case of a diatomic molecule considered above,

$$F \propto \sum_n \frac{\langle 1s_n|D'e^{-\imath\mathbf{k}'\cdot\mathbf{r}}|\psi_{v\mathbf{p}'}\rangle\langle\psi_{c\mathbf{p}}|De^{\imath\mathbf{k}\cdot\mathbf{r}}|1s_n\rangle}{\omega - \omega_{c\mathbf{p}} + \imath\Gamma}. \tag{15}$$

The resonant energy of photoabsorption is approximately equal to the difference between the energies of the electron in the conduction band and in the $1s$ level: $\omega_{c\mathbf{p}} \approx \epsilon_{c\mathbf{p}} - \epsilon_{1s}$. Using Bloch's theorem, $\psi_{\mathbf{p}} = e^{\imath\mathbf{P}\cdot\mathbf{r}}u(\mathbf{r})$, where $u(\mathbf{r}) = u(\mathbf{r} + \mathbf{R}_n)$ is a periodic function, the dipole approximation for the atomic matrix transition element, and

$$\sum_n e^{\imath(\mathbf{p}'-\mathbf{p}-\mathbf{q})\cdot\mathbf{R}_n} \propto \sum_{\mathbf{G}} \delta(\mathbf{p}' - \mathbf{p} - \mathbf{q} - \mathbf{G}) \tag{16}$$

we obtain (Gel'mukhanov and Ågren, 1998b; Gel'mukhanov $et$ $al.$, 2000, 1977b)

$$\sigma(\omega', \omega) \propto \sum_{\mathbf{G}} \int d\mathbf{p} |D'_{v\mathbf{p}'} D_{i\mathbf{p}}|^2$$
$$\times \Delta(\omega - \omega_{v\mathbf{p}}, \Gamma) \Delta(\omega' - \omega - \omega_{c\mathbf{p}, v\mathbf{p}'}, \Gamma_f),$$
$$\mathbf{p}' = \mathbf{p} + \mathbf{q} + \mathbf{G}, \tag{17}$$

where $\mathbf{G}$ is the reciprocal lattice vector, $\omega_{c\mathbf{p}, v\mathbf{p}'} \approx \epsilon_{c\mathbf{p}} - \epsilon_{v\mathbf{p}'}$, $D_{c\mathbf{p}'}$ and $D'_{v\mathbf{p}'}$ are matrix elements of X-ray transitions to the conduction band (CB) and from the valence band (VB), respectively. In the soft X-ray range, the photon momentum transferred to the electrons is small, $q \ll G$. Since the momenta of the valence electron and the conduction electron approximately coincide

$$\mathbf{p}' \approx \mathbf{p}, \tag{18}$$

the scattering process is vertical. The spectral features of RIXS are determined by the interband density of states $\rho(\omega', \omega)$ (Gel'mukhanov $et$ $al.$, 2000, 1977b)

$$\rho(\omega', \omega) = \sum_{v<F, c>F} \int d\mathbf{p} \delta(\omega - \omega_{c\mathbf{p}}) \delta(\omega' - \omega_{v\mathbf{p}}), \tag{19}$$

where the summation is carried out over the zones above and below the Fermi level (F). Interband density of states is related to the formation of the RIXS spectrum of periodic structures. The frequency of the initial photon determines the crystal momentum $\mathbf{p}$ ($\omega_{c\mathbf{p}} = \omega$) and, hence, the resonant frequency of emission transition $\omega' = \omega_{v\mathbf{p}}$ (see. Fig. 5 a).

The variation of $\omega$ changes the resonance value of the momentum $\mathbf{p}$ and the position of the emission peak $\omega' = \omega_{v\mathbf{p}}$ changes accordingly (see Fig. 5 a). This explains the evolution of the RIXS spectrum when $\omega$ changes (Carlisle $et$ $al.$, 1995, 1999; Shirley, 2000) and allows to solve the inverse problem of reconstruction of the band structure from experimental RIXS spectra (Kanász-Nagy $et$ $al.$, 2016; Lüning $et$ $al.$, 1997).

Obviously, the RIXS process ceases to be vertical (Ament $et$ $al.$, 2011; Gel'mukhanov $et$ $al.$, 2000, 1977b) in the hard X-ray region ($q \gtrsim G$) due to the transfer of large momentum from the photons to the electrons. In this case, one should use the strict law of momentum conservation (17) instead of Eq. (18). The $\mathbf{q}$-dependence of the RIXS cross section is a powerful tool to study the dispersion of low-energy excitations in solids (Kim $et$ $al.$, 2012; Le Tacon $et$ $al.$, 2014; Schlappa $et$ $al.$, 2012; Ulrich $et$ $al.$, 2009) (See Sec. IX C and Sec. XIII C.)
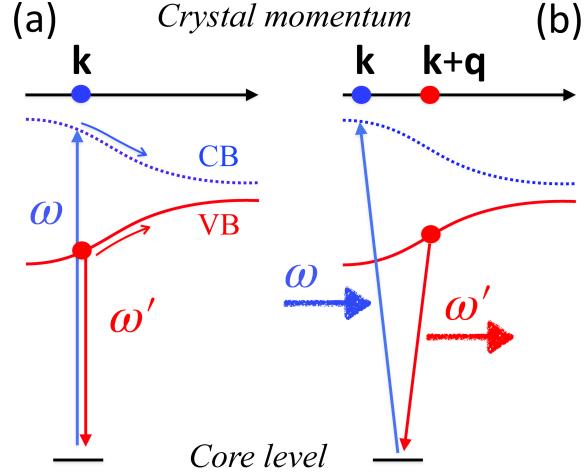
FIG. 5 Physical picture of the evolution with detuning of RIXS resonance in a crystal. a) The momentum transfer $\mathbf{q}$ is negligible for soft X-rays. Due to this the final state consists of a vertical VB-to-CB excitation, whose crystal momentum is selected by the energy of the incoming photon as indicated. A nice showcase of this is the RIXS of graphite (Carlisle *et al.*, 1995). b) The RIXS transitions cease to be vertical in hard X-ray region.

The electron-phonon scattering, involving linear (Gel'mukhanov *et al.*, 1998c; Privalov *et al.*, 1999) and the angular momentum (Beye *et al.*, 2009; Privalov *et al.*, 1999) of the phonon, violates the law (18). The RIXS profile becomes sensitive to temperature due to electron phonon scattering which increases the incoherent scattering. Angular momentum of the phonon opens the symmetry forbidden p-p decay channels as shown in RIXS from crystalline silicon (Beye *et al.*, 2009).

Sudden appearance of the core-hole leads to infinite number of low energy electron-hole pairs generated in the vicinity of the Fermi surface. This results in the edge singularity in the soft XAS and XES spectra of metals known as the Mahan- Noziéres-deDominicis (MND) effect (Doniach and Sondheimer, 1998). This dynamical effect in RIXS was studied in (Hancock *et al.*, 2010; Noziéres and Abrahams, 1974; Privalov *et al.*, 2001).

## C. Life-time vibrational interference

Modern RIXS and RAS spectroscopy resolve the vibrational structure (see VI.B), which is extremely sensitive to the dynamics of nuclei in the intermediate electronic state. It is firmly established that the formal reason for the nuclear dynamics is the interference of intermediate

19

vibrational states (Gel'mukhanov *et al.*, 1977a), which for RIXS on the vibrational ground state coherently forms the scattering amplitude

$$F_{\nu_f} = \sum_{\nu_i} F_{\nu_f,\nu_i} = \sum_{\nu_i} \frac{\langle \nu_f | V_{fi} | \nu_i \rangle \langle \nu_i | D_{i0} | 0 \rangle}{\omega - \omega_{i0} - w_{\nu_i,0} + \imath \Gamma} \tag{20}$$

which also can be formulated as the projection of the wave packet $|\Psi\rangle$ onto the final vibrational state $|\nu_f\rangle$

$$F_{\nu_f} = -\imath \langle \nu_f | \Psi \rangle,$$
$$|\Psi\rangle = \imath \sum_{\nu_i} \frac{V_{fi} |\nu_i\rangle \langle \nu_i | D_{i0} | 0 \rangle}{\omega - \omega_{i0} - w_{\nu_i,0} + \imath \Gamma}, \tag{21}$$

Here $\omega_{i0} = E_i - E_o$ and $w_{\nu_i,0} = \varepsilon_{\nu_i} - \varepsilon_0$ is a difference of energies of electronic and vibrational states, respectively. As can be seen from Eq. (21), the wave packet $|\Psi\rangle$ is a coherent superposition of intermediate vibrational states $|\nu_i\rangle$. This is denoted Life-Vibrational Interference (LVI) (Skytt *et al.*, 1997), since it captures vibrational dynamics occurring during the lifetime of the core-excited state $2/\Gamma$. Eqs. (20) and (21), obtained in the Born-Oppenheimer (BO) approximation from the general KH formula (2), are valid for both RIXS and RAS processes with one intermediate electronic state $i$. In the first case, $V_{fi} = D'_{fi}$, and in the second, $V_{fi} = Q_{fi}$ is a matrix element of the Coulomb interaction between the electrons. Here and below, the vibrational states of electronic state $i$ is denoted by Greek letters, $|\nu_i\rangle$, $D_{i0} = (\mathbf{e} \cdot \mathbf{d}_{i0})$, $D'_{fi} = (\mathbf{e}' \cdot \mathbf{d}_{fi})$.

To demonstrate the crucial role of interference, we divide the cross section into direct and interference contributions (Gel'mukhanov *et al.*, 1977a)

$$\sigma(\omega', \omega) = \sigma_{\mathrm{dir}}(\omega', \omega) + \sigma_{\mathrm{int}}(\omega', \omega), \tag{22}$$
$$\sigma_{\mathrm{dir}}(\omega', \omega) = \sum_{\nu_f, \nu_i} |F_{\nu_f,\nu_i}|^2 \Delta(\varepsilon, \Gamma_f),$$
$$\sigma_{\mathrm{int}}(\omega', \omega) = \sum_{\nu_f, \nu_i \neq \nu'_i} F^*_{\nu_f,\nu_i} F_{\nu_f,\nu'_i} \Delta(\varepsilon, \Gamma_f),$$

where $\varepsilon = \omega' - \omega - \omega_{f0} - w_{\nu_f,0}$. Fig. 6 shows that taking into account only the direct contribution of $\sigma_{\mathrm{dir}}$ leads to a strong deviation from the total cross section of $\sigma$. The physical reason for this is that a description of the dynamics of nuclei is impossible without taking into account vibrational interference. The decisive role of interference for intermediate states in a continuous spectrum, as in the case of dissociative states, is obvious. It is worth noting,
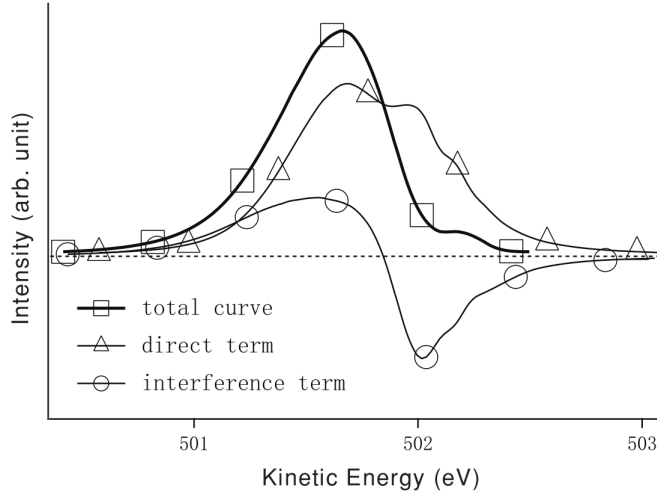
FIG. 6 The LVI line shape of the normal Auger spectral component $1^3\Delta_u$ of the $O_2$ molecule. The thick line with ($\square$) is the total LVI line shape $\sigma(E,\omega)$; the line with ($\triangle$) is calculated by the direct term $\sigma_{\text{dir}}(E,\omega)$ in the LVI formula (22); the line signed with signs ($\bigcirc$) shows the LVI interference term $\sigma_{\text{int}}(E,\omega)$. Reprinted from Bao $et$ $al.$, 2008 by permission from IOP Science, license 1106314-1.

that in the wave packet technique, presented in Sec. VI.A, the interference is taken into account automatically through the completeness condition

$$\sum_\nu |\nu\rangle\langle\nu| = 1. \tag{23}$$

RIXS and RAS theory, which takes into account the LVI of scattering channels through closely spaced intermediate states (Gel'mukhanov $et$ $al.$, 1977a), is a necessary tool for a correct description of RIXS and RAS experimental spectra (Kjellsson $et$ $al.$, 2021; Neeb $et$ $al.$, 1994). As examples of recent progress, let us mention successful applications of the LVI theory to describe the RIXS and RAS spectra of polyatomic molecules with a large number of vibrational modes and their overtones, for example in water (Vaz da Cruz $et$ $al.$, 2017), methanol (Vaz da Cruz $et$ $al.$, 2019b), acetone (Sun $et$ $al.$, 2011a), ethene (Liu $et$ $al.$, 2011b), etc.

### 1. Sum rules. Optical theorem

There are certain sum rules for resonant scattering (Gel'mukhanov and Ågren, 1996a; Gel'mukhanov $et$ $al.$, 1996a). The first one follows directly from the optical theorem, which makes the link between total RIXS cross-section and imaginary part of the scattering am-

plitude Im$F$ which is proportional to the XAS cross-section. This sum rule implies also that the integral of the interference term is equal to zero

$$\int \sigma_{\mathrm{int}}(\omega', \omega)d\omega' = 0 \qquad (24)$$

in the FC approximation. There are also sum rules for the center of gravity and for the width of the RIXS and RAS profiles (Gel'mukhanov and Ågren, 1996a; Gel'mukhanov *et al.*, 1996a), which were investigated recently in experiment (Piancastelli *et al.*, 2020).

### 2. X-ray absorption measured in X-ray Raman mode

An important property of RIXS and RAS is the spectral resolution which is not influenced by a lifetime broadening of core-excited states. This is the origin of the idea to resolve the transitions in XAS beyond the lifetime broadening limit of core-excited states. Tulkki and Åberg, 1982 suggested that lifetime broadening free XAS can be achieved by scanning over the frequencies of the incoming photons while keeping the emission frequency fixed at the maximum of an X-ray fluorescence line. Narrowing of X-ray absorption resonances was experimentally evidenced in RIXS (Hämäläinen *et al.*, 1991) and RAS (Hikosaka *et al.*, 2008) modes (see also (Glatzel and Bergmann, 2005; de Groot, 2001)). It even has been given a special name "High-energy resolution fluorescence detected (HERFD) XAS (Glatzel *et al.*, 2005, 2002; Safonova *et al.*, 2006). Let us point out that XAS profile measured in scattering mode is sensitive to the final RIXS/RAS state and can strongly deviate from true XAS profile (Carra *et al.*, 1995; Gel'mukhanov and Ågren, 1999; Glatzel *et al.*, 2009; Hikosaka *et al.*, 2008). Measurement of XAS in RIXS mode was recently studied theoretically for the vibrationally excited water molecule (Ignatova *et al.*, 2017a,b), where it was shown that this technique allows for distinction of XAS contributions from different initial vibrational states.

The second opportunity was recognized by Rubensson, 2000 who showed that the low-energy tail of the RIXS spectrum resembles inverted XAS profile for large negative detuning from the XAS edge (Kikas *et al.*, 2004; Magnuson *et al.*, 2003), giving an alternative way to measure the XAS and EXAFS spectra (Błachucki *et al.*, 2014; Kikas *et al.*, 2004).

## VI. DYNAMICS OF RESONANT SCATTERING

Despite that RIXS and RAS measurements are essentially stationary experiments there are, as we will see below, many spectral manifestations of nuclear dynamics in resonant scattering. The main characteristic time of this dynamics is the duration of the resonant X-ray scattering; this is due to a purely quantum mechanical effect of interference suppression of the long time contribution to the scattering amplitude. Using the variation of the duration time with the excitation energy detuning from the resonance $\Omega$, one can monitor and even control various microscopic dynamical processes, revealed by RIXS and RAS spectral features.

### A. Scattering duration

The simplest way to rewrite the KH equations in the time domain is to apply the identity

$$\frac{1}{x + \imath\Gamma} = -\imath \int_0^\infty e^{\imath(x+\imath\Gamma)t} dt \tag{25}$$

to the wave packet $|\Psi\rangle$ (21), and to replace the Lorentzian $\Delta(x,\Gamma) = -\text{Im}(1/(x+\imath\Gamma))$ in the cross section (2) by an integral over time (25). Then using the completeness condition (23) and the identity $\exp(-\imath\varepsilon_f t) = \exp(-\imath h_f t)$, it is possible to rewrite the KH formula (2) in a temporal representation (Gel'mukhanov $et\ al.$, 1977a; Sałek $et\ al.$, 1999)

$$\sigma(\omega',\omega) = \frac{1}{\pi}\text{Re}\int_0^\infty e^{\imath(\omega-\omega'-\omega_{f0}+\varepsilon_0+\imath\Gamma_f)t}\sigma(t)dt,$$

$$\sigma(t) = \langle\Psi|e^{-\imath h_f t}|\Psi\rangle, \quad |\psi_i(t)\rangle = e^{-\imath h_i t}D_{i0}|0\rangle,$$

$$|\Psi\rangle = V_{fi}\int_0^\infty e^{-\Gamma t}e^{\imath\Omega t}e^{\imath\varepsilon_0 t}\psi_i(t)dt, \tag{26}$$

where $h_i$ is the nuclear Hamiltonian of the electronic state $i$. The time

$$\tau = \frac{1}{\Gamma - \imath\Omega} = |\tau|e^{\imath\phi}, \quad \Omega = \omega - \omega_{i0} \tag{27}$$

of formation of the wave packet

$$|\Psi\rangle = V_{fi}\int_0^\infty e^{-\frac{t}{\tau}}e^{\imath\varepsilon_0 t}\psi_i(t)dt \tag{28}$$
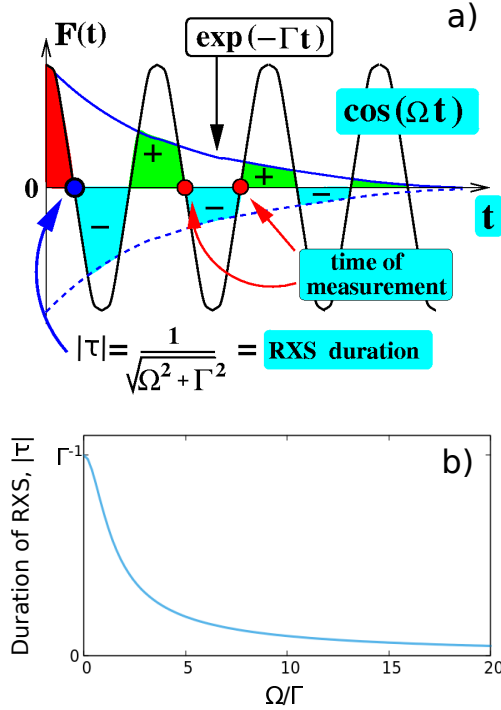
FIG. 7 a) Irreversible $\exp(-\Gamma t)$ and reversible $\cos(\Omega t)$ quenching of scattering amplitude $F$. b) Scattering duration $|\tau| = 1/\sqrt{\Omega^2 + \Gamma^2}$ (Cesar *et al.*, 1997; Gel'mukhanov *et al.*, 1999; Skytt *et al.*, 1996).

is a complex number. This time determines the scattering duration (Cesar *et al.*, 1997; Gel'mukhanov *et al.*, 1999; Marchenko *et al.*, 2015; Skytt *et al.*, 1996), controlled experimentally by changing the detuning $\Omega$ of the frequency of the initial photon $\omega$ from the absorption resonance. In practice, the real time $|\tau| = 1/\sqrt{\Gamma^2 + \Omega^2}$ is used for description of the scattering duration; its dependence on $\Gamma$ and $\Omega$ is shown in Fig. 7 b). However, the roles of $\Gamma$ and $\Omega$ in the scattering duration are qualitatively different.

The finite lifetime $1/\Gamma$ leads to the decay term $\exp(-\Gamma t)$ in the wave packet $|\Psi\rangle$ (26) and results in irreversible quenching of the excited state. Unlike $\Gamma$, the detuning $\Omega$ describes undamped, in principle, reversible, dephasing oscillations $\exp(\imath\Omega t)$. Obviously, these sign-changing oscillations effectively quench the contribution to $|\Psi\rangle$ (26) from the times $t > 1/|\Omega|$ due to the destructive interference of contributions from different $t$ (Fig. 7 a).

As we will see below, the concept of the scattering time varied by the detuning (Cesar *et al.*, 1997; Gel'mukhanov *et al.*, 1999; Skytt *et al.*, 1996) allows to study the electronic-vibrational dynamics with a femtosecond time resolution without using pump-probe methods with short (fs) X-ray pulses. There is yet another powerful method to study ultrafast

dynamics, namely core-hole-clock spectroscopy (Brühwiler *et al.*, 2002). The method is used to study, for example, the charge transfer dynamics at interfaces and surfaces with the lifetime of the core-hole as an internal reference clock to follow the charge transfer process.

In conclusion, let us note that the time-dependent wave packet technique (Eq. (26)) is one of the main numerical methods for calculation of RIXS and RAS spectra and dynamics. The advantages of this method as compared to the time-independent KH formula (21) are most pronounced in the case of dissociative states.

## B. Dynamical spatial quantum beats in quasi-elastic RIXS

In Secs. V.A and V.B we considered the interference of nearly degenerate electronic intermediate states. Often there are several core-excited states close in energy that can interfere in RIXS. Kosugi and coworkers (Adachi *et al.*, 2005) have shown that the $1s$ core-ionized paramagnetic oxygen molecule has doublet ($D$) and quartet ($Q$) states, with total spin $S = 1/2$ and $3/2$. Similarly, with X-ray excitation of the neutral $O_2$ molecule into the lowest unoccupied MO (LUMO), $1\sigma_g \rightarrow 3\sigma_u$, the doublet and quartet states of the ion, pairing with the electron spin on this orbital, form two closely spaced singlet $\Sigma$ states (Fig. 8). These dissociative $\Sigma$ states are also denoted by the letters $D$ and $Q$. RIXS at excitation energies close to these interfering states was studied in (Kimberg *et al.*, 2012; Pietzsch *et al.*, 2011). Of particular interest here is the quasi-elastic scattering channel, the final state of which is the electronic ground state. An extended oscillatory progression in this channel experiences smoothly damped oscillations (Pietzsch *et al.*, 2011) (Fig. 9).

In order to investigate the unusual nature of these beats, one can employ the extended smoothly damped oscillatory progression in quasi-elastic RIXS, characteristic for dissociation in the intermediate state(Couto *et al.*, 2017; Niskanen *et al.*, 2019; Vaz da Cruz *et al.*, 2019a,b) (see Sec. XI). We can verify that the cross section for scattering to the final vibrational state $\nu$ is proportional to the Frank-Condon factor (FC) $|\langle\nu|\Psi\rangle|^2$, which is nothing else than the square of the projection of the wave packet in an intermediate dissociative state

$$\Psi = \Psi_D + \Psi_Q \tag{29}$$

onto $|\nu\rangle$. The superposition expressed in Eq. (29) is valid, since the wave packet propagates along the potential energy surface $E$ simultaneously in the field of dissociative potentials
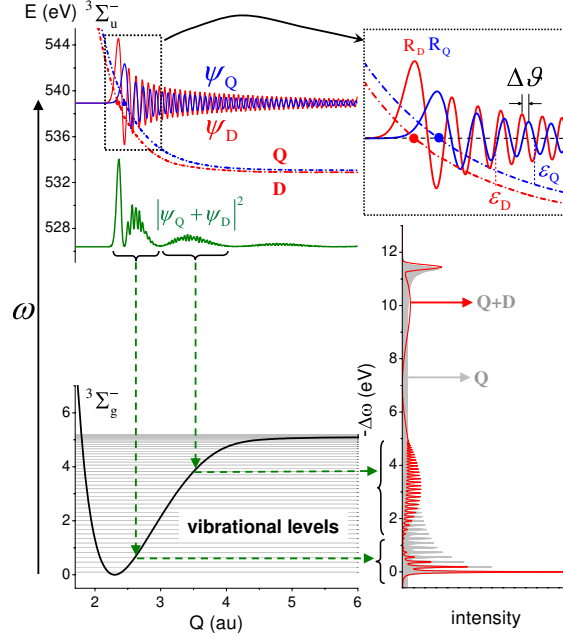
FIG. 8 Dynamical interference of the Q and D core-excited states of $O_2$ results in the quantum beats of the RIXS cross-section. $\Delta\omega = \omega' - \omega$. From Pietzsch *et al.*, 2011.
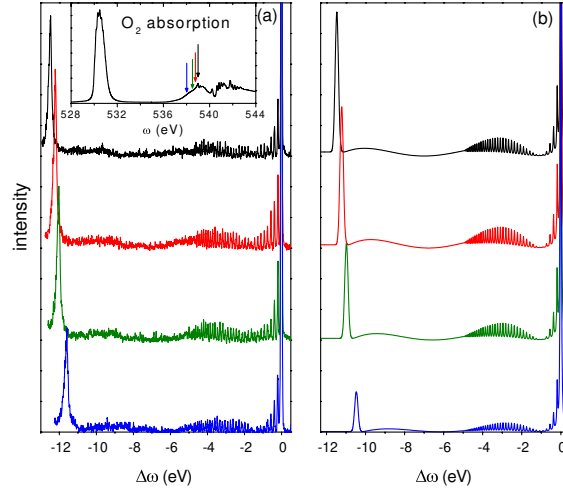


FIG. 9 Experimental (a) and theoretical (D) RIXS spectra of $O_2$ for $\chi = 90°$ for excitation energies $\omega$ shown in by arrows in the XAS spectrum. $\Delta\omega = \omega' - \omega$. Adapted from Pietzsch *et al.*, 2011.

$E_D(R)$ and $E_Q(R)$ of states $D$ and $Q$. The idea now is to compute the phase shift $\Delta\vartheta$ between the wave packets $\Psi_D$ and $\Psi_Q$. To do this, we use the semiclassical approximation

$$\Psi_i(R) \propto \exp \int_{R_i}^{R} \{\imath P_i(R')dR' - \Gamma dt\}, \quad t = \frac{dR'}{v_i(R')}. \tag{30}$$

Here $i = D, Q$, $P_i(R') = \sqrt{2\mu\varepsilon_i(R)}$, $\varepsilon_i(R) = E - E_i(R)$, $\mu$ is the reduced mass. Calculations

based on this equation (Pietzsch *et al.*, 2011) lead to the following expression for the phase shift we are interested in

$$\Delta\vartheta \approx (P_Q - P_D)(R - R_Q) = \Delta t \Delta E - \varphi, \tag{31}$$

where $\Delta t = (R - R_Q)/v$ is the propagation time of the wave packet to the point $R$ with an average speed $v = (P_D + P_Q)/2\mu$, $\Delta E = E_Q(R_0) - E_D(R_0) \approx 2$ eV is the splitting between the states $D$ and $Q$ near the equilibrium bond length $R_0$, and $\varphi$ is the phase shift independent of $R$. As a result, $|\Psi_D + \Psi_Q|^2$ experiences a beating with increasing bond length $R$

$$\cos(\Delta t \Delta E + \varphi)e^{-2\Gamma\tau}, \tag{32}$$

which decays due to the finite lifetime of the intermediate state $2/\Gamma$. Despite the semiclassical approximation (30), Eq. (32) perfectly explains the spatial modulation of the squared wave packet $|\Psi_D + \Psi_Q|^2$, strictly computed by the quantum wave packet method shown in Fig. 8.

With the help of the reflection principle (Gel'mukhanov and Ågren, 1996b; Schinke, 2009) it is possible to obtain an approximate spectral shape from the spatial distribution of the squared nuclear wave function, namely by reflecting of the $|\Psi_D + \Psi_Q|^2$ onto the potential energy curve (PEC) of the final state, as illustrated in Fig. 8. This gives a unique opportunity to image nuclear wave functions (Gel'mukhanov and Ågren, 1996b; Kjellsson *et al.*, 2021; Pietzsch *et al.*, 2011). Altogether we obtain a clear physical picture of the effect. The discussed quantum beats were previously observed also in RAS spectra from $O_2$ (Feifel *et al.*, 2008). Fig. 8 shows that the reflection principle allows to solve an inverse problem: to reconstruct approximately the square of the wave packet $|\Psi|^2$ from the RIXS or RAS spectrum.

In conclusion, it should be noted that the considered effect of quantum beats is inherently dynamical, occurring when the coherent evolution of nuclei along two potential surfaces plays a decisive role. Furthermore, the role of interference between the direct ionization and different resonant ionization channels was studied in the C K RAS spectra of the $CH_3Cl$ molecule (Nandi *et al.*, 2017).

## C. Dynamical collapse of vibrational structure and quenching of soft modes

We proceed considering another dynamic effect that is inherent in all RIXS spectra and has also been observed in a number of RAS experiments, namely, the collapse of vibrational structure. Let us discuss two qualitatively different transition schemes, typical for both RIXS and RAS processes.

**Collapse of type 1**: Let us first consider a special case when the shapes of PECs of the initial $E_0(R)$ and final $E_f(R)$ states are identical. Obviously, this is the case in quasi-elastic RIXS, where the final state is the same at the initial state. When the photon frequency coincides with the vertical transition frequency, $\Omega = \omega - \omega_{i0}(R_0) = 0$, the scattering duration is quite long, $|\tau| = 1/\Gamma$ (Eq. (27)), so that the initial wave packet $|0\rangle$ has time to propagate and get deformed in the intermediate state. Due to difference in the shape of the intermediate $E_i(R)$ and final $E_f(R)$ states' PEC and the small life-time broadening, the RIXS spectrum shows a vibrational structure. Let us now tune the excitation frequency away from the absorption resonance

$$|\Omega| \equiv |\omega - \omega_{i0}(R_0)| \gg \varepsilon_0, \tag{33}$$

making the scattering duration $|\tau|$ (Eq. (27)) shorter than the vibrational period $T = 4\pi/\varepsilon_0$. In this case, the nuclear wave packet $|\Psi\rangle$, has no time to move away from the vertical transition point $R_0$ and it decays to the final state without changing of the original shape, $|\Psi\rangle = |0\rangle$. Obviously, the amplitude of the RIXS is now proportional to the FC amplitude of the direct transition from the initial to the final state

$$F_f \propto \langle \nu_f | 0 \rangle, \quad |\tau| = \frac{1}{\sqrt{\Gamma^2 + \Omega^2}} \ll T. \tag{34}$$

Taking into account the identical shape of the initial and final states' PEC, and, hence $\nu_f | 0 \rangle = \delta_{\nu_f,0}$, we conclude that at large detuning, the spectrum collapses into a single vibrational peak, $\nu_f = 0$. Here it is assumed that only lowest vibrational state is initially populated in the ground electronic state. It worth noting that due to the dependence of the condition (34) on the vibration frequency, the "soft" vibrational modes in polyatomic molecules collapse before stiff modes as a function of detuning (Vaz da Cruz *et al.*, 2019b).

This effect, predicted in by Gel'mukhanov *et al.*, 1997a, almost immediately received experimental confirmation in RAS of CO molecule (Sundin *et al.*, 1997), and later in $N_2$ molecule (Feifel *et al.*, 2002). This collapse in quasi-elastic RIXS has been observed for
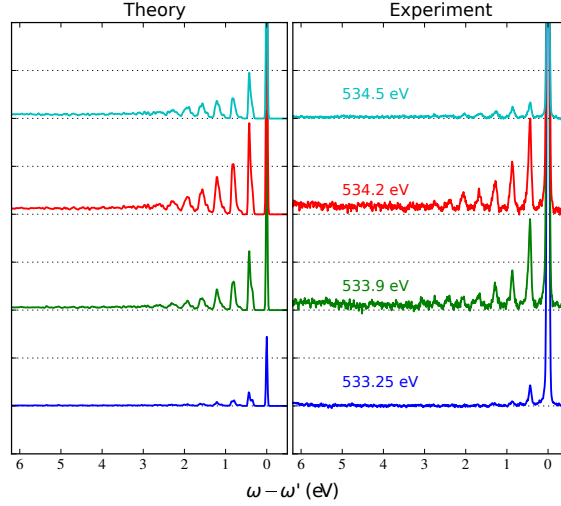
FIG. 10 The detuning from the absorption resonance leads to the collapse of vibrational structure (Gel'mukhanov *et al.*, 1997a) in RIXS of liquid water (Vaz da Cruz *et al.*, 2019a).

different systems, for example, in liquid acetone (Sun *et al.*, 2011a), liquid ethylene (Hennies *et al.*, 2005), liquid methanol (Vaz da Cruz *et al.*, 2019b), and gaseous and liquid water (Fig. 10) (Vaz da Cruz *et al.*, 2017). Recently, the dynamical collapse of the vibrational structure made it possible to extract the electron-phonon interaction constant, $\approx 0.17$ eV, from the $\Omega$-dependence of the phonon-resonance in a RIXS experiment (Rossi *et al.*, 2019a) on the superconductor $NdBa_2Cu_3O_3$.

**Collapse of type 2:** The second type of dynamic collapse of the vibrational structure is realized in the systems where the shapes of PECs of the intermediate and final states coincide (Piancastelli *et al.*, 2020; Sundin *et al.*, 1997). This situation is realized in RIXS transitions between two core hole states, e.g. $K_\alpha$ RIXS in the HCl or $H_2S$ molecules (Piancastelli *et al.*, 2020; Simon *et al.*, 2006)

$$\omega + HCl \rightarrow HCl(1s^{-1}\sigma^*) \rightarrow HCl(2p^{-1}\sigma^*) + \omega'. \tag{35}$$
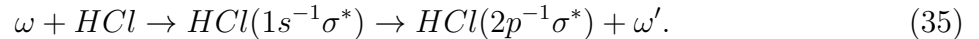
Since the intermediate $|1s^{-1}\sigma^*\rangle$ and the final $|2p^{-1}\sigma^*\rangle$ states differ only by the character of the core hole, the PEC shapes for these states match with high precision (Simon *et al.*, 2006). In spite of the short lifetime ($1/2\Gamma \approx 1$ fs) of the state $|1s^{-1}\sigma^*\rangle$, the narrowing of both components of the $K_{\alpha_{1,2}}$ doublet when $\Omega \rightarrow 0$ unambiguously indicates dynamical nature of the collapse (Fig. 11).

This phenomenon is explained by the fact that for $\Omega = 0$ the spectral form of RIXS is determined by the set of frequencies of the emission transitions $\omega_{if}(R) = E_i(R) - E_f(R)$,
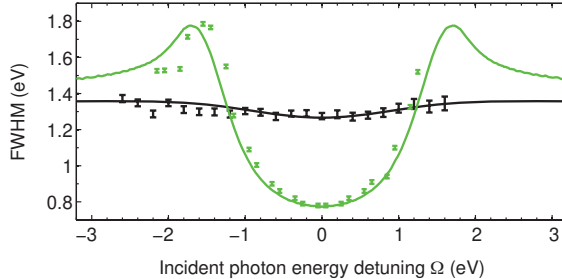
FIG. 11 Collapse of vibrational structure in RIXS: Full width at half maximum (FWHM) of the I $L_3$-$N_{4,5}$ of $CH_3I$ (black) and Cl K-L of $CH_3Cl$ (green/grey) emission lines as a function of the incident photon energy detuning with respect to the resonance energy. Adapted from Marchenko *et al.*, 2011, with the permission of AIP Publishing.

which collapses into a single narrow resonance when $E_i(R)$ and $E_f(R)$ are parallel ($\langle \nu_f | \nu_i \rangle = \delta_{\nu_f,\nu_i}$). At the large detuning, the direct channel is strong (see Eq. (34)) and the vibrational broadening occurs (see. Fig. 11) as $\langle \nu_f | 0 \rangle \neq \delta_{\nu_f,0}$, due to different shape of $E_f(R)$ and $E_0(R)$. Thus, unlike the collapse of the first type, the broadening occurring at the large $|\Omega|$ is followed by the narrowing of the peak at $\Omega \to 0$.

An additional confirmation of the dynamic nature of the phenomenon is obtained from the comparison of the $\Omega$-dependence of the resonance width for the molecules $CH_3Cl$ and $CH_3I$ (Fig. 11). The intermediate state lifetime with a hole in the $L$ shell of the iodine atom (0.23 fs) in $CH_3I$ is much shorter than one for the intermediate state with a hole in the $K$ shell of the chlorine atom (0.94 fs) in the $CH_3Cl$ molecule. This means that during the lifetime of the intermediate state, the nuclei in $CH_3I$ molecule have much less time to shift their position, as compared to $CH_3Cl$. This explains the less pronounced line narrowing for $CH_3I$ as compared to $CH_3Cl$. The second type of the collapse of the vibrational structure was first observed in RAS from the CO (Sundin *et al.*, 1997). It is worth noting that the observation of the collapse provides information about the PECs of the states involved in the process.

## D. Extraction of potential energy surfaces from RIXS and RAS spectra

Thanks to modern spectrometers with super-high resolution, in many cases it has become possible to resolve vibrational structure in the RIXS and RAS spectra, which allows to extract PEC along different vibrational modes from the experimental spectra, as demonstrated
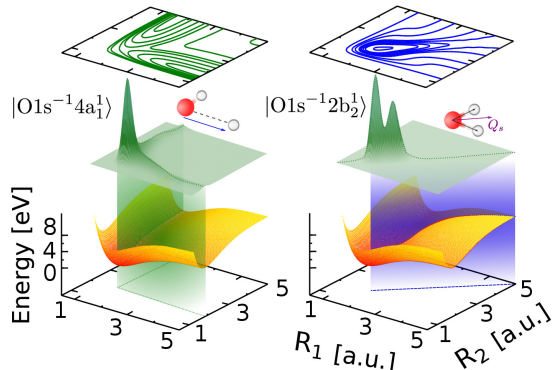
FIG. 12 During the emission transition, a nuclear wave packet of an intermediate state, being projected onto the ground state, allows one to obtain a slice of the potential surface of the ground state along the direction of propagation of the wave packet.

in a number of cases (Eckert *et al.*, 2018; Marchenko *et al.*, 2017; Miron *et al.*, 2012; Schreck *et al.*, 2016; Vaz da Cruz *et al.*, 2019a). For example, the RIXS and RAS spectra made it possible to determine from experimental data the dissociative potentials of the intermediate and final single and double hole states of the $CH_3Cl$ and $CH_3I$ molecules (Marchenko *et al.*, 2017). The extended vibrational progression of $1s_O^{-1}\pi^{*1}$ of the quasi-elastic RIXS channel of liquid acetone and liquid acetone mixed with chloroform made it possible to determine the potentials of the ground electronic state along the C = O coordinate (Schreck *et al.*, 2016). The potentials of the final ion states $1^2\Pi_g$ and $1^2\Phi_g$ of the $N_2$ molecule were extracted from the RAS spectra (Kimberg and Miron, 2014; Miron *et al.*, 2012).

It is worth noting that in a disordered system, like liquid, it is impossible to determine a unique potential energy surface of a molecule due to the fluctuating local environment around it (see Sec. XI.C.3). Therefore, only the confidence interval of the PECs distribution can be extracted from the experiment, as it was done for liquid water (Vaz da Cruz *et al.*, 2019a).

It is advisable to illustrate one of the methods of extracting potential energy surface details using the example of RIXS from the water molecule, limited to symmetric and anti-symmetric stretching vibrations. Fig. 12 shows potential energy surfaces of the two lowest intermediate core-excited $|1s_O^{-1}4a_1^1\rangle$ (dissociative) and $|1s_O^{-1}2b_2^1\rangle$ (bound) states (Eckert *et al.*, 2018), selectively populated by changing the frequency $\omega$ of X-rays. The excited nuclear wave packet propagates along the individual OH bonds in the first (dissociative) case and simultaneously along both OH bonds in the second case. Since the emission transition to the core hole is determined by the projection of the wave packet onto the ground state, we have a
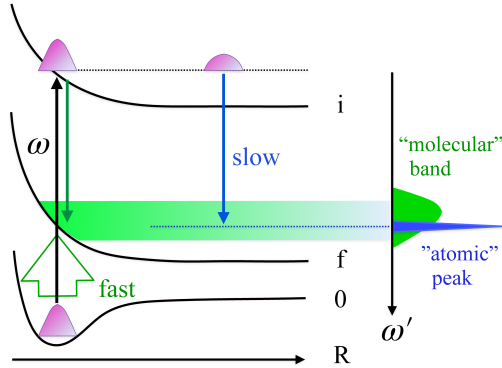
FIG. 13 Physical picture of the formation of fast ("molecular") and slow ("atomic") scattering channels. In the limit of fast scattering, RIXS corresponds to a sudden transition directly to the final state $0 \to f$ (Eq. (34)).

unique opportunity to obtain specific cuts through the potential surface along and between the OH bonds (Fig. 12) by tuning the photon frequency $\omega$ to specific intermediate states with the corresponding orientation of the potential valleys surfaces (Eckert *et al.*, 2018).

### E. RIXS and RAS under dissociation in core-excited state

Fig. 9 shows an unusual narrow resonance near $\Delta\omega \equiv \omega' - \omega = -11$ eV. The reason for this, so-called atomic peak, is emission transition in the core-excited oxygen atom in the region of dissociation of an core-excited oxygen molecule, $[O_2]^* \to O^* + O$. This phenomenon was discovered by Morin and Nenner, 1986 who studied RAS spectra of the HBr molecule core-excited into a dissociative state. To date, this effect has been observed in the RIXS and RAS spectra of many two- and polyatomic molecules (Björneholm *et al.*, 1997; Couto *et al.*, 2017; Ertan *et al.*, 2018; Fuchs *et al.*, 2008; Kimberg *et al.*, 2012; Pietzsch *et al.*, 2011; Sałek *et al.*, 2001; Vaz da Cruz *et al.*, 2019b).

As we will see below, the physical mechanism inherent in this effect served as an impetus for the discovery of new phenomena. Fig. 13 illustrates the physical picture of the process that occurs in both RIXS and RAS. The photon excites the initial wave packet $|0\rangle$ to the point of vertical transition, $R = R_0$, where the kinetic energy is zero. We see two qualitatively different peaks, narrow and wide. A wide peak corresponds to the fast decay of the intermediate state to the final one near the equilibrium distance $R_0$, where the kinetic energy is again close to zero (classical turning point) and the energy of the final state is

$E_f(R_0)$. This explains the Raman dispersion law (6) of this so-called molecular peak. The width of this peak is determined (Gel'mukhanov and Ågren, 1999) by the spatial size of the initial vibrational wave function $|0\rangle$. A narrow atomic peak is formed in the dissociation region, far from the equilibrium distance, where the potential is $E_i(R) = E_i(\infty) = \text{const}$. In this region, the decay occurs with the conservation of kinetic energy $P^2/2\mu$ (Gel'mukhanov and Ågren, 1999) and the total energy of the final state $P^2/2\mu + E_i(\infty)$ is a continuous function of nuclear momentum, $P$. As a result of integration over $P$ in the expression for the cross section, the Lorentzian responsible for the Raman dispersion (6) disappears. As a result of this, the position of the narrow resonance ceases to depend on the frequency of the initial photon $\omega$ and is equal to the frequency of the emission transition in the core-excited fragment of dissociation (in the case of RAS: $\omega' \to E$)

$$\omega' = E_i(\infty) - E_f(\infty) = \text{const}. \tag{36}$$

For the same reason, the width of the resonance is approximately equal to the natural width of the intermediate state $\Gamma$. The transitional region, where $E_i(R)$ deviates slightly from the constant also contributes to the formation of the narrow peak. Therefore, usually it's width exceeds $\Gamma$. Due to the fact that the atom is a fragment of dissociation for diatomic molecules, the name "atomic peak" is generally used. In the case of polyatomic molecules, the fragments of dissociation are not only atoms but molecules. In this case the "atomic" peak may have a vibrational structure characteristic of this fragment (Ertan *et al.*, 2018).

For the appearance of an atomic peak, time is required. This is the time of propagation of the wave packet into the region of dissociation. Consequently, the atomic peak should disappear (Sałek *et al.*, 1999) with a shorter scattering time $|\tau|$ achieved by increasing $|\Omega|$. This dynamic effect was experimentally observed in (Björneholm *et al.*, 1997; Sałek *et al.*, 2001).

## F. Dynamical interference hole

Due to the difference in dispersion law of the molecular (6) and atomic (36) peaks, these peaks can intersect at the corresponding initial photon frequency $\omega$. Quantum mechanically, the "molecular" and "atomic" scattering channels are indistinguishable, since they lead to the same final state of the continuous spectrum. Therefore, interference from these channels
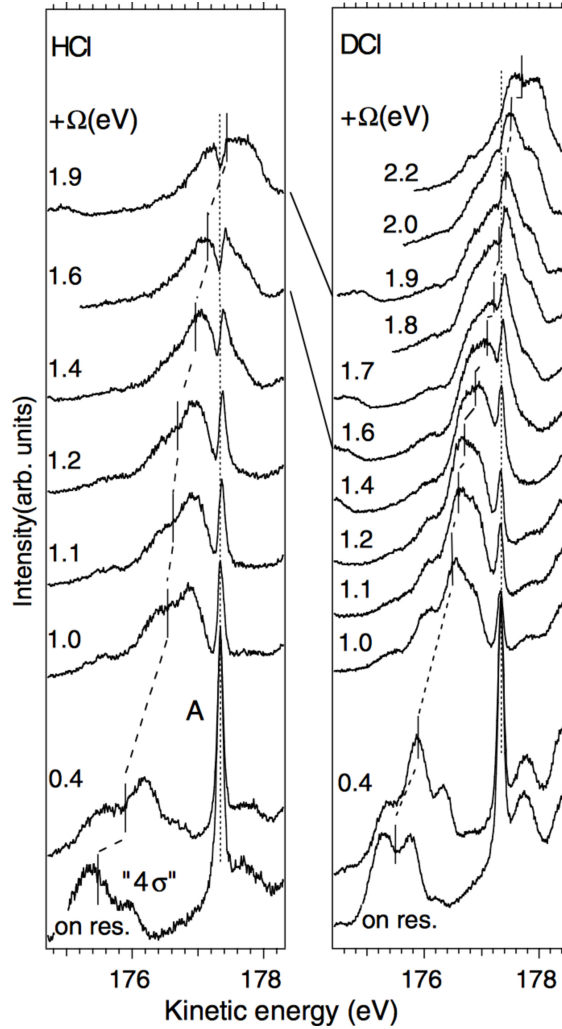
FIG. 14 RAS spectra of HCl and DCl. The spectral hole seen in HCl for $\Omega = 1.9$ eV has completely disappeared for DCl for the same detuning value in full agreement with the theoretical prediction (Sałek *et al.*, 1999). From Feifel *et al.*, 2000.

should be expected. In the case of destructive interference, a narrow dip or spectral "hole" may appear in the region of intersection of the peaks. This effect, predicted by Sałek *et al.*, 1999, was subsequently experimentally confirmed by Feifel *et al.*, 2000 in the RAS from the HCl molecule (Fig. 14), where the isotopic sensitivity clearly evidences the dynamical origin of the effect (Sałek *et al.*, 1999).

## VII. DOPPLER EFFECT CAUSED BY ULTRAFAST DISSOCIATION

The atomic peak is formed far from the equilibrium point $R_0$, where the potentials of the intermediate $E_i(R)$ and final $E_f(R)$ states are practically constant, and therefore the fragment of dissociation moves freely with the momentum $\mathbf{P}_i$ and $\mathbf{P}_f$, respectively. This allows to obtain the momentum conservation law from the FC amplitude of the Auger transition (Gel'mukhanov *et al.*, 1998a), $\langle \mathbf{P}_f | \exp(-\imath \mathbf{p} \cdot \mathbf{R}) | \mathbf{P}_i \rangle \propto \delta(\mathbf{P}_f + \mathbf{p} - \mathbf{P}_i)$. Consider a RAS of diatomic molecule in the soft X-ray region, where the small photon momentum $\mathbf{k}$ can be neglected compared to the Auger electron momentum $\mathbf{p}$:

$$k \ll p. \tag{37}$$

Applying the momentum and energy conservation laws for the transition from the intermediate core-excited to the final state, we find the energy shift of the Auger electron ($E = k^2/2$) (Gel'mukhanov *et al.*, 1998a)

$$E = \omega_{if}(\infty) + \mathcal{D} + E_{\mathrm{rec}}, \tag{38}$$

which consists of the electron Doppler shift $\mathcal{D}$ and the recoil energy $E_{\mathrm{rec}}$, experienced by the dissociation fragment when the Auger electron leaves it

$$\mathcal{D} = \mathbf{p} \cdot \mathbf{v}, \quad E_{\mathrm{rec}} = \frac{p^2}{2\mu}. \tag{39}$$

Here $\omega_{if}(\infty) = E_i(\infty) - E_f(\infty)$ is the transition energy and $\mathbf{v} = \mathbf{P}_f/\mu$ is the fragment velocity in the final state. We neglect here the small recoil energy. Taking into account the kinetic energy released upon the dissociation $\Delta E = \mu v^2/2 \sim 5$ eV, we obtain for atoms of the oxygen type $\mathcal{D} \sim 1$ eV, which is more than an order of magnitude greater Doppler broadening due to thermal motion. This makes the effect easily observable (Gel'mukhanov *et al.*, 1998a), at least by measuring the broadening of the atomic peak.

### A. Doppler splitting of RAS resonance

There is an elegant way to visualize the effect under discussion (Björneholm *et al.*, 2000). To do this, remember that the probability of excitation of a molecule is highly anisotropic

$$\sigma_{\mathrm{abs}} \propto (\mathbf{e} \cdot \mathbf{d}_{i0})^2 \tag{40}$$
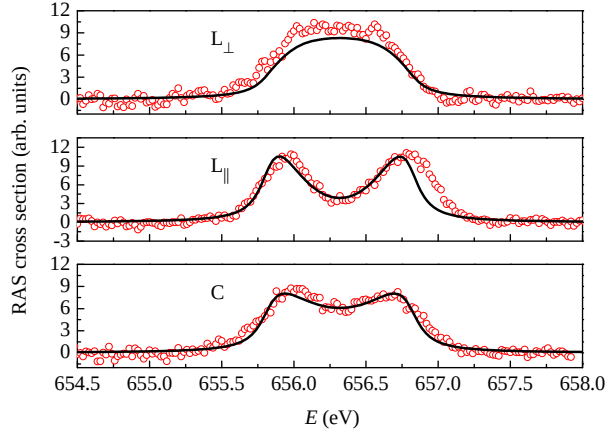
FIG. 15 Doppler splitting of the "atomic peak" in RAS from the $SF_6$ molecule. $L_\parallel$ and $L_\perp$ mark parallel ($\mathbf{e} \parallel \mathbf{k}$) and perpendicular ($\mathbf{e} \perp \mathbf{k}$) geometries for linear polarization. C: circular polarization. Circles show the experimental data. The theoretical simulations are drawn by sold lines. From Travnikova $et$ $al.$, 2010.

and it reaches a maximum when $\mathbf{d}_{i0} \parallel \mathbf{e}$. When $1s \to \sigma^*$ is excited, the dipole moment of the transition $\mathbf{d}_{i0}$ is parallel to the axis of the molecule $\mathbf{R}$ along which it dissociates. This means that the velocity $\mathbf{v}$ of the fragment is predominantly parallel or antiparallel to the polarization vector $\mathbf{e}$. Thus, half of the fragments move preferentially along $\mathbf{e}$, and the other half against.

If the electron detector is installed on the axis $\mathbf{e}$, the atomic resonance splits into two peaks with the opposite Doppler shifts: $\mathcal{D} = \pm pv$. Obviously, $\mathcal{D} \approx 0$ if the momentum of Auger electron $\mathbf{p}$ is perpendicular to $\mathbf{e}$. Experimental data (Travnikova $et$ $al.$, 2010) on Fig. 15 perfectly illustrates the Doppler splitting at $\mathbf{p} \parallel \mathbf{e}$ and its absence if $\mathbf{p} \perp \mathbf{e}$ for the RAS of the $SF_6$ molecule when $\omega$ is tuned to the $F1s \to a_{1g}^*$ dissociative resonance (688 eV). The Doppler splitting was observed also for the circular polarized light when the Auger electron was detected in the polarization plane (Travnikova $et$ $al.$, 2010).

It is necessary to explain why Doppler splitting was not observed in RIXS. The main reason is the small momentum of the photon (37), which makes the photon Doppler shift negligible as compared to the width of the atomic peak and the electronic Doppler shift, $kv \ll pv \sim 1$ eV.

The effect of Doppler splitting has been identified in a few applications. Doppler Auger splitting of the atomic peak confirmed in RAS experiments with molecules $O_2$ (Baev $et$ $al.$, 2002; Björneholm $et$ $al.$, 2000), CO (Sorensen $et$ $al.$, 2007), $O_3$ (Rosenqvist $et$ $al.$, 2001),

36
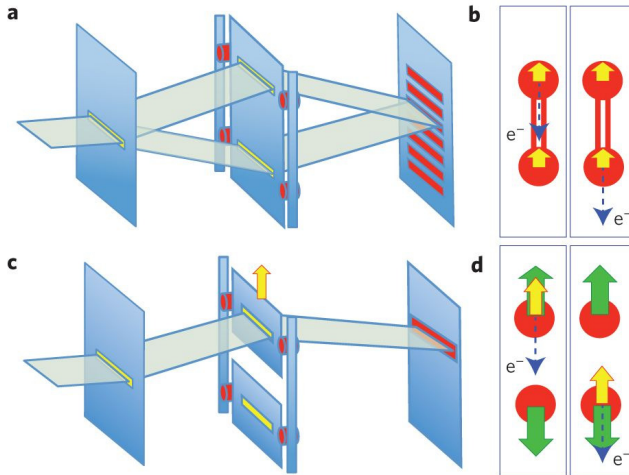
FIG. 16 Analogy of the YDSE experiment with macroscopic slits and RAS implementation of the YDSE experiment with fixed-in-space oxygen molecules. The RAS experiment was performed with oriented molecules by simultaneously detecting the electron and the cation $O^+$ using the coincidence technique. From Liu *et al.*, 2015.

CF$_4$ (Ueda *et al.*, 2003), CH$_3$F (Liu *et al.*, 2005), SF$_6$ (Kitajima *et al.*, 2003; Travnikova *et al.*, 2010). The effect unequivocally allows us to establish that the resonance under study is an atomic peak, which, in turn, unambiguously indicates dissociation in the intermediate state. The magnitude of the splitting determines an important parameter; Namely the kinetic energy released during dissociation (Björneholm, 2001). The dependence of the Doppler splitting on $\omega$ provides information on the femtosecond dynamics of dissociation (Björneholm, 2001; Kitajima *et al.*, 2003).

## B. Einstein-Bohr recoiling double-slit gedanken experiment performed at the molecular level

The Doppler effect in RAS recently allowed (Liu *et al.*, 2015) to experimentally confirm the validity of Bohr's reasoning in his discussion with Einstein about wave-particle duality in YDSE experiment on two slits (Fig. 16 a), where they discussed the question whether the measurement of the momentum exchange between the particle and the movable slit, highlighting the slit through which the particle passed, can destroy the interference structure in the YDSE (Bohr, 1983). Einstein believed that the measurement of recoil on the moving slit after the particle has passed cannot affect the process and the interference on the screen
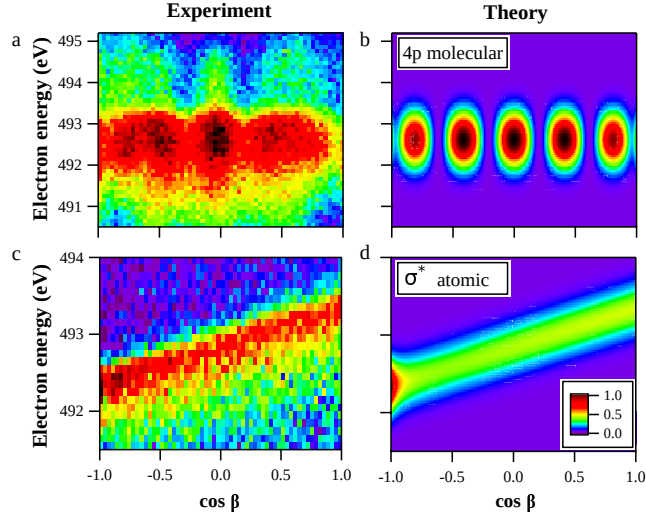
FIG. 17 The absence of the interference structure of the atomic peak upon dissociation in the $|1\sigma_g^{-1}3\sigma_u\rangle$ state (c, d), in contrast to the "rigidly bonded" atoms in the bound $|1\sigma_g^{-1}4p\sigma_u\rangle$ condition, is consistent with Bohr's conclusion. Here $\beta$ is the angle between the Auger momenta of the electron and the cation $O^+$. Adapted from Liu *et al.*, 2015.

should remain. Bohr, on the basis of the uncertainty principle, argued that this is impossible - any attempt to select the slit (particle path) leads to degradation of the interference structure (Fig. 16 c).

Two RAS channels were studied, with a bound $|1\sigma_g^{-1}4p\sigma_u\rangle$ and a dissociative $|1\sigma_g^{-1}3\sigma_u\rangle$ core-excited state, respectively. These states decay to the final state, emitting Auger electrons detected in coincidence with the product of fast dissociation in one of the final states $O^+$. The direction of cation propagation "fixes" the molecular axis. A channel with a bound state corresponds to motionless slits (Fig. 16 a, b), where the Auger electron momentum is transferred to the whole molecule (center of gravity) $O_2$. In this case, the experiment shows the interference structure $\cos(\mathbf{p}\cdot\mathbf{R}) = \cos(pR\cos\beta)$ (Fig. 17 a, b), as it should be for stationary atoms / slits. A similar structure was previously discussed for photon scattering (12). In the case of a dissociating molecule, the momentum is transmitted to a freely moving atom (mobile slit), from which the Auger electron is ejected, as shown in Fig. 16 c, d. Recall that Auger decay in a freely moving atom corresponds to an atomic peak and this atom is marked with a Doppler shift. This shift has the opposite sign for the second atom moving in the opposite direction. Fig. 17 c, d demonstrates the absence of any interference structure, which is consistent with Bohr's prediction.

## VIII. DYNAMICAL MANIFESTATIONS OF ELECTRON-VIBRATIONAL INTERACTION

In the previous sections, we investigated resonance scattering in the framework of the adiabatic BO approximation, which allows us to separate nuclear and electronic degrees of freedom. The justification for this approximation is the smallness of the electron mass in comparison with the mass of nuclei. However, instead of this rather crude criterion, one should use the strict condition of applicability of the BO approximation (Köuppel $et$ $al.$, 2007)

$$|V_{VC}| = |\langle \psi_i |V| \psi_j \rangle| \ll |E_i(R) - E_j(R)|, \tag{41}$$

where $V$ is the operator of electron-vibrational, also known as vibronic coupling (VC), or electron-phonon (in the case of a solid) interaction. This relation means that the BO approximation is completely violated if the diabatic potential surfaces intersect or are close in the region of the spectral transition. The corresponding adiabatic surfaces, computed by most conventional quantum-chemical methods, are split at the intersection point of the diabatic surfaces by a distance of $2|V_{VC}|$. According to calculations, typical magnitude of this splitting

$$2|V_{VC}| \sim \omega_0 \tag{42}$$

is comparable with the vibrational frequency $\omega_0$, which means a need to take into account electron-vibrational interaction (Köuppel $et$ $al.$, 2007) in this case. Without claiming to give a complete overview of this dynamic problem, we consider two important cases, namely, violation of the BO approximation in the intermediate and final states in soft X-ray RIXS process.

### A. Breakdown of selection rules in RIXS

In this section, we restrict ourselves to analyzing the situation in symmetric molecules ($CO_2$, $C_2H_4$, etc.), which will also allow us to understand the physics of the phenomenon in crystals. Omitting the details of the theory, which is described in the literature (Cesar $et$ $al.$, 1997; Gel'mukhanov $et$ $al.$, 1997b; Hennies $et$ $al.$, 2007; Köuppel $et$ $al.$, 2007; Privalov $et$ $al.$, 1999), we will only focus on the physical picture of the phenomenon, considering RIXS in the planar symmetric $C_2H_4$ ethylene molecule with gerade ground state $|^1A_g\rangle$ (Hennies
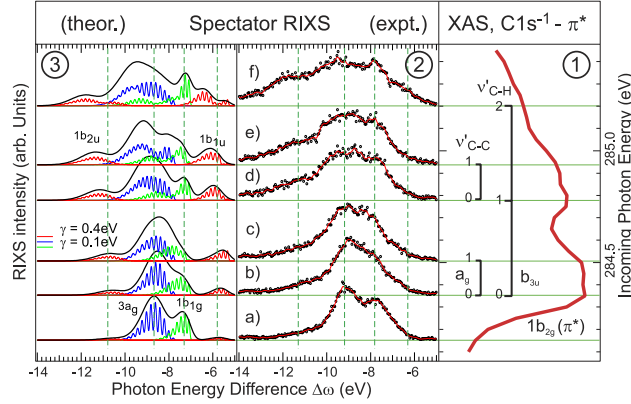
FIG. 18 Restoration of the selection rules in RIXS of the $C_2H_4$ molecule for $C1s \rightarrow 1b_{2g}$ core excitation (Hennies *et al.*, 2007, 2005), $\Delta\omega = \omega' - \omega$. RIXS to the final (forbidden by symmetry) ungerade states $|1b_{2u}^{-1}1b_{2g}^1\rangle$ and $|1b_{1u}^{-1}1b_{2g}^1\rangle$ becomes forbidden under shortening the scattering duration $|\tau|$ by increasing the detuning $|\Omega|$. From Hennies *et al.*, 2005.

*et al.*, 2007, 2005). The excitation photon frequency $\omega$ is set near the resonance with the transition of the carbon $1s$ electron to the first unoccupied MO $1b_{2g}(\pi^*)$. Let us consider the emission transitions from the first occupied MOs $1b_{1u}$, $1b_{1g}$, $3a_g$ and $1b_{2u}$, taking into account that due to the weak interaction of $1s$ electrons localized at different carbon atoms, the $1s$ shell is only slightly split $(2|V_{VC}| < 0.1 \text{ eV})$ to gerade $1a_g$ and ungerade $1b_{3u}$ levels. Applying the dipole selection rules to the absorption and emission processes and ignoring the nuclear vibrations for a while, we obtain the following allowed transition for RIXS

$$\omega + |^1A_g\rangle \rightarrow |1b_{3u}^{-1}1b_{2g}^1\rangle \rightarrow \begin{cases} |1b_{1g}^{-1}1b_{2g}^1\rangle \\ |3a_g^{-1}1b_{2g}^1\rangle. \end{cases} \tag{43}$$

Scattering into ungerade final states $|1b_{2u}^{-1}1b_{2g}^1\rangle$ and $|1b_{1u}^{-1}1b_{2g}^1\rangle$ is prohibited. We now take into account the antisymmetric C-H stretch vibration $b_{3u}$. During this vibration, a periodic symmetry breaking occurs, which obviously mixes intermediate states of opposite parity

$$|\psi\rangle = a|1b_{3u}^{-1}1b_{2g}^1\rangle + b|1a_g^{-1}1b_{2g}^1\rangle, \tag{44}$$

thereby periodically creating a hole in the $1a_g$ shell, and therefore, opening the forbidden decay channels to a ungerade final states $|1a_g^{-1}1b_{2g}^1\rangle \rightarrow |1b_{2u}^{-1}1b_{2g}^1\rangle$ and $|1a_g^{-1}1b_{2g}^1\rangle \rightarrow |1b_{1u}^{-1}1b_{2g}^1\rangle$ (see Fig. 18).

40
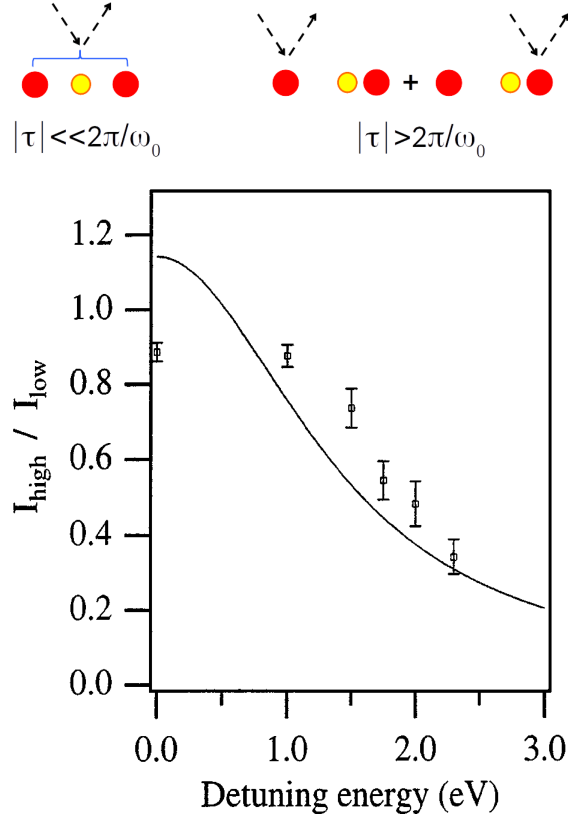
FIG. 19 A decrease in the relative intensity of the symmetry-forbidden peak $|1\pi_g^{-1}2\pi_u^1\rangle$ in the RIXS of the $CO_2$ molecule. Upper panel illustrates symmetry breaking in the course of the vibration. Adapted from Skytt *et al.*, 1996.

## B. Dynamical restoration of selection rules

The described dynamic symmetry breaking takes time. Indeed, a violation of the symmetry will occur as a result of the symmetry breaking vibration, which is characterized by a period of vibration, $2\pi/\omega_0$. Obviously, symmetry breaking will not occur if the scattering duration (27) $|\tau|$ is shorter than $2\pi/\omega_0$. Considering the dependence (27) $|\tau|$ on the detuning $\Omega$, we should expect a violation of the selection rules at $\Omega \approx 0$ and their restoration with increasing $|\Omega|$ ($|\tau| < 2\pi/\omega_0$) (Cesar *et al.*, 1997; Gel'mukhanov *et al.*, 1997b; Privalov *et al.*, 1999).

Given qualitative picture of the phenomenon explains the results of RIXS experiments with the ethylene (Hennies *et al.*, 2007, 2005) and $CO_2$ (Cesar *et al.*, 1997; Maganas *et al.*, 2014; Skytt *et al.*, 1996; Söderström *et al.*, 2020) molecules, presented in Fig. 18 and Fig. 19, respectively, as well as RIXS experiments with benzene (Hennies *et al.*, 2007) molecule and

crystalline silicon (Shin *et al.*, 1996) and graphite (Harada *et al.*, 2004).

## C. Electron-vibrational interaction in the final states of RIXS

In the previous Sec. VIII.B, the mixing of electronic states in symmetric systems by exclusively electron-vibrational interaction was considered. In most cases, the diabatic Hartree-Fock (HF) electronic states of $\psi_i^{\mathrm{el}}$ are mixed by the Coulomb interaction $V_{ij}$. The effect of such a mixing of close-lying configurations

$$\Psi(R, r, t) = \sum_i \psi_i(R, t) \psi_i^{\mathrm{el}}(r) \tag{45}$$

may be important in both the intermediate and final state (Ekholm *et al.*, 2020; Vaz da Cruz *et al.*, 2019b). Obviously, the mixing of the electronic states with different potential energy curves $E_i(R)$, strongly affects the electron-vibrational spectrum, since the nuclear wave packet propagating near the crossing of the diabatic states $E_i(R)$ and $E_j(R)$ jumps between the PECs according to the equations

$$i\frac{\partial \psi_i}{\partial t} = \sum_j h_{ij} \psi_i, \tag{46}$$

$$h_{ij} = \delta_{ij} \left( -\frac{d^2}{dR^2} + E_i(R) \right) + (1 - \delta_{ij}) V_{ij}.$$

This can be demonstrated in RIXS from the CO molecule ($X^1\Sigma^+[1\sigma^1 2\sigma^2 3\sigma^2 1\pi^4 5\sigma^2]$) with scattering through the intermediate $O1s^{-1}$ state $|1\sigma^{-1}2\pi^1\rangle$. Here the strong state mixing happens in the final states manifold (Couto *et al.*, 2016a,b) due to the intersection of PECs of $E^1\Pi(5\sigma^{-1}3p_\pi^1)$ and $G^1\Pi(5\sigma^{-1}3d_\pi^1)$ states with the PEC of the state $E'^1\Pi(4\sigma^{-1}2\pi^1)$ (Fig. 20). In the HF approximation, only the one-electron emission transition $|1\sigma^{-1}2\pi^1\rangle \rightarrow E'$ is allowed, while the two-electron transitions $|1\sigma^{-1}2\pi^1\rangle \rightarrow E$ and $|1\sigma^{-1}2\pi^1\rangle \rightarrow G$ are forbidden. The admixture of the $E'$ allowed state to the $E$ and $G$ states opens these forbidden RIXS channels. Calculations using the wave packet technique (26, 46) reproduce the experimental data (Fig. 21).

## IX. VIBRATIONAL SCATTERING ANISOTROPY

In Sec. VII.A we discussed the Doppler splitting of the atomic peak in RAS, that shows abnormally strong sensitivity of the nuclear dynamics to the polarization of incoming radia-
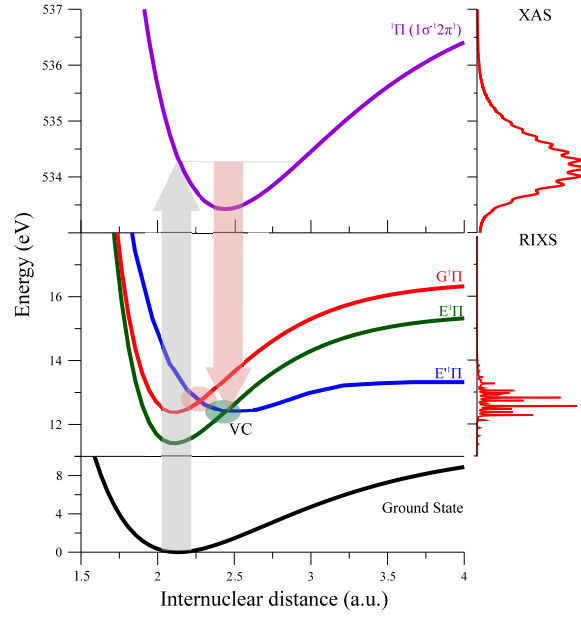
FIG. 20 Potential energy curves of the ground, core-excited $O1s^{-1}2\pi^1$ and final valence-excited states of CO. XAS and RIXS spectra are shown at the right panel. Adapted from Couto *et al.*, 2016b.
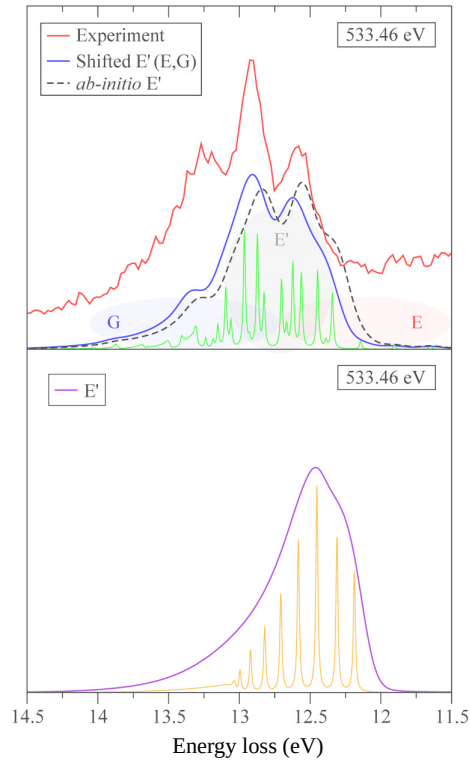


FIG. 21 The experimental and theoretical RIXS spectra of CO vs energy loss $\omega - \omega'$. Lower panel shows the RIXS profile computed without accounting for the VC between the final states. Adapted from Couto *et al.*, 2016b.

43
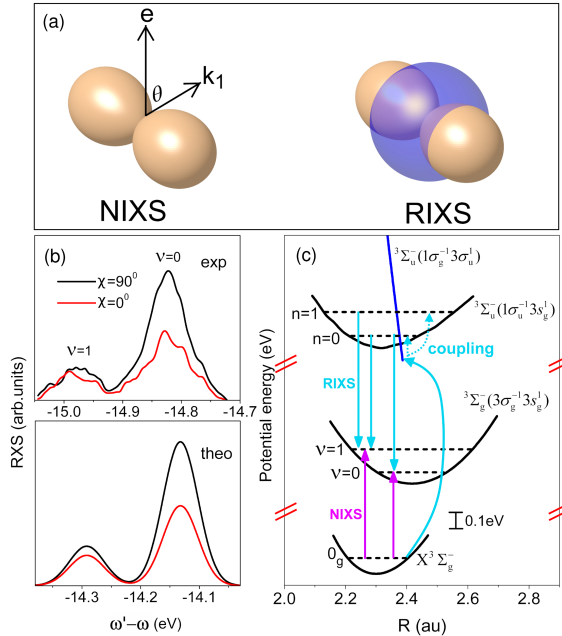
FIG. 22 The interference of the Thomson and resonance scattering channels in $O_2$ leads to a different polarization dependence of the vibrational resonances $\nu = 0$ and $\nu = 1$. Adapted from Sun *et al.*, 2013.

tion. Naturally the question arises: Does the form of the vibrational progression of RIXS and RAS depend on polarization? The first impression is that the answer is negative. Indeed, in the framework of the BO approximation the nuclear and electronic degrees of freedom are separated, providing that the polarization dependence, which affects only the amplitudes of the electronic transitions, enters as just a prefactor for the vibrational part of the scattering amplitude (21), if the $R$-dependence of these transition amplitudes is neglected. Apparently, the polarization dependence of a vibrational progression appears when the BO approximation is violated and electronic states of different symmetries are mixed (see VIII.A), giving rise to the phenomenon of vibrational scattering anisotropy (VSA).

Let us consider two qualitatively different cases that demonstrate a strong dependence of the vibrational progression on polarization in the RIXS (Sun *et al.*, 2013) and RAS (Miron *et al.*, 2010) spectra.

## A. Interference of resonant and Thomson inelastic scattering channels

In the soft X-ray range, Thomson scattering (2) is associated with an elastic peak ($\nu_f = 0$). For elastic scattering, the Thomson term, proportional to the number of electrons $\propto N$, far

exceeds the contribution of resonance scattering (Pietzsch *et al.*, 2011). The first term in the expansion of the Thomson amplitude ($\exp(\imath \mathbf{q} \cdot \mathbf{r}) \approx 1 + \imath \mathbf{q} \cdot \mathbf{r}$) opens an inelastic Thomson channel through a dipole transition, known in the hard X-ray region as Compton scattering (Hämäläinen and Manninen, 2001). Nevertheless, the amplitude of Thomson inelastic scattering or non-resonant inelastic X-ray scattering (NIXS), being $N$ times smaller than the amplitude of elastic scattering, becomes comparable with the amplitude of the resonant term (2), thereby making the interference of these channels significant, as experimentally found in the RIXS from $O_2$ (Sun *et al.*, 2013). In this experiment, the incoming X-ray photon resonantly populated the dissociative intermediate state $X^3\Sigma_g^- \rightarrow^3 \Sigma_u^-(1\sigma_g^{-1}3\sigma_u^1)$. Then, due to the electron-vibrational interaction, the molecule jumps to the bound state $^3\Sigma_u^-(1\sigma_u^{-1}3s_g^1)$, from which the radiative decay to the final state $^3\Sigma_g^-(3\sigma_g^{-1}3s_g^1)$ takes place. Besides the RIXS channel (Fig. 22c), the same final state can be populated by the direct dipole transition $X^3\Sigma_g^- \rightarrow^3 \Sigma_g^-(3\sigma_g^{-1}3s_g^1)$ from the ground state by the Thomson inelastic scattering channel (NIXS). Taking into account different scattering anisotropy in NIXS ($\propto \sin^2\chi$) and in RIXS ($\propto 1 + \sin^2\chi$) (Fig. 22a) and different FC amplitudes of direct $\langle 0|\nu_f\rangle$ and resonant $\langle 0|\nu_i\rangle\langle\nu_i|\nu_f\rangle$ channels, it is possible to understand the dependence of the relative intensities of the vibrational resonances $\nu = 0$ and $\nu = 1$ on the scattering angle $\chi = \angle(\mathbf{k}', \mathbf{e})$ (Fig. 22b).

The contribution of Thomson scattering to the elastic peak was studied for acetone (Sun *et al.*, 2011a) and oxygen molecule (Pietzsch *et al.*, 2011). In Ref. (Carniato *et al.*, 2012), interference of the elastic Thomson and resonance channels in Cl K-edge RIXS of the HCl molecule was found.

## B. Interference of direct and resonant ionization scattering channels in RAS

Let us now consider the second mechanism of VSA, observed in RAS (Miron *et al.*, 2010) from the acetylene molecule $C_2H_2$ near the $1\sigma_u \rightarrow 1\pi_g$ absorption resonance. X-ray excitation of the intermediate state $1\sigma_u^{-1}1\pi_g^1$ is accompanied by the subsequent Auger decay to the final state $1\pi_u^{-1}\psi_{\mathbf{k}}^1$. The final electronic state can also be reached by the direct ionization of the valence electron $1\pi_u \rightarrow \psi_{\mathbf{k}}$. Different orientations of the dipole moments of the interfering resonant and direct ionization channels explains the difference in polarization dependence of these channels (see Eq. (4)). In turn, different FC amplitudes of the direct
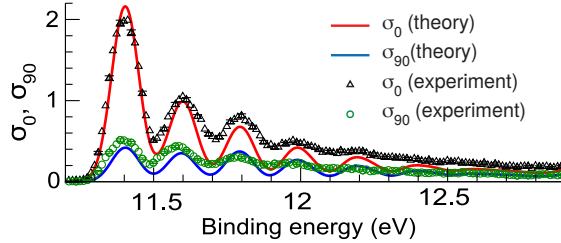
FIG. 23 The interference of the direct and resonant scattering channels leads to a different polarization dependence of the vibrational resonances – the VSA effect – in RAS from the acetylene molecule $C_2H_2$. Adapted from Miron *et al.*, 2010.

and resonant channels (see the previous section) lead to a strong change of vibrational progression in RAS measured for difference angle between the X-ray polarization vector and the photoelectron moment, $\angle(\mathbf{e}, \mathbf{k}) = 0°$ and $90°$ (see Fig. 23).

Difference in the anisotropy parameters for different final vibrational states was observed in RAS experiments with NO (Demekhin *et al.*, 2010a,b) and CO (Demekhin *et al.*, 2010c) molecules. This was quantitatively described taking into account the LVI interference as well as the interference of the direct and resonant ionization channels. For N K ionization of $N_2O$, another mechanism, caused by non-Frank-Condon transitions near shape resonances, is active for the polarization dependence of the vibrational progression (Lucchese *et al.*, 2007).

## C. Recoil-induced inelastic Thomson scattering

In the hard X-ray region the recoil effect opens inelastic channel in the Thomson scattering amplitude. As we mention already (Sec. IX.A) the momentum exchange between the hard X-ray photon and electrons results in the Compton scattering. The momentum exchange between photon and phonons results in a phonon band near the elastic peak. Thomson scattering $S(\mathbf{q}, \omega - \omega')$ (2), playing a dominant role in the non-resonant scattering, is a powerful phonon research tool. In studies of cuprates (Blackburn *et al.*, 2013; Le Tacon *et al.*, 2014) it was possible to resolve low-energy phonons (Fig. 24), due to the ultrahigh spectral resolution ($\sim 1$ meV) for X-ray photons with energy 23.7 keV. This enabled measurements of their temperature dependence in the dispersion in the temperature range $T = 5 - 150$ K in the high-temperature superconductor $YBa_2Cu_3O_{6.6}$.
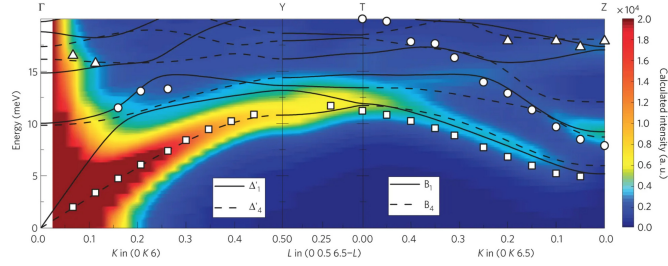
FIG. 24 Phonon dispersion along the lines of high symmetry of a superconductor YBa$_2$Cu$_3$O$_{6.6}$: Γ-Y, Y-T T-Z (T≈ 300 K). White symbols - momentum resolved RIXS experiment, color map and lines - density functional theory (DFT) calculation. Adapted by permission from Springer Nature Customer Service Centre GmbH: Le Tacon *et al.*, 2014.
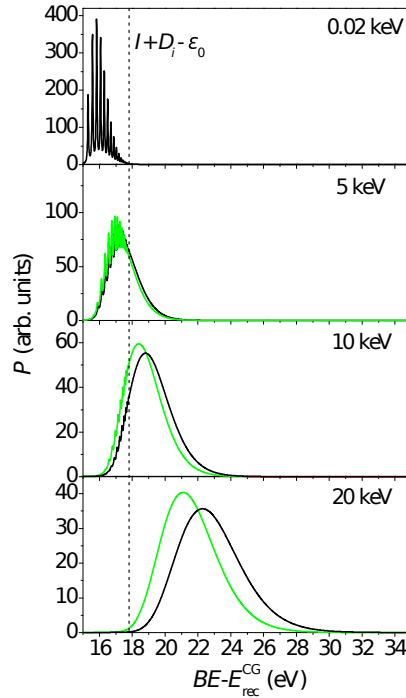


FIG. 25 Photoelectron spectrum of the H$_2$ molecule for $\omega$ =0.02, 10, and 20 keV . Binding energy $BE = E - \omega$, $E_{\mathrm{rec}}^{CG}$ is the recoil energy of the center of gravity. Green (grey) and black lines correspond to the angle between momenta of the photon and photoelectron 90° and 145°, respectively. The vertical dashed line marks the dissociation threshold. Adapted from Liu *et al.*, 2019b.

## D. Recoil induced Doppler splitting

The degree of manifestation of the recoil effect is determined by the momenta of the photon and photoelectron. In the soft X-ray range, the role of the photon momentum in the recoil is small. This explains why the recoil effect in this area is studied mainly by means
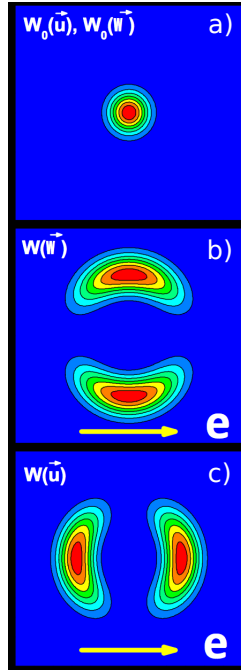
FIG. 26 Distributions over velocities (c) and angular velocities (b) induced by recoil from ejected fast photoelectron. The panel (a) shows the initial Boltzmann distribution. Adapted from Céolin *et al.*, 2019.

of photoelectron spectroscopy. Significant attention in X-ray photoelectron spectroscopy is payed to the recoil-induced excitation of vibrations in free molecules (Domcke and Cederbaum, 1978; Felicíssimo *et al.*, 2005; Gel'mukhanov *et al.*, 2007; Kukk *et al.*, 2018; Liu *et al.*, 2019b, 2006; Suga *et al.*, 2009; Ueda *et al.*, 2009, 2006) and phonons in solids (Takata *et al.*, 2008, 2007) accompanied by corresponding shift of the center of gravity of the photoelectron line. Calculations show (Liu *et al.*, 2019b) that the contributions of the photon and electron momenta are balanced in the hard X-ray range, $\omega \gtrsim 10$ keV. One of the most striking manifestations of the photonic recoil effect is the Compton effect (Hämäläinen and Manninen, 2001; Kane, 1992) (see Sec. IX.A). Below, we will discuss a recent development in studies devoted to the excitation of rotational degrees of freedom (Thomas *et al.*, 2009). To get a general idea of the role of the recoil effect in the motion of nuclei, let us take a look at the photoelectron spectrum of the $H_2$ molecule in a wide energy range (Liu *et al.*, 2019b). Fig. 25 shows that the recoil effect not only leads to the excitation of vibrations, but also to the dissociation of the molecule, when the recoil energy exceeds the dissociation energy $D_i$.

## X. RECOIL EFFECT: TRANSLATIONAL AND ROTATIONAL MOTION

In the previous sections, we showed that the momenta of photons and Auger electrons can lead to specific effects. Here we will focus on the Auger process after photoionization by the initial photon. We will investigate the role of recoil by the emitted photoelectron, which obviously affects the initial state of the Auger decay.

### A. Preparation of initial state for Auger decay

One can consider RIXS and RAS as experiments with an intrinsic pump-probe character, where the incoming photon pumps the system and the emitted photon or Auger electron probes it.

If the photon energy is much larger than the $1s$ ionization potential $(I)$ of the atom, a fast photoelectron with a momentum $\mathbf{p}_i$ is ejected. As a result of the recoil, the atom acquires momentum $\mathbf{p}_{\mathrm{at}} \approx -\mathbf{p}_i$, which far exceeds the thermal momentum $\bar{p}_{\mathrm{at}} = M\bar{v}_{\mathrm{at}} = \sqrt{2k_B T}$. Probability of $1s$ ionization

$$\sigma_{\mathrm{ion}} \propto |\mathbf{e} \cdot \mathbf{d}_{i0}|^2 \propto |\mathbf{e} \cdot \mathbf{p}_i|^2 \tag{47}$$

reaches the maximum for photoelectrons emitted along the polarization vector $(\mathbf{p}_i \parallel \mathbf{e})$, since the dipole moment of $1s$ ionization is parallel to the momentum: $\mathbf{d}_{i0} \parallel \mathbf{p}_i$. This means that as a result of the recoil, a far from equilibrium distribution of atomic velocities (Gavrilyuk *et al.*, 2010) with two islands moving in opposite directions along $\mathbf{e}$ (see Fig. 26 c).

### B. Experimental observation of recoil induced non equilibrium distribution over velocities

The created nonequilibrium distribution can be probed using the corresponding Doppler splitting (Gavrilyuk *et al.*, 2010) of the resonance of fluorescence or Auger resonance, as was done in the Auger experiment with Ne atoms (Simon *et al.*, 2014) (Fig. 27). In latter case, the nonequilibrium distribution is probed by the Auger electron with the momentum $\mathbf{p}$, which has certain orientation with respect of $\mathbf{e}$ in angular resolved measurements. When the Auger electron is detected along the polariaation vector, $\mathbf{p} \parallel \mathbf{e}$, two islands in the velocity distribution (Fig. 26 c ) results in two peaks with opposite Doppler shifts $\mathcal{D} =$
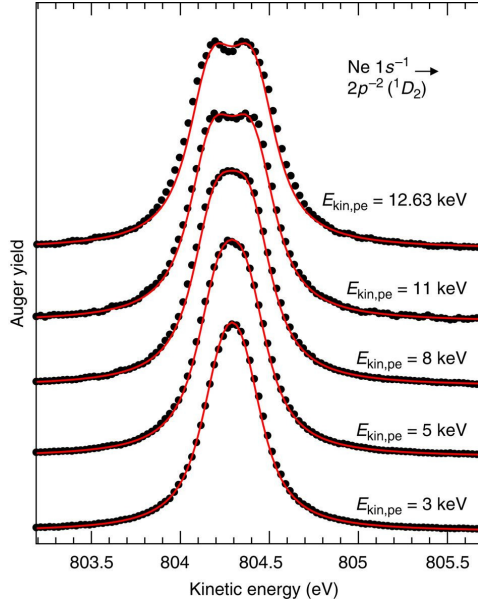
FIG. 27 Recoil-induced Doppler splitting of an Auger resonance in an Ne atom. Reprinted by permission from Springer Nature Customer Service Centre GmbH: Simon *et al.*, 2014.

$\mathbf{p}_i \cdot \mathbf{k}/M \approx \pm p_i (\mathbf{e} \cdot \mathbf{p})/M = \pm p_i p/M$. Since the Doppler splitting $2\mathcal{D} \approx 2p_i p/M$ depends on on the photoelectron momentum $p_i \propto \sqrt{\omega - I}$, the splitting increases with increasing $\omega$ in agreement with the measurements (Fig. 27).

## C. Dynamical rotational Doppler effect

Obviously, the Doppler splitting considered above should also be observed in molecules. But in molecules, in addition to the "translational" Doppler effect, as was predicted earlier there is also a rotational Doppler effect (Sun *et al.*, 2010c). The reason for this effect is that in the course of core ionization of the diatomic molecule AB, the photoelectron is ejected only from atom A where $1s$ is localized. Therefore, the recoil momentum $\mathbf{k}$ creates an angular momentum $\mathbf{j_p} = \eta[\mathbf{R} \times \mathbf{p}]$, where $\eta = M_B/M$ and $M = M_A + M_B$. Using the analogy between rotational and translational degrees of freedom, one can guess the expression for the rotational Doppler shift (Sun *et al.*, 2010c) $\mathcal{D}_{\mathrm{rot}} = \mathbf{j_p} \cdot \mathbf{w}$, where $\mathbf{w}$ is the initial angular velocity of the molecule (for example, thermal velocity). Rotational Doppler shift leads to additional broadening of X-ray photoelectron resonances, which was experimentally verified for $N_2$ (Miao *et al.*, 2015; Thomas *et al.*, 2011) and HCl (Miron *et al.*, 2014).

We now consider an Auger experiment (Céolin *et al.*, 2019) on the $CO$ molecule, in which
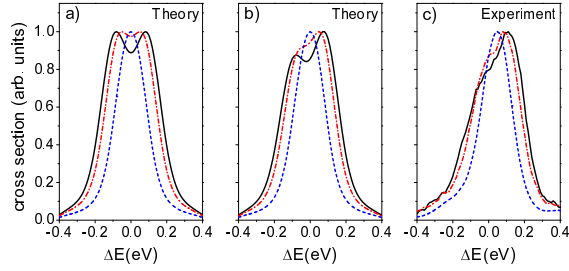
FIG. 28 The delay of Auger decay with respect to ionization leads to a change in the Doppler shift with time (48). This makes the Doppler doublet (a) asymmetric (b, c). From Céolin *et al.*, 2019.

photons with energy $\omega = 2.5$, 8 and 12 keV ionized the $1s$ electron of the carbon atom with the momentum $\mathbf{p}_i$. Due to the recoil, the molecule passed into a state of ultrafast rotation with an angular velocity $\mathbf{w} = \eta[\mathbf{R} \times \mathbf{p}_i]$. The created nonequilibrium distribution over angular velocities $w = |\mathbf{w}|$, similar to translational velocities, depends on the polarization vector $\mathbf{e}$ and has two islands as it is shown in Fig. 26 b. After a short time, the intermediate core-ionized state $i$ decays into a final state, emitting an Auger electron with a momentum $\mathbf{p}$ creating the angular momentum $\mathbf{j}_\mathbf{p}(t) = \eta[\mathbf{R}(t) \times \mathbf{p}]$. Similar to translational recoil-induced Doppler splitting one can expect similar splitting for rotational degrees of freedom into a symmetric doublet. This is the case if we assume that ionization and Auger decay happen at the same instant (see Fig. 28 a). However, there is on average a time delay ($t \approx 1/\Gamma$) between the ionization act and the Auger decay. During this delay the molecule will reorient its molecular axis $\hat{\mathbf{R}} \to \hat{\mathbf{R}}(t)$ and thereby change the Doppler shift $\mathcal{D}_{\mathrm{rot}}(t)$

$$\dot{\hat{\mathbf{R}}}(\mathbf{t}) = [\mathbf{w} \times \hat{\mathbf{R}}(\mathbf{t})], \quad \mathcal{D}_{\mathrm{rot}}(\mathbf{t}) = \mathbf{j}_\mathbf{p}(\mathbf{t}) \cdot \mathbf{w}. \tag{48}$$

This happens due to the large angular velocity $w$ imparted to the molecule by the recoil. Here $\hat{\mathbf{R}}(t)$ is the unit vector along $\mathbf{R}(t)$ at the instant $t$. The rotation of the molecular axis during the Auger process makes the rotational Doppler double asymmetric (Fig. 28 b) in full agreement with the experiment (Fig. 28 c).

## XI. RIXS OF LIQUIDS

Unlike gaseous and crystalline media considered above, a liquid is a more difficult object of study due to its inherent disorder and fluctuations of the local structure. The absence of crystalline ordering makes the diffraction peaks in X-ray and neutron scattering weaker and more diffuse than Bragg peaks in crystals (Fischer *et al.*, 2006; Sivia, 2011; Soper and

51

Ricci, 2000). For the same reason, theoretical modeling of fluids is much more complicated and less informative. For computational reasons it is also less accurate. Accordingly, more sophisticated methods of analysis of experimental data are required in order to extract useful quantitative information from them about the local structure and other properties. Therefore, the use of a set of complementary physical methods (diffraction, X-ray spectroscopy (XAS, RIXS, RAS, XPS), NMR, Raman, IR) is necessary to obtain a consistent picture of the liquid. Taking into account the main direction of the review, we will try to answer the question - Which useful information can we extract from RIXS measurements on liquids and solutions? Due to the fact that intermediate states in RIXS are created as a result of X-ray absorption, we briefly highlight the role of XAS in the study of liquids. In order for the discussion to be substantive, we consider four different fluids: acetone, water, methanol, and acetic acid.

As demonstrated in previous section, RIXS is a proper tool for studying electron-nuclear dynamics since modern spectrometers can the used to acquire RIXS spectra of liquids with vibrational resolution.

However, also previously at much lower resolution dynamical effects has been identified by comparison between valence XPS and XES (Brena *et al.*, 2004), which share the same final valence-ionized states. Furthermore, isotope substitution has been widely employed to study dynamical effects in RIXS of hydrogen bonded solutions and liquids (Blum *et al.*, 2012; Fuchs *et al.*, 2008; Jeyachandran *et al.*, 2014; Lange and Aziz, 2013; Lange *et al.*, 2011; Odelius *et al.*, 2005; Tokushima *et al.*, 2008; Weinhardt *et al.*, 2015; Yin *et al.*, 2015). The phenomenon that the introduction of ions into the water network reduces the dissociative character of the water molecules was observed in the spectator emission (Jeyachandran *et al.*, 2014; Yin *et al.*, 2015). Besides the reduction of the dissociation, also a direct influence of the ions on the electronic structure of the water molecules can be observed. The derived third spectral component (dR), associated with the water molecules which are influenced by the KCl ions, shows a spectral signature similar to the signature of intact water molecules. This again indicates that the salt ions cause a molecular reorganization of the water molecules around the ions. The recently achieved super-high resolution in RIXS opens for more detailed studies.

Due to intrinsic fluctuating disorder in liquid phase one can not use the solid state theoretical tools. Instead, the simulations of vibrationally resolved RIXS spectra of liquids

have to be carried out employing a hybrid classical-quantum approach. First, the liquid is simulated using ab initio molecular dynamics (AIMD) of a N-molecule model in periodical boundary conditions. In the second step, transition dipole moments and cuts through the potential energy surfaces along vibrational modes are sampled from the MD simulation. In a study of liquid water (Vaz da Cruz *et al.*, 2019a), the sampling was performed over molecules in a single configuration for comparison against earlier classical simulations of the core-hole dynamics (Odelius, 2009a,b). These potential energy curves are used in quantum wave packet simulations of the partial RIXS cross-sections $\sigma_k(\omega', \omega)$ for each k-th molecule in the configuration. The total RIXS cross-section is calculated as the sum over these partial contributions

$$\sigma(\omega', \omega) = \sum_{k=1}^{N} \sigma_k(\omega', \omega). \tag{49}$$

## A. RIXS of liquid acetone: Mechanisms of line broadening

Acetone is a typical representative of aprotic polar liquids with a relatively weak dipole-dipole interaction which was studied both experimental and theoretical in Ref. (Sun *et al.*, 2011a). The role of the hydrogen bond, as we will see below, is negligible for pure acetone liquid, since the C-H groups have limited hydrogen bonding capability. However, in mixed solutions of acetone with chloroform, the RIXS spectrum shows sensitivity to hydrogen bonding (Schreck *et al.*, 2016).

The acetone molecule $(CH_3)_2CO$ has 24 vibrational modes (3N-6 modes for N=10 atoms). Of these modes, as many as 8 can be considered active in RIXS and the most active modes are CO stretching, CO-out-of-plane wagging and $CH_3$ torsion modes (Sun *et al.*, 2011a). Soft intermolecular modes where neglected in the analysis (Sun *et al.*, 2011a).

The scheme of transitions and experimental RIXS spectra of liquid acetone for the $1s_O^{-1}\pi^{*1}$ core-excited state are shown in Fig. 29. The measurements displays a clearly resolved CO vibrational progression in quasielastic RIXS. However, the RIXS in the excited final state $f = n^{-1}\pi^*$ does not display vibrational structure. According to single-mode simulations of the free acetone molecule (Sun *et al.*, 2011a) here should be resolved CO vibrations. The motivates to look more carefully on the mechanism of line broadening.

First we should understand the role of the environmental broadening given by the dipole-

dipole interaction

$$\gamma_S \approx \frac{4}{3}\sqrt{\pi \ln 2}|\mu_S \Delta d_{f0}|\sqrt{\rho/a^3}, \tag{50}$$

where $\Delta d_{f0} = d_{ff} - d_{00}$, $\rho$ is the concentration of the solvent molecules. while $a$ is the radius of the solute (Weisskopf radius). This broadening is absent for quasi elastic RIXS, since $\Delta d_{f0} = 0$. More advanced calculations of the environmental broadening based on the QM/MM method (Aidas $et$ $al.$, 2011) coupled to the dynamical averaging scheme give the same broadening in neat acetone $\gamma_S^{MD}(HWHM) \approx 0.04$ eV which is not sufficient to wash out the vibrational structures in RIXS. However, it is expected that the environmental broadening for aqueous acetone ($\gamma_S^{MD} \approx 0.11$ eV, Fig. 31) will play a more important role on the spectral broadening due to the effect of the hydrogen bond between the "solute" acetone molecule and "solvent" water molecules.

However, to our surprise we discovered that the environmental inhomogeneous broadening is not the dominant source of the broadening in the lowest inelastic feature. Instead in pure acetone, the large broadening of the $n^{-1}\pi^*$ band is due to the low frequency torsion modes, i.e., to the two $CH_3$ rotors and the C O bending mode (Fig. 31). During the short lifetime of core-excited state ($\omega_{\text{tors}}/\Gamma \approx 0.14$) the methyl groups do not have time to rotate. Hence, the ground state torsion wave packet is directly transferred to the final $n^{-1}\pi^*$ state. As a result, the soft torsion modes affect only the "direct transition" $0 \to f$ characterized by the FC amplitude $\langle 0|\nu_f \rangle$. In this limit of fast scattering the dynamics of the soft modes in the intermediate state can be neglected. This is nicely confirmed by the lack of soft mode broadening in the scattering to the ground electronic state. The prediction is that the broadening of the $n^{-1}\pi^*$ band will be observed also in RIXS of gas phase acetone.

Thus, the total broadening of the profile is caused by following three different broadening mechanisms: (1) the width of incident light and instrumental broadening ($\approx$0.025 eV), (2) environmental broadening ($\approx$0.04 eV) and (3) multimode excitation including CO out-of-plane wagging mode and torsion modes ($\approx$0.075 eV). All this together results in a good agreement between the theory and the experiment (Fig. 32). One can also clearly see the narrowing of the RIXS band as a function of detuning due to the shortening of the scattering duration.
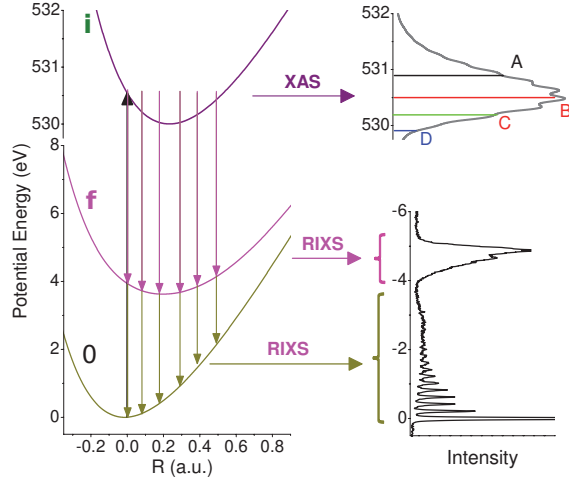
FIG. 29 Transition scheme and experimental RIXS spectrum of liquid acetone. $\omega =$529.9 (D), 530.2 (C), 530.5 (B), and 530.9 eV (A). Adapted from Sun *et al.*, 2011a.
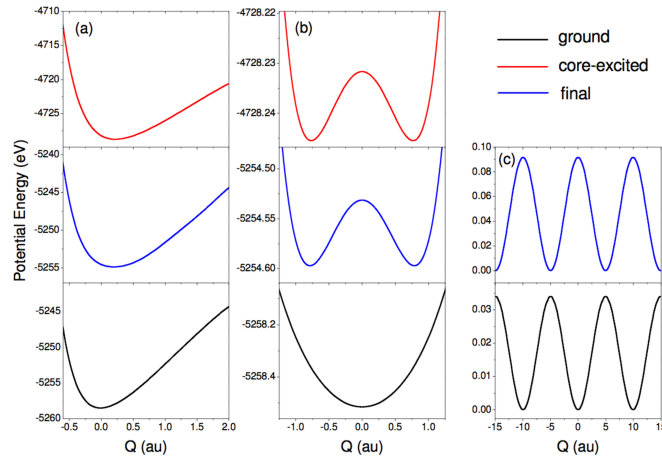


FIG. 30 The potential energy surfaces of the three most active modes. (a) CO stretching mode. (b) CO out-of-plane wagging mode. (c) $CH_3$ torsion mode. The ground (lower panels), core-excited (upper panels) and the final (middle panels) state potentials are shown; in (b) and (c) potentials are extracted from experimental UV data (Baba *et al.*, 1985).

## B. Nuclear dynamics in RIXS of free water molecules

To understand the X-ray spectra of water in liquid phase it is instructive to shed light on RIXS of water in gas phase. The water molecule has three vibrational modes: bending (b) and symmetric (s) and antisymmetric (a) stretching modes. The vibrational energy levels up to the dissociation limit of the ground electronic state of free water molecules have been studied by one- (Carleer *et al.*, 1999; Coheur *et al.*, 2002; Kassi *et al.*, 2005; Naus *et al.*,
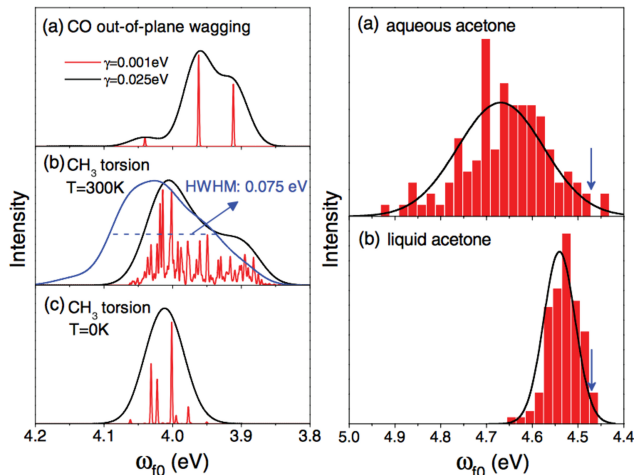
FIG. 31 The broadening mechanisms of $n^{-1}\pi^{*1}$ RIXS of the acetone spectrum. Left panel: The spectra of the "direct transition" $0 \to f$ for the CO out-of-plane wagging mode (a), torsion mode at T = 300K (b) and at T = 0K (c). The blue (thick grey) line in panel (b) displays a spectrum taking into account both modes for $\gamma = 0.025$ eV. The spectra are computed using potential energy curves shown in Fig. 30. Right panel: The distribution of transition energy $\omega_{f0}$ for pure liquid acetone (a) and aqueous acetone (b) from MD simulations. The blue arrow corresponds to the vertical transition energy for gas acetone. From Sun *et al.*, 2011a.

2001), two-(Grechko *et al.*, 2008) , an three- (Grechko *et al.*, 2009) photon IR techniques and using high-level ab initio calculations (Barletta *et al.*, 2006; Császár *et al.*, 2010; Polyansky *et al.*, 2013) to interpret the measurements. It was established that the strongly coupled symmetric and antisymmetric stretching modes can be treated independently of the bending motion.

### 1. Quasi-elastic RIXS of free water molecules

The advantage of quasi elastic RIXS is that it allows to probe highly excited vibrational levels of the electronic ground state, with a selectivity arising from the shape of the potential energy surfaces of different core-excited states. The reason for this is that the nuclear wave packet can move far away from the equilibrium in the core-excited state. This is illustrated in Fig. 33, where the PESs of the ground and first three core-excited states are presented together with the simulated X-ray absorption spectrum in Fig. 33 a. In Fig. 33 b, we notice that the bending potential is merely softened in the $|1s_O^{-1}4a_1^1\rangle$ core-excited state relative to
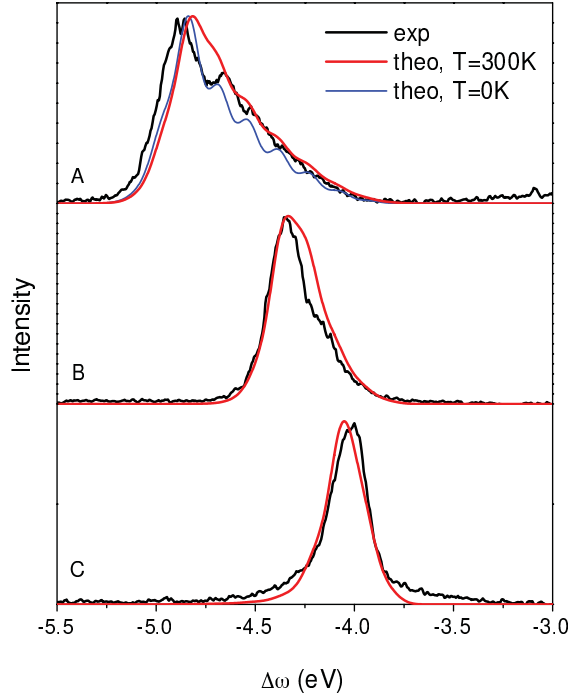
FIG. 32 The experimental and theoretical $n^{-1}\pi^{*1}$ RIXS profiles (Sun *et al.*, 2011a) of liquid acetone for excitation frequencies from Fig. 29. $\gamma$=0.025 eV. $\angle(\mathbf{k}', \mathbf{e}) = 90°$. $\Delta\omega = \omega' - \omega$. From Sun *et al.*, 2011a.

the ground state, whereas $|1s_O^{-1}2b_2^1\rangle$ and $|1s_O^{-1}2b_1^1\rangle$ exhibit an opening of the H-O-H angle. The $|1s_O^{-1}2b_1^1\rangle$ core-excited state is of Rydberg character and has a stretching potential with a shape similar to the ground state, as seen in Fig. 33 c. The $|1s_O^{-1}4a_1^1\rangle$ PES is dissociative along the individual OH bonds, whereas in the bound $|1s_O^{-1}2b_2^1\rangle$ PES there is a valley along the symmetric normal coordinate. These qualitative differences of the PESs are crucial to understand the RIXS, as it can probe the wave packet propagation in each of the core-excited states (Fig. 33).

Fig. 34 shows how vibrational modes are excited differently depending on the intermediate states. One can see how the specific direction of the propagation of the wave packet in the dissociative $|1s_O^{-1}4a_1^1\rangle$ and bound $|1s_O^{-1}2b_2^1\rangle$ states determines the vibrational structure of the stretching overtones $(\nu_s, \nu_a)$. This is observed in the experiment (Couto *et al.*, 2017) via slight shifts of the stretching vibrational peaks, although the actual fine structure is not resolved in the current experiment. As it was shown in Sec. VI.D, the state-specific high confinement of the nuclear wave packet in the core-excited state allows to reconstruct from experimental spectra 1D cuts of the ground state potential energy surface in different
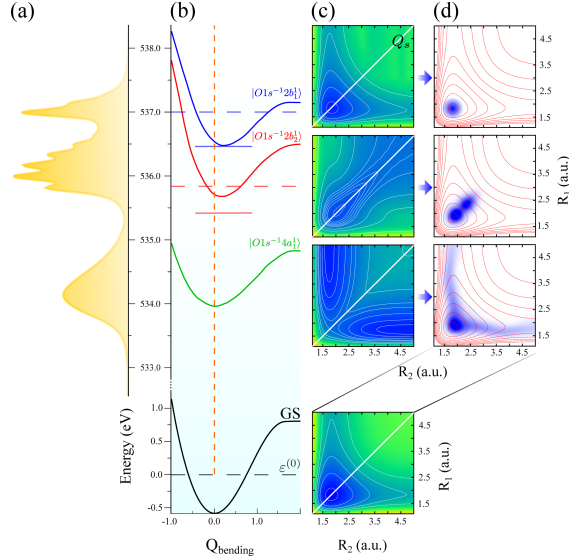
FIG. 33 X-ray absorption spectrum and potential energy surfaces of gas-phase water. (a) Simulated XAS spectrum for the three lowest core-excited states of water. (b) Potential energy curves (1D) of the bending vibrational mode for the ground (GS) and core-excited states. (c) Stretching potential energy surfaces (2D) as a function of bond lengths for the core-excited states. The color bars represent the energy range of the surfaces in eV, relative to the bottom of GS potential. Qs is the symmetric stretching coordinate. (d) The squared integral wave packet $|\Psi|^2$ for each of the core-excited states for 2D stretching motion in 2D stretching potential energy surfaces of the ground electronic state. From Couto *et al.*, 2017.

directions.

### 2. Dynamical origin of the splitting lone pair RIXS resonance in gas phase water and methanol

As it was noticed in Sec. VI.C, the potentials surfaces of core-excited and final states are very similar for decay transitions between core hole states, e.g. $K_\alpha$ RIXS in the HCl or $H_2S$ molecules. Here, we show that this situation happens also in soft X-ray region where the final state has the hole in the valence lone pair orbital. Let us consider the RIXS channels which lead to the first valence excited final state $1b_1^{-1}4a_1^1$ of the water molecule with a hole in the lone pair $1b_1$. This has been studied experimentally (Weinhardt *et al.*, 2012) and theoretically (Ertan *et al.*, 2018; Vaz da Cruz *et al.*, 2019a). As we will see below, the gas phase RIXS sheds light on the dynamical origin of the observed splitting of the lone pair resonance in liquid water ($1b_1$) (Fuchs *et al.*, 2008; Tokushima *et al.*, 2008; Vaz da Cruz
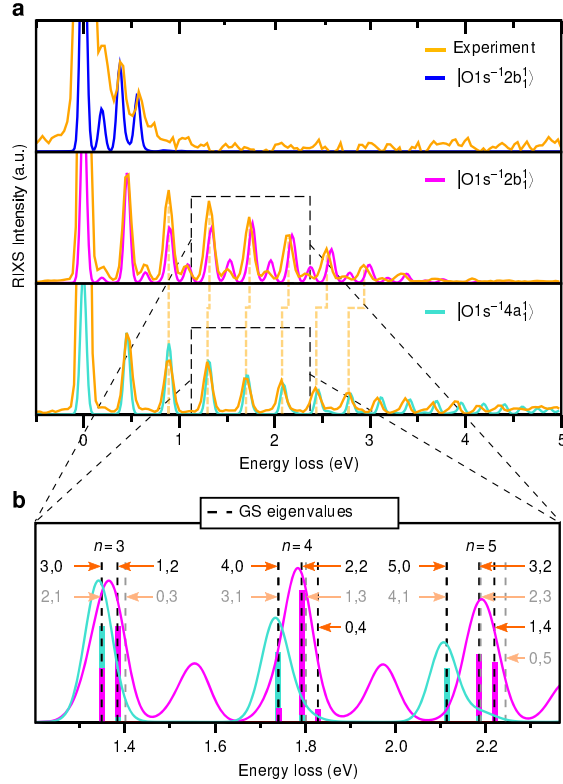
FIG. 34   a) Quasi-elastic RIXS spectra for the $|1s_O^{-1}2b_1^1\rangle$ and $|1s_O^{-1}2b_2^1\rangle$, $|1s_O^{-1}4a_1^1\rangle$ core-excited states of water molecule. b) The fine structure of RIXS caused by overtones. Adapted from Couto *et al.*, 2017.

*et al.*, 2019a) and methanol ($2a''$) (Benkert *et al.*, 2016; Schreck *et al.*, 2014; Vaz da Cruz *et al.*, 2019b).

The similar non-bonding characters of $1s_O$ and lone-pair $1b_1$ orbitals make the potential surfaces of the core-excited and final states almost parallel already at moderate distortions (see Fig. 35e). Decay transition at these distances have the same transition energy as the decay transition in the fragment of dissociation $O^*H$ in the region of dissociation. Notice that due to the small lifetime quenching of the wave packet for small propagation distances, the intensity of these transitions is significantly higher than intensity of the "atomic" peak. We name this transition "pseudo-atomic" to distinguish it from the "atomic" transition which occurs in the region of dissociation, far away from equilibrium (Sec. VI.E).

Simulations shown in Fig. 35 c explain the splitting of the $1b_1$ peak, discussed above, in terms of molecular and pseudo-atomic peaks. The dynamical origin of this splitting is confirmed by the observed (Weinhardt *et al.*, 2012) dependence of the $1b_1$ doublet on the isotope substitution. Theory nicely reproduces the isotope sensitivity (Ertan *et al.*, 2018;
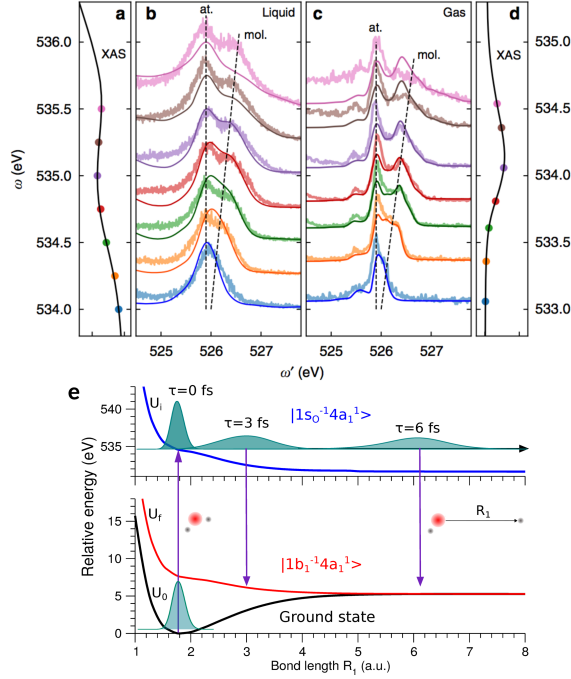
FIG. 35 Dynamical origin of the splitting of the $1b_1$ peak. Comparison of the dispersion of the split components in experimental RIXS spectra of liquid (b) and gas-phase water (c) at the pre-edge region. Solid lines in the panel b and c show theoretical spectra. Both liquid (b) and gas-phase (c) spectra display a nondispersive component (pseudo-atomic peak) and a molecular band following the Raman dispersion law. Panel (e) illustrates schematically how the pseudo-atomic peak is formed near equilibrium (R = 3 a.u.) as the PECs of the core-excited $E_i(R)$ and final $E_f(R)$ states become almost parallel: $\Delta U = E_i(R) - E_f(R) \approx const$. The splitting between molecular and pseudo-atomic peaks on top of the XAS resonance is approximately 0.45 eV. Adapted from Ertan *et al.*, 2018; Vaz da Cruz *et al.*, 2019a.

Vaz da Cruz *et al.*, 2019a).

A very similar effect was observed also for free methanol molecules (Vaz da Cruz *et al.*, 2019b) for the $|2a''^{-1}8a'^1\rangle$ final state. Simulations (Vaz da Cruz *et al.*, 2019b) explain nicely the dynamical origin of splitting of the lone-pair $2a''$ peak seen in the experiment through the sensitivity to isotope substitution (Fig. 36).

It is obvious that exactly the same phenomenon should be present in liquid phase, because both molecular and pseudo-atomic peaks are formed near the *equilibrium* distance where the influence HB surrounding on the shape of the potentials is weak (see Sec. XI.C).
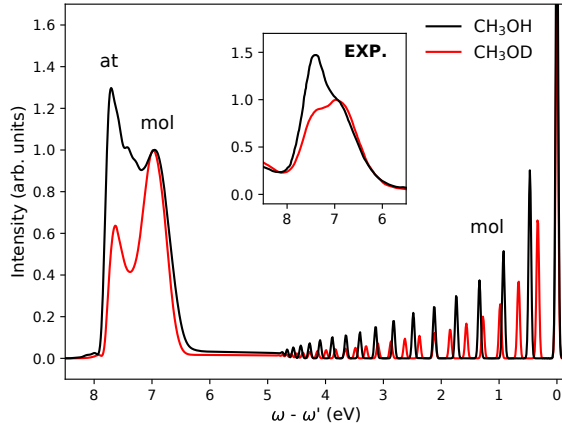
FIG. 36 Isotope effect for $2a''$ RIXS in gas phase methanol: theory and experiment. From Vaz da Cruz *et al.*, 2019b.

## C. RIXS of liquid water and methanol

Water is a highly polar liquid with strong hydrogen bonds and a number of unusual thermodynamic properties (Men'shikov *et al.*, 2020; Millot *et al.*, 2018; Palmer *et al.*, 2013). For example, unlike ordinary liquids, its density decreases at low temperatures. The anomalous behavior of water's thermodynamic response functions begins near ambient conditions and can be significantly more pronounced in the supercooled state, when liquid water becomes metastable with respect to ice. To understand the thermodynamic behavior of supercooled water the hypothesis of coexistence of low density (LDL) and high density (HDL) liquids has been invoked (Caupin and Anisimov, 2019; Röntgen, 1892).

However, it remains an experimental challenge to reach the deeply supercooled region of water (so called "no-man's land"), due to crystallization in the region of expected liquid-liquid phase transition (Palmer *et al.*, 2013; Soper and Ricci, 2000), although liquid droplet (Kim *et al.*, 2017) and thin water film (Kringle *et al.*, 2020) experiments are used to delay crystallization. Recently this problem was attacked by decompressing the high-density amorphous ice (Kim *et al.*, 2020).

### 1. RIXS vs X-ray and neutron scattering, IR, Rayleigh-Brillouin scattering and XAS

The elemental sensitivity of X-ray diffraction is determined by the dynamical structure factor of this element $S(\mathbf{q}, \omega) \propto Z$. Therefore, this method provides extremely limited information about hydrogen with $Z = 1$ (Fischer *et al.*, 2006). X-ray scattering, which is mainly

sensitive to oxygen, measures the O-O radial distribution, providing information about the first three coordination spheres. From the measurement data, it is very difficult to single out information about the O-O correlations of higher order. The situation with neutron scattering is quite similar, with the exception of hydrogen, because neutron scattering also gives the positions of the hydrogen atoms, particularly if hydrogen/deuterium isotope contrast is used (Fischer *et al.*, 2006). Both methods require theoretical modeling for accurate and reliable interpretation. Usually, classical molecular dynamics (MD) and Monte Carlo methods, possibly in combination with the Feynman quantum path integral method, are used. Modern X-ray and neutron experiments indicate that water is homogeneous under normal conditions (Clark *et al.*, 2010; Soper, 2019; Soper and Ricci, 2000; Soper *et al.*, 2010), in contrast to the rather widespread hypothesis that HDL and high LDL fractions are present in water. These diffraction experiments have recently been strengthened in experiments on the Rayleigh-Brillouin scattering of optical radiation (532 nm) (Zykova *et al.*, 2017) over the range from 249 to 365 K. The theoretical modeling also support the homogeneity of water in under stationary conditions(English and Tse, 2011). One can expect the coexistence of HDL and LDL during the phase transition liquid-ice. There is an interesting approach (Russo and Tanaka, 2014; Shia *et al.*, 2018) which support the two-state model. This theory is based on an order parameter which determines how close the nearest nonbonded molecule is to any given water molecule. However the bimodal distribution obtained here is a consequence of the way the order parameter is defined rather than representing different populations of two states of water (Soper and Ricci, 2000). In spite of this remark, the search the proper order parameter (Russo and Tanaka, 2014; Shia *et al.*, 2018) is crucial for understanding the possible liquid-liquid phase transition in water.

It should be noted that one can not infer that ambient water may be described as a mixture of two liquids (Röntgen, 1892), HDL and LDL(Nilsson and Pettersson, 2015; Wernet *et al.*, 2004) as stressed by recent re-examination of small-angle X-ray scattering (SAXS)(Clark *et al.*, 2010; Head-Gordon and Johnson, 2006; Soper, 2019; Soper and Ricci, 2000; Soper *et al.*, 2010), XAS (Chen *et al.*, 2010; Kühne and Khaliullin, 2013; Niskanen *et al.*, 2019; Sun *et al.*, 2017) and MD studies (English *et al.*, 2013; English and Tse, 2011). However, there is uninterrupted interest in supercooled water, named the no man's land (Palmer *et al.*, 2018), where one can expect the coexistence of two phases. However, no definitive experimental proof exists to date (Amann-Winkel *et al.*, 2016). Due to this, the

simulations play an important role in this area. Whether really two liquid phases have been identified in computer experiments (Palmer *et al.*, 2018; Shi and Tanaka, 2020; Smallenburg and Sciortino, 2015) or not (Chandler, 2016; English *et al.*, 2013; English and Tse, 2011; Limmer and Chandler, 2013) is currently vigorously debated.

**The X-ray absorption spectra** are used to probe properties of different liquids(Nagasaka *et al.*, 2020) and especially local structure of liquid water. Some time ago, an XAS study of liquid water (Nilsson and Pettersson, 2015; Wernet *et al.*, 2004) stirred a storm of controversy by the conclusion that a majority ($> 80\%$) of H bonds are broken in the liquid water in contrast to the conventional near-tetrahedral picture supported by diffraction(Clark *et al.*, 2010; Head-Gordon and Johnson, 2006; Soper, 2019; Soper and Ricci, 2000; Soper *et al.*, 2010), X-ray photoelectron data (Nishizawa *et al.*, 2011), thermodynamic, and spectroscopic data (Stillinger, 1980). Moreover, later higher level simulations, based on the Bethe-Salpeter equation (Chen *et al.*, 2010; Sun *et al.*, 2017), does not support the main conclusion made in Ref. (Wernet *et al.*, 2004), which also is in contradiction with MD simulations of liquid water (Chen *et al.*, 2010; Nilsson and Pettersson, 2011; Sun *et al.*, 2017) (see also Ref.(Kühne and Khaliullin, 2013)). Recently (Niskanen *et al.*, 2019), the areas of the pre-edge XAS peak ($\approx 534 - 535$ eV) of gas phase, liquid water and ice were used to attack this problem. This peak in free water molecule corresponds to the core-excitation to dissociative $1s_O^{-1}4a_1^1$ state (see Fig. 33). The comparison of areas of the pre-edge peaks for gas, liquid and ice was used to determine the average number of hydrogen bonds per molecule $N = 3.48$ for liquid water under ambient conditions (Niskanen *et al.*, 2019). This value, being very different from $N = 2.2$ (Wernet *et al.*, 2004), agrees with the X-ray and neutron scattering data (Soper and Ricci, 2000), as well as with the MD simulations (Vaz da Cruz *et al.*, 2019a).

*2. Dynamical origin of the lone-pair peak splitting in RIXS of liquid water and methanol*

The local HB environment has also been probed in electronically inelastic processes (Fuchs *et al.*, 2008; Odelius, 2009a,b; Pietzsch *et al.*, 2015; Tokushima *et al.*, 2008; Zhovtobriukh *et al.*, 2018); Decay channels for RIXS and XES in which the $1s_O$ core-hole is filled by a transition from the occupied lone-pair orbital $1b_1$. This transition forms a split peak (Fig. 35 b), which in XES of liquid water has been attributed either to two distinct ground state structural motifs (Nilsson and Pettersson, 2015; Tokushima *et al.*, 2008; Zhovtobriukh

*et al.*, 2018) or to nuclear motion after core-excitation(Ertan *et al.*, 2018; Fuchs *et al.*, 2008; Niskanen *et al.*, 2019; Odelius, 2009a,b; Pietzsch *et al.*, 2015; Vaz da Cruz *et al.*, 2019a). The importance of improved spectral resolution in RIXS and XES also for liquid measurement is striking in the gradually increased insight from the early observations of dynamical effects in XES (Odelius *et al.*, 2005), of the peak splitting in high-resolution RIXS and XES (Fuchs *et al.*, 2008) and the direct evidence of proton-dynamics in vibrationally resolved RIXS (Pietzsch *et al.*, 2015).

The experimental RIXS spectra shown in Fig. 35 b display a striking quantitative co-incidence of the $\omega$-dependence of the $1b_1$ splitting in liquid and gas phases of water. This together with the isotope effect (Fuchs *et al.*, 2008) is a clear indication that the splitting in RIXS at the pre-edge resonance is of the same dynamical origin as for the gas-phase (Ertan *et al.*, 2018) associated with the different dispersion laws of the pseudo-atomic and molecular peaks (see Sec. XI.B.2). This conclusion is also supported by simulations (Ertan *et al.*, 2018; Vaz da Cruz *et al.*, 2019a). The main idea behind of simulations is that the physical mechanism of the splitting for free water molecules is the same for the liquid water because the formation of the molecular and pseudo-atomic peaks happens near the equilibrium where the role of the HB surrounding is weak (Sec. XI.B.2).

A similar splitting is observed also in RIXS for scattering in the main- and post-edge regions and for non-resonant XES (Fuchs *et al.*, 2008; Nilsson *et al.*, 2013; Tokushima *et al.*, 2008; Yamazoe *et al.*, 2019). According to DFT-based MD simulations, the doublet in the region of the $1b_1$ peak for non-resonant excitations is related to "atomic"/"pseudo-atomic" features arising from the $3a_1$ and $1b_1$ levels, which approach each other in the course of the OH bond elongation in the core-ionized state, which as confirmed by the simulations (Odelius, 2009b), is dissociative in the local hydrogen bond environment in liquid water. It is important to notice that this splitting for higher excitation energies is absent in the gas-phase (Weinhardt *et al.*, 2012) where (contrary to liquid-phase) the OH potential is bound (Odelius, 2009a). Since both molecular and pseudo-atomic $1b_1$ peaks arise from decay near the equilibrium, the splitting under excitation into the lowest core-excited state is not sensitive to differences in HB environments (Vaz da Cruz *et al.*, 2019a). Hence, we conclude that the splitting cannot be regarded as a fingerprint of specific local structures. It is important to notice that the lone-pair $2a''$ splitting observed for liquid methanol (Schreck *et al.*, 2014) can also be described in a dynamical context (Vaz da Cruz *et al.*, 2019b) but
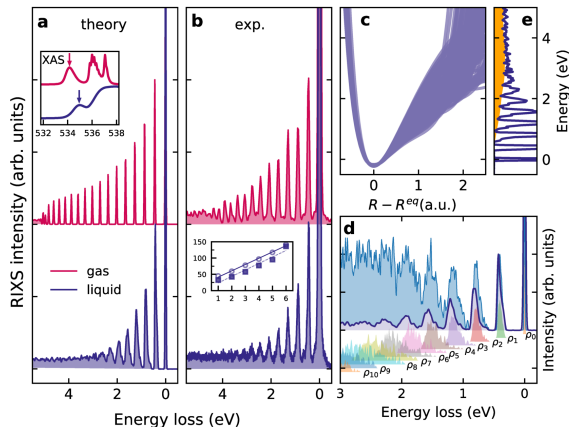
FIG. 37 Quasielastic RIXS of water in gas/liquid-phase under $4a_1$ pre-edge core-excitation. Theory takes into account only OH vibrations. From Vaz da Cruz *et al.*, 2019a.

also here there is alternative interpretation of this splitting for liquid methanol based on the two structural motives (Ljungberg *et al.*, 2017).

### 3. Role of hydrogen bond on vibrations and fluctuations of OH potential energy curves. RIXS vs IR spectroscopy

A holy grail of the RIXS of liquids is to understand the competition roles of nuclear dynamics in the core-excited state and strongly fluctuating the HB surrounding. A step toward a more detailed understanding can be taken by comparing the vibrational progression in quasielastic RIXS of gas and liquid (Fig. 37) under core-excitation in the dissociative sate. Theoretical this was achieved by determining, based on configurations from an MD simulation, the stretching potentials (OH PECs) of water molecules in different environments in the liquid, which occasionally deviate strongly from the potential of the gas phase molecule (Vaz da Cruz *et al.*, 2019a). The propagation of the nuclear wave packet results in the long vibrational progression seen in both theory and experiment. In the liquid, however, we observe a strong shortening of the vibrational progression in comparison to the gas-phase (Fig. 37 a, b). This shortening arises from variations in the OH PECs, reflecting the different local HB environments (Fig. 37 c) in liquid water. These variations affect mainly the long-range part of the OH PEC and result in a variation of the high vibrational levels, seen in the partial density of vibrational states of OH vibrations (Fig. 37 d).

RIXS provides a vibrational probe complementary to IR spectroscopy. Therefore, it is
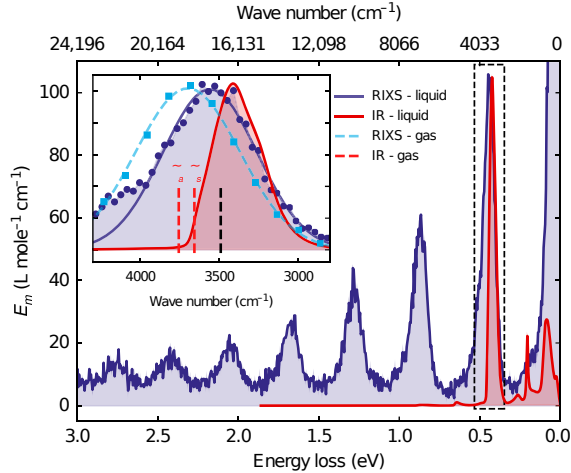
FIG. 38 Comparison of RIXS under pre-edge core-excitations and IR spectra of water in gas and liquid phases. From Vaz da Cruz *et al.*, 2019a.

pertinent to compare the RIXS and IR spectra of water (Fig. 38). Contrary to RIXS, the main contribution in IR absorption originates from the $0 \rightarrow 1$ dipole allowed OH transition (higher lying dipole forbidden IR transitions are more than two orders of magnitude smaller (Bertie and Lan, 1996)). Hence, the majority of IR studies of liquid water (Bakker and Skinner, 2010; Perakis *et al.*, 2016) has focused only on this transition, which probes the bottom of the OH potential well. However, we notice that the liquid-gas shift in IR absorption ($\approx 280 cm^{-1}$) is significantly larger than in RIXS ($\approx 140 cm^{-1}$) and the RIXS and IR peaks are shifted in opposite directions with respect to the theoretically derived maximum of the OH vibrational density of states at $\approx 3490 cm^{-1}$ (Fig. 38).

The sensitivity of IR spectroscopy to a large extent stems from the strong dependence of the IR intensity of the OH stretch on the hydrogen bond environment (Auer and Skinner, 2008; Perakis *et al.*, 2016; Yang and Skinner, 2010). The IR absorption transition dipoles of the OH stretching modes with a broken HB (located in the high-frequency region) are significantly smaller than those of hydrogen-bonded OH modes (located in the low-frequency region) (Yang and Skinner, 2010). The situation is reversed in RIXS, where the molecules with a weak/broken hydrogen bond are excited preferentially. This explains the opposite shifts of the RIXS and IR absorption resonances with respect to the maximum of the density of vibrational states (see inset in Fig. 38). Thus, IR and RIXS spectroscopy complement each other and deliver structural information already at the lowest $0 \rightarrow 1$ transition: this OH transition in IR absorption predominantly shows the existence of structures with strong
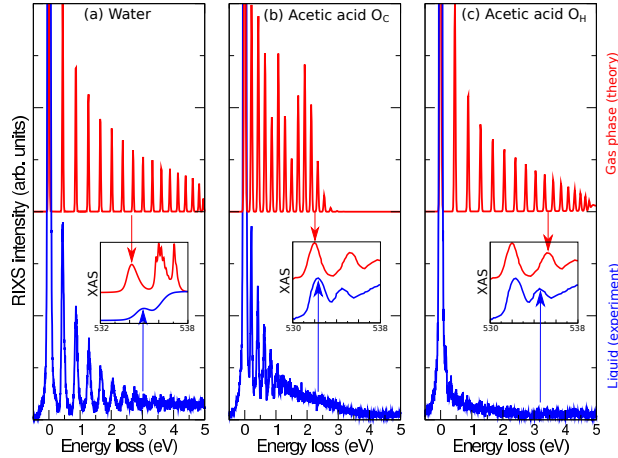
FIG. 39 Quasi-elastic RIXS of acetic acid and water. Top panels-gas phase, bottom panels - liquid. From Savchenko *et al.*, 2021.

HB contrary to RIXS where the peak position of the $0 \to 1$ transition is associated with both broken and strong HBs structures (Vaz da Cruz *et al.*, 2019a). One should mention that IR Raman spectra (Auer and Skinner, 2008; Perakis *et al.*, 2016; Yang and Skinner, 2010) show a similar trend as the IR absorption spectra.

Because of long-range nuclear dynamic in the intermediate dissociative state, OH bonds stretch into the long-range part of the potential energy curve, which makes the X-ray probe more sensitive than IR spectroscopy to the local environment. This makes the OH potential sensitive to the local surrounding and results in a broad distribution of the potentials (Fig. 37 c). One can exploit this property to effectively probe hydrogen bond strength via the distribution of intramolecular OH potentials derived from measurements (Vaz da Cruz *et al.*, 2019a). The role of soft vibrational modes (bending and intermolecular) was discussed in Refs. (Harada *et al.*, 2017; Pietzsch *et al.*, 2015; Vaz da Cruz *et al.*, 2019a).

There is a nontrivial consequence of strong sensitivity of the OH potential to the local structure (Fig. 37 c). Namely, there is not necessary (Vaz da Cruz *et al.*, 2019a) a strict one-to-one correspondence (Harada *et al.*, 2013) between the peak number in the RIXS spectrum and the actual quantum number of the vibrational state that contribute to it. The reason for this is random shifts of vibrational levels starting from $\nu = 3$ caused by the fluctuating HB network (see Fig. 3e from Vaz da Cruz *et al.*, 2019a).
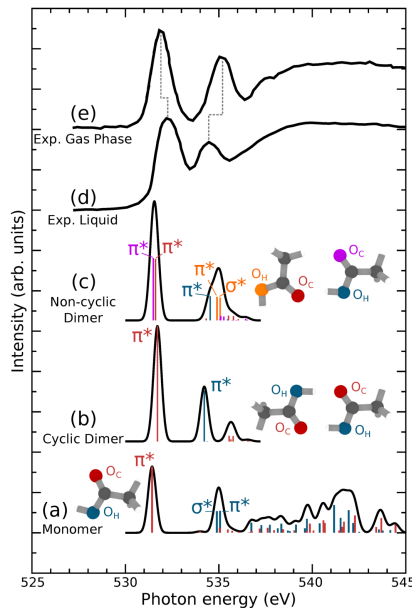
FIG. 40 Calculated XAS spectra of (a) the acetic acid monomer, (b) regular dimer and (c) inverted dimer, showed in comparison to measured XAS spectra of (d) acetic acid liquid from Ref. (Tokushima *et al.*, 2009) and (e) gas phase from Ref. (Robin *et al.*, 1988). The calculated oscillator strengths are shown as bar graphs, where each bar is colored according to the atom of origin depicted in the molecular structure next to each spectrum. Adapted from Savchenko *et al.*, 2021.

## D. Anomalous role of hydrogen bond on RIXS of liquid acetic acid

Carboxylic acids have received a lot of experimental and theoretical interest over more than a century. The local structure of liquid ACA is more complex and is still heavily debated (see Ref. (Savchenko *et al.*, 2021) and references therein). Recent RIXS measurements of liquid acetic acid (ACA) and simulations (Savchenko *et al.*, 2021) show the absence of a vibrational progression of the OH stretch mode under pre-edge core-excitation of the hydroxyl oxygen contrary to liquid water and methanol (see Sec. XI.C). This behavior was attributed to an unusually strong influence of the HB, which changes the character of the intermediate state, and quenches the vibrational progression in RIXS (Savchenko *et al.*, 2021). To understand this effect let us look on two distinct dimers, namely the regular dimer (centrosymmetric cyclic dimer, which also exist in the gas phase) and the inverted dimer (asymmetric noncyclic dimer which is the shortest representative of the chain present in the liquid). Calculations show that only "in" OH groups are affected by HB: The $1s_{O_H}^{-1}\sigma^*$

dissociative core-excited state (only which leads to the long OH vibrational progression in RIXS) does not contribute at all in the 535-eV peak in the XAS (Fig. 40). This effect allowed to put an upper limit to the average concentration of "end" OH groups in the liquid ACA that are not strongly involved in HBs, implying that the average length of chains must be larger than 3 and/or there must be a significant abundance of cyclic structures (Savchenko *et al.*, 2021).

## XII. RIXS IN STUDIES OF CORRELATED MATERIALS

The elementary excitations in solids (van den Brink, 2016) span a broad range of physical processes from charge-transfer (CT) excitations at a 4-10 eV, metal centered dd excitations $\lesssim 4$ eV, and magnons ($\lesssim 0.5$ eV) down to phonons ($\sim 10 - 50$) meV at the meV scale (see also Fig. 24 and Ref.(Schlappa *et al.*, 2018)). Since the X-ray photon transfers significant momentum to the material, RIXS can measure the momentum transfer (17) dependence or dispersion of the excitation energy of these modes (Ament *et al.*, 2011; Comin and Damascelli, 2016; Dean *et al.*, 2016; Hariki *et al.*, 2020a; Le Tacon *et al.*, 2014; Schlappa *et al.*, 2012) (See Sec. V.B, Fig. 24 and below). Similar to free molecules (Sec. IV) the polarization of X-rays gives rise to new opportunities for RIXS experiments on solids. A polarization analysis of the spectral features allows to gain information on the symmetry of the excitations and therefore on their nature (Braicovich *et al.*, 2014; Hunault *et al.*, 2018; Murakami *et al.*, 1998a).

Spin waves (spinons), also referred to as magnons quasi-particles are energetically low-lying excitations of the spin lattice in crystalline materials (Doniach and Sondheimer, 1998; Faddeev and Takhtajan, 1981; Haldane, 1981; Khaliullin and Oudovenko, 1997; Kitaev, 2006). A special attention was payed to 1D (Giamarchi, 2016; Giamarchi and Press, 2004; Haldane, 1981; Voit, 1995) and 2D (Hermanns *et al.*, 2018; Kitaev, 2006) spin liquids due to unusual physical properties and because these systems can be described by possess strictly solvable models.

Systems with strongly correlated electrons, in particular, transition metal (TM) compounds, present a very interesting class of materials with extremely rich properties (Ishihara, 2017; Ishii, 2017; Kugel' and Khomskii, 1982; Streltsov and Khomskii, 2017). Among them are metals, insulators (of a special kind), and systems with metal-insulator transitions;
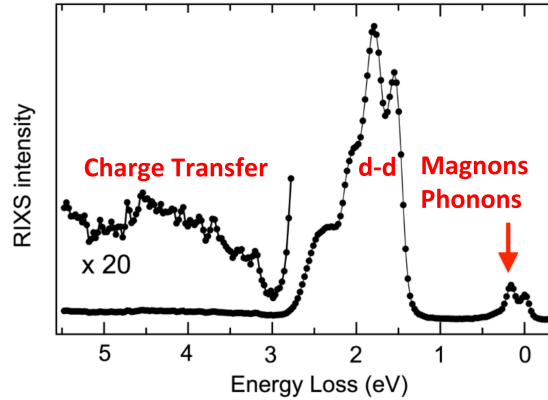
FIG. 41 The typical energy scale of elementary excitations in solids is exemplified for RIXS spectrum at the Cu $L_3$ edge of the cuprate antiferromagnet $Ba_2Cu_3O_4Cl_2$ (see also Rossi *et al.*, 2019a). The elastic peak is at energy loss $\omega - \omega' = 0$. From Fatale *et al.*, 2017.

they exhibit different types of ordering [magnetic, charge ordering (CO), orbital ordering (OO)], the cooperative Jahn-Teller (JT) effect, and high-temperature superconductivity. All this richness is mainly due to strong electron correlations and the many degrees of freedom involved in mutual interplay: charge, spin, and orbital, and all of this, of course, on the background of the lattice, with which all these electronic degrees of freedom often strongly interact.

Spin-resolved valence band excitations were also studied using magnetic circular dichroism and magnetic linear dichroism (Elnaggar *et al.*, 2020; Luo *et al.*, 1997; Miyawaki *et al.*, 2017; Yablonskikh *et al.*, 2001; Zimmermann *et al.*, 2018) in RIXS (RIXS-MCD and RIXS-MLD) using an external magnetic field for magnetisation of the sample (Elnaggar *et al.*, 2019; Magnuson *et al.*, 2006; Umetsu *et al.*, 2019).

### A. Charge transfer

Charge transfer (CT) excitations TM compounds lead to final states in which electrons are transferred between the ligand band and the $3d$ orbitals at the TM site. In particular, ligand-to-metal CT (LMCT) is frequently detected in RIXS. These excitations are typically at higher energies than the $dd$ excitations (as shown in Fig. 41), and are also inherently broader since they involve transitions involving the broad ligand band.

In the RIXS and RAS (Woicik *et al.*, 2018, 2020) studies of CT excitations in solids one uses the polarization, momentum and excitation energy dependence of the spectra. The

stage of this direction of investigations until 2010 was reviewed previously (Ament *et al.*, 2011; Rueff and Shukla, 2010). Here, we stress only the main physical processes involved.

Charge transport in solids is determined by the energetics of moving electrons from one site to another. The process in TM compounds is defined by competition between the energy of charge-transfer $\Delta_{CT} = E(d^{n+1}L^{-1}) - E(d^n)$ and the *dd* Coulomb interaction $(U = E(d^{n-1}) - E(d^n) - [E(d^n) - E(d^{n+1})])$. The later of which is associated with moving a $d$ electron from one metal site to another. Here $L^{-1}$ denotes a hole on the ligand site. This nontrivial problem was solved strictly by Zaanen et al (Zaanen *et al.*, 1985) in the framework of the single-ion Anderson model (SIAM). The SIAM approach invented by Anderson (Anderson, 1961) has been extended for the interpretation of core-level spectra (Gunnarsson and Schönhammer, 1983).

For the case of a Mott-Hubbard (MH) insulator $\Delta_{CT} > U$, the top of the valence band is composed primarily of $3d$ states, and the band gap is of a *dd* type $(U)$. For the case of a CT insulator $U > \Delta_{CT}$, the $U$ is large enough to push the occupied $3d$ states deep in the VB, meaning the top of the valence band has primarily ligand $2p$ character (see Fig. 42). The transition-metal oxides, including the cuprates, nickelates, and manganites are the CT insulators with the CT lowest optical excitations across the optical gap. According to the nonresonant X-ray emission experiment (Olalde-Velasco *et al.*, 2011) (Fig. 43 ) almost all $MF_2$ difluorides are MH insulators in an agreement with the Zaanen-Sawatzky analysis (Zaanen and Sawatzky, 1990). Fig. 43 shows a MH to CT insulator transition between CoO and NiO, leaving CuO as an obvious CT insulator.

One can identify two approaches used in simulations of RIXS: the cluster method and more accurate SIAM approach.

A widely used and computationally efficient cluster method is the semi-empirical ligand-field multiplet (LFM) model. In this atomic model (de Groot *et al.*, 1990) which takes into account spin-orbital (SO) interaction, electron correlation is accounted by a full configuration interaction (CI) including the $3d$ orbitals and by reducing of the Hartree-Fock electron-electron repulsion integrals. Ligands are described by an empirical ligand-field splitting of the $3d$ orbitals. For highly covalent complexes, the effects of CT excitations is modeled using additional configurations, where one electron has been transferred from or to the ligand. Adding these configurations to the CI gives the semi-empirical charge-transfer multiplet (CTM) model (de Groot, 2005; de Groot and Kotani, 2008; Tanaka and Jo, 1994). There

are also ab initio cluster methods (Josefsson *et al.*, 2012; Kunnus *et al.*, 2016b; Pinjari *et al.*, 2014) which offer better predictive power than semi-empirical methods, at least in principle. In the ab initio model, the basis for the CI calculations are molecular orbitals (MOs) calculated for small clusters, typically the central atom and first-shell ligands. An alternative powerful approach to model X-ray spectra in condensed phase has been developed on the basis of localized Wannier orbitals from periodic DFT calculations (Haverkort *et al.*, 2012). Thereby, a multiconfigurational treatment can be obtained which takes the crystal environment into account.

The cluster methods describes rather well the dd excitation in RIXS ($\omega - \omega' \lesssim 4$ eV) but not the CT band ($\omega - \omega' \sim 4 - 10$ eV) which is too localized and strong. The main shortcoming of the cluster model is that it only takes into account hybridization with nearest neighbors, leading to CT configurations centered at a single energy $\Delta_{\mathrm{CT}}$. However, in real solid , the ligand 2p electrons form a wide band. To proper understand and describe the CT excitations it was recognized that only taking into account the ligand band structure leads to the wide band of CT excitations seen in the experiment (Fig. 41)). Such a extension of the cluster approach leads to the single-ion Anderson model (SIAM) with full multiplet effects which is widely used in modern semiempirical simulations of RIXS (Chiuzbăian *et al.*, 2008; Ghiringhelli *et al.*, 2005, 2006; Magnuson *et al.*, 2002a,b) of the RIXS. The combination of the local density approximation (LDA) to the density-functional theory and the dynamical mean-field theory (DMFT) (Hariki *et al.*, 2020b) eliminates most of the empirical parameters of the traditional cluster method.

The RIXS together with XAS is used to get information about valence and conductivity band, parameter of the SIAM model, as well as the band gap of materials. Applications of band gap engineering are extensive in material science, and are found in fields such as optoelectronics, water-splitting photocatalysts, solar cells etc. For example, an ideal photocatalyst should have a band gap of around 2 eV. However, the native band gap of promising materials, such as different forms of $TiO_2$, are in the range of 3.0-3.2 eV. Thus one need to reduce the band gap of $TiO_2$ and other potential materials such as ZnO, $In_2O_3$, and GaN in into a desired region 2 eV by insertion of other transition metals into semiconductors and insulators. For example, a band reduction from 8 eV (pure $TiO_2$) to 4.1 eV was found for $SiO_2$: $TiO_2$ mixtures (Green *et al.*, 2013) and from 3.4 eV for pure ZnO down to 2.9 eV in $Zn_{1-x}NiO$ (Das *et al.*, 2013).
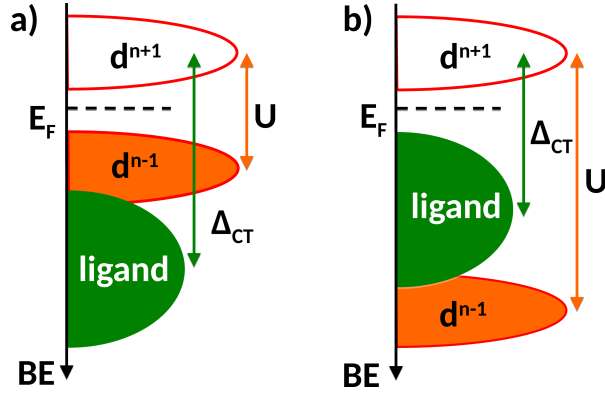
FIG. 42 Sketch of the Zaanen-Sawatzky-Allen (Zaanen *et al.*, 1985) classification of transition-metal compounds into (a) a d-d character Mott-Hubbard insulator and (b) a character charge- transfer insulator. Idea of Figure adopted from Ref. (Chainani *et al.*, 2013). Filled areas show the occupied d-states of metal and ligand states while hollow areas depict electron affinity states $d^{n+1}$. $\Delta_{\mathrm{CT}}$ is the charge-transfer energy while $U$ is the Coulomb repulsion energy of D-electrons on the same site.
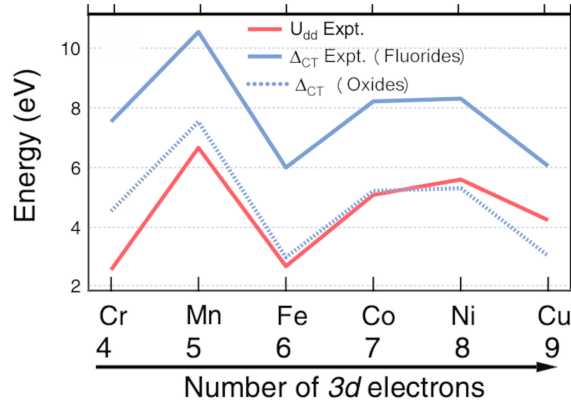


FIG. 43 Experimental picture (Olalde-Velasco *et al.*, 2011) of the MH to CT transition for 3d-TM difluorides $MF_2$ and oxides $MO_2$ with M = Cr-Zn. The values for $\Delta_{CT}$ were decreased by 3 eV for oxides to compensate the difference in the electronegativity between F and O. Adapted from Olalde-Velasco *et al.*, 2011.

The non-resonant X-ray scattering (NIXS) governed by the Thomson term $F_f^T$ (see Eq. (2)) gives in crystals unique opportunity of imaging of core-orbitals to probe the orbital anisotropy in solids without the necessity of any modeling (Yavaş *et al.*, 2019).

Wang *et al.*, 2017 studied high-resolution $2p3d$ RIXS of $CoF_2$, $CoCl_2$, $CoBr_2$, and $CoS$ compounds. The improved spectral resolution allowed to analyze $dd$ and CT excitations in more detail. Systematical analysis allowed accurately determine the charge-transfer parameters of the LMCT model.
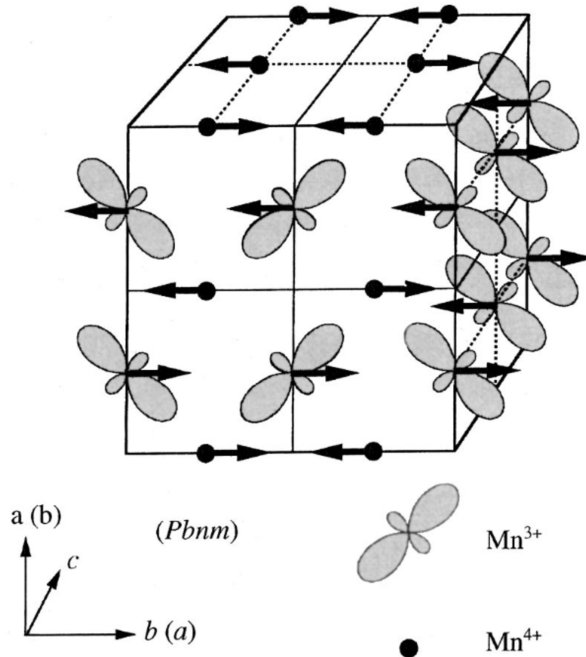
FIG. 44 Spin, charge, and orbital ordering pattern of the charge–exchange (CE) antiferromagnetic type. From Salamon and Jaime, 2001.

## XIII. RESONANT ELASTIC X-RAY SCATTERING IN SOLIDS. ORBITAL AND CHARGE ORDERING

The elastic resonant X-ray scattering (Anomalous X-ray scattering) deserves a special attention not only because of the enhancement of the cross section near the XAS resonance, but mainly due to the qualitatively different polarization dependence of the resonant term in the KH amplitude (2) at resonance (Ishihara, 2017), $\propto (\mathbf{e}' \cdot \mathbf{d}_{0i})(\mathbf{e} \cdot \mathbf{d}_{i0})$, to a magnitude comparable with the non-resonant Thomson contribution, $\propto (\mathbf{e}' \cdot \mathbf{e})$.

### A. Hard X-ray region. Orbital ordering vs Jahn-Teller distortion

A while ago pioneering RIXS experiments (Murakami *et al.*, 1998a,b) demonstrated the possibility to use this effect to shed light on properties of perovskite-type manganites $La_{0.5}Sr_{1.5}MnO_4$ and $LaMnO_3$. Depending on the composition, manganites show a variety of magnetic and electric phenomena, including ferromagnetic, antiferromagnetic, charge, and orbital ordering (OO), and leading to high-temperature superconductivity and colossal magnetoresistance (Salamon and Jaime, 2001). These highly correlated systems, where
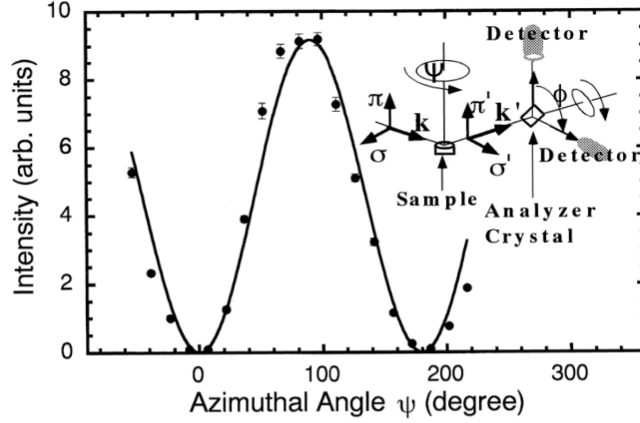
FIG. 45    Azimuthal-angle dependence of the intensity of the orbital ordering reflections (3,0,0). From Murakami *et al.*, 1998a.

charge, spin, and lattice degrees of freedom are intimately interrelated (see Fig. 44), deserve a microscopic understanding of their properties.

Contrary to non-resonant Thomson scattering, the polarization of X-rays is rotated in the resonant scattering $\mathbf{e}^\sigma \to \mathbf{e}^{\pi'}$ due to the crystal field anisotropy in the $4p$ shell, in which the components are split by $\Delta$ components of. Here $\mathbf{e}^\sigma$ and $\mathbf{e}^\pi$ denote the polarizations parallel and perpendicular to the scattering plane, respectively.

For usual (Thomson) reflection, the intensity is independent of the azimuthal angle, but a resonant reflection shows a characteristic oscillation (Fig. 45)(Murakami *et al.*, 1998a,b)

$$\sigma_{\sigma\pi'}^{\mathrm{res}} \propto \frac{\Delta^2 \sin^2 \psi}{[(\Omega - 2\Delta)^2 + \Gamma^2][(\Omega + \Delta)^2 + \Gamma^2]} \tag{51}$$

The azimuthal angle $\psi$ is zero when the crystal stacking vector (c axis) is normal to the scattering plane and $\psi = 90°$ when it is in the scattering plane (see Fig. 44 and Ref. (Murakami *et al.*, 1998a). The resonant $1s \to 4p$ dipole-allowed transitions at the Mn $K$-edge correspond to core-excitations to the $4p$ band, which is split by $\Delta$ due to both the Coulomb interaction with the polarized $3d$ band (related to OO) and because of JT distortion (Fabrizio *et al.*, 1998; Murakami *et al.*, 1998a)

$$\Delta = \Delta_{OO} + \Delta_{JT} \tag{52}$$

The sign of the splitting is opposite for these mechanisms (Murakami *et al.*, 2007) which were studied for different compounds both theoretically (Elfimov *et al.*, 1999; Fabrizio *et al.*, 1998; Mizokawa *et al.*, 1999) and experimentally (Iga *et al.*, 2004; Murakami *et al.*, 2007)
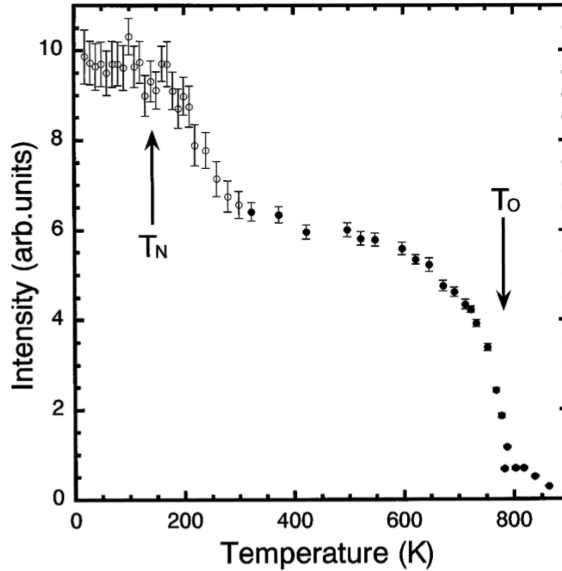
FIG. 46  Temperature dependence of the normalized intensity of the orbital ordering reflection (3,0,0) at $\omega$ = 6.555 keV. Open symbols correspond to results obtained at an azimuthal angle $\psi = 127°$ and cooling with a displex cryostat; closed symbols were obtained for $\psi = 90°$ and heating with an oven. The two data sets were scaled to be equal at T = 300 K. From Murakami *et al.*, 1998a.

The experiment, Fig. 46, shows that the orbital ordering persists until $T_O$=780 K, while magnetic order occurs at or below $T_O$(Turner *et al.*, 2008). This transition is accompanied by a dramatic increase in the intensity observed at the fundamental reflection (2, 0, 0), which was interpreted (Murakami *et al.*, 1998a) in terms of an orthorhombic-to-orthorhombic structural phase transition. This transition in $LaMnO_3$ has been studied earlier (Jonker, 1966; Wold and Arnott, 1959).

Later a rather similar technique was applied to study charge and orbital order in doped manganites (v. Zimmermann *et al.*, 1999), $Pr_{1-x}Ca_xMnO_3$, with $x = 0.4$ and 0.5. Orbital (and charge) order below $T_O \approx 245$ K enhances the antiferromagnetic correlations, and thereby promotes the magnetic phase transition. It was found that the (0,1,0) charge order reflection for $x = 0.5$ shows only a slight broadening corresponding to a correlation length of $\geq 2000$ Å. While, the (0, 2.5, 0) orbital order reflection is substantially broadened, with a correlation length of $\approx 160$ Å. Below the first-order-like phase transition at $T_O$ the charge and orbital order parameters exhibit identical temperature dependencies.

The resonant enhancement of coherent X-ray scattering allowed to study the slow (few
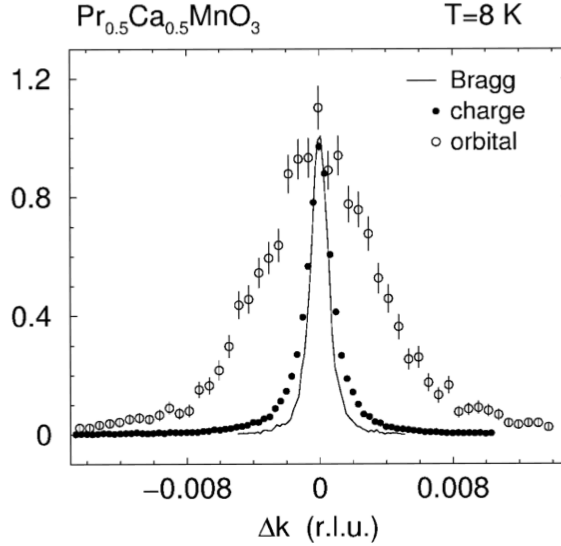
FIG. 47 Longitudinal scans of the (0, 2, 0) Bragg reflection, the (0, 1, 0) charge order peak, and the (0, 2.5, 0) orbital order peak. The orbital order peak is significantly broadened. From v. Zimmermann *et al.*, 1999.

minutes) orbital domain dynamics in a half-doped manganite near the orbital-order phase transition temperature (Turner *et al.*, 2008).

## B. Charge density waves in the cuprates

We now turn to the discussion of resonant X-ray scattering studies of charge order, or equivalently a charge-density wave (CDW), which competes and coexists with superconductivity in underdoped cuprates. In 1986 Bednorz and Müller (Bednorz and Müller, 1986) found a new family of high-temperature superconducting materials, cuprate superconductors, made of layers of copper oxides ($CuO_2$) alternating with layers of other metal oxides, which act as charge reservoirs. The electrons within a CDW form a periodic pattern incompatible with the periodicity of the underlying lattice. Referring readers interested in a detailed description to an excellent review (Comin and Damascelli, 2016), we outline some key achievements in this field below.

Both resonant (Achkar *et al.*, 2012; Blanco-Canosa *et al.*, 2013; Comin *et al.*, 2015; Ghiringhelli *et al.*, 2012; Le Tacon *et al.*, 2014; Thampy *et al.*, 2013) and non-resonant (Blackburn *et al.*, 2013; Chang *et al.*, 2012) X-ray scattering experiments demonstrated CDW order with domain sizes up to 20 unit cells. CDW has emerged as a universal feature of

hole-doped cuprates. Resonant Soft X-ray Scattering (RSXS) measurements of the electron-doped cuprate $Nd_{2-x}Ce_xCuO_4$ (NCCO) indicate CDW formation also in electron-doped cuprates (da Silva Neto *et al.*, 2015).

The electron–phonon interaction is a major factor influencing the competition between collective instabilities in correlated-electron materials. The role of phonons (Fig. 24) in a narrow range of momentum space around the CDW ordering vector and the interference of dynamical CDW excitations with the lattice were studied in $YBa_2Cu_3O_{6.6}$ (Le Tacon *et al.*, 2014), $Bi_2Sr_2LaCuO_{6+\delta}$ (Bi2201) and $Bi_2Sr_2CaCu_2O_{8+\delta}$ superconductors (Chaix *et al.*, 2017; Li *et al.*, 2020a).

High-brightness X-ray sources opened a new frontier in the context of high-magnetic field studies (Comin and Damascelli, 2016). Femtosecond XFEL pulses synchronized with the high-magnetic-field (32.1 T) pulses were used to explore the magnetic field-induced 3D CDW correlations in high quality ortho-II and ortho-VII $YBa_2Cu_3O_x$ (YBCO) crystals by resonant soft X-ray scattering (RSXS) measurements at the Cu $L_3$-edge (Jang *et al.*, 2016).

## C. RIXS from low dimensional systems

The lowering of the real or effective dimensionality of the systems brings unusual physical properties. A two-dimensional electronic gas can be formed at the interface between appropriate materials. A typical example of 2D materials is graphene. Nano wires are representative of 1D fermions. Quite often real 3D system exhibits strong 1D properties due to effective lowering of the dimensionality along certain orientation of the orbitals in the solids (for example d-orbitals). There are many families of organic and inorganic quasi-1D materials which deviate strikingly from 3D Fermi liquid behavior in their normal state, and undergo a variety of low-temperature phase transitions into, e.g., charge or spin density wave insulating phases or even become superconducting (Dressel, 2018; Jérome and Schulz, 1982). The excitations in the 1D electron gas are approximate bosons, rather than fermions, and bear resemblance to the Tomanaga-Luttinger liquid model (Luttinger, 1963; Tomonaga, 1950), which was solved exactly by Mattis and Lieb (Mattis and Lieb, 1965). Efetov and Larkin (Efetov and Larkin, 1976) and Haldane(Haldane, 1981) gave Luttinger liquid theory the form it has today.

Although the state of an electron is characterized by spin, charge and orbital degrees of

freedoms, the electronic excitations break up into deconfined spinons, holons and orbitons in 1D systems. This effect is one of the most unusual manifestations of collective low energy quantum physics of interacting particles in low dimensional systems.

**Spin-charge separation in 1D**

In one-dimensional (1D) electron systems, theory predicts that collective excitations of electrons produce, instead of the quasiparticles in ordinary Fermi liquids, two new particles known as 'spinons' and 'holons' . Unlike ordinary quasiparticles, these particles surprisingly do not carry the spin and charge information of electrons together. Instead, they carry spin and charge information separately and independently. Unlike spinons, which have spin $1/2$ but no charge, holons carry zero spin and charge $e$. The spinon and holon are decoupled and propagate with different velocities. This novel and exotic phenomenon was predicted theoretically (Haldane, 1981; Lieb and Wu, 1968) and is commonly known as spin-charge separation. The spin-charge separation, thus spinons and holons was observed in 1D copper-oxide chain compound $SrCuO_2$ using angle-resolved photo-emission spectroscopy (ARPES)(Kim *et al.*, 2006, 1996, 1997). The interpretation of the experiment is supported by the observed distinct dispersions of spinon and holon and quantitative agreement with the theory.

**Spin-orbiton separation in 1D**

In addition to spin, the orbital degrees of freedom play an important role in the low-energy physics of various correlated TM compounds. In MH insulators, the Kugel-Khomskii (KK) model (Kugel' and Khomskii, 1982; Streltsov and Khomskii, 2017) is the effective low-energy superexchange model for coupled spin and orbital excitations. Jackeli and Khaliullin (Jackeli and Khaliullin, 2009) recognized that SO coupling in crystals results in an exchange interaction which depends on the spatial orientation of a given bond $ij$. Instead of the Heisenberg interaction $H = J \sum_{ij} \mathbf{S}_i \mathbf{S}_j$, the interaction of pseudo-spins is described by the Kugel-Khomskii-Kitaev Hamiltonian (Kitaev, 2006; Kugel' and Khomskii, 1982; Streltsov and Khomskii, 2017)

$$H = \sum_{\langle ij \rangle} K^\gamma S_i^\gamma S_j^\gamma \tag{53}$$

which entangles in general the orbital and spin degrees of freedom. In the exactly solvable and experimentally relevant Kitaev honeycomb model (Hermanns *et al.*, 2018; Kitaev, 2006) the spin degrees of freedom interact via a strongly anisotropic nearest-neighbor Ising
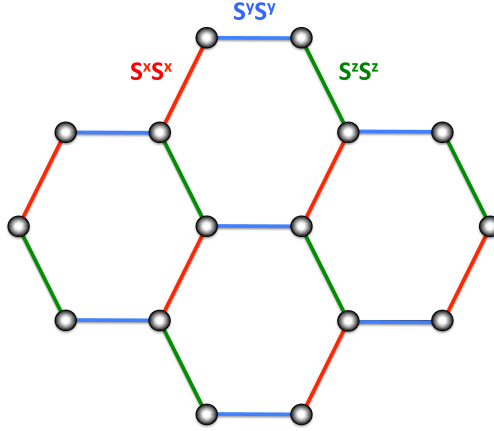
FIG. 48 Kitaev interactions on a honeycomb lattice indicating the three kinds of bonds x, y and z and spins sitting on the vertices of a lattice.

exchange, where the easy axis $\gamma = x, y, z$ depends on the bond direction $\langle ij \rangle$ (Fig. 48).

However, the orbital and spin degrees of freedom are decoupled in the 1D systems in the peculiar regime where spinons are propagating faster than orbitons. The spin-orbital (spinon and orbiton) separation is conceptually analogous to the spin-charge separation in the 1D system and it was predicted in Ref. (Chen *et al.*, 2015; Wohlfeld *et al.*, 2011). The spin-orbiton separation was observed using (RIXS)(Bisogni *et al.*, 2015; Schlappa *et al.*, 2012) (see Fig. 49).

The electronic quasiparticle is unstable in 1D systems and the elementary excitations in low energy region are the spinon, the holon and the orbiton, propagating with different velocities. However, real materials are never strictly 1D. In spite of this, RIXS measurements of the anisotropic ladder system $CaCu_2O_3$ combined with simulations (Bisogni *et al.*, 2015) show that spin-orbital separation occurs along the leg direction x through the xz orbital channel as in a 1D system,- while no fractionalization is observed for the xy orbital, which extends in both leg (x) and rung (y) direction, contrary to a 1D system. Therefore the $3d_{xy}$ orbital excitation is affected by interladder couplings and, hence, behaves as in a 2D system. This means that various orbital symmetries allows to select different degrees of dimensionality in the same system. Moreover, it is shown (Bisogni *et al.*, 2015) that spin-orbital separation is, in general, much more robust than spin- charge separation.
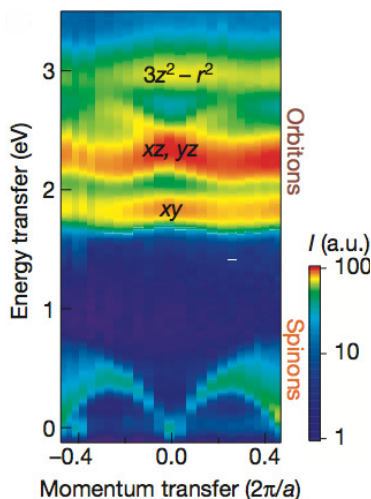
FIG. 49 Measured spin-orbital separation process in an antiferromagnetic spin chain, emerging after exciting an ground-state copper $3d_{x^2-y^2}$ orbital to an excited copper $3d_{xy}$ or $3d_{xz}$ orbital. RIXS intensity map of the dispersing spin and orbital excitations in quasi-one-dimensional Mott insulator $Sr_2CuO_3$ as functions of photon momentum transfer along the chains and photon energy transfer. Adapted by permission from Springer Nature Customer Service Centre GmbH: Schlappa *et al.*, 2012.

### D. Dynamics of multi-spinon excitation in RIXS

RIXS is an adequate and unique tool to study magnetic excitations (Ishii, 2017) and it provides access to non-local spin correlation functions as it was recently demonstrated in the experiment (Schlappa *et al.*, 2018). The theoretical details of spinon excitation in RIXS one can find in Ref. (Ament *et al.*, 2009, 2011; Haverkort, 2010; Kumar *et al.*, 2018). To explain the magnetic spin-flip transitions one needs the combination of core and valence SO coupling, crystal-field splitting, core-valence and valence-valence electron-electron interactions (Das *et al.*, 2018; Elnaggar *et al.*, 2019; Nag *et al.*, 2020). Double spin-flip RIXS (Fig. 50 a) across two Cu sites at the oxygen K-edge along -Cu-O-Cu- chains in the quasi-1D spin-chain cuprate $Sr_2CuO_3$ allows to probe two-and four-spinon continuum excitations (Fig. 50 b) (Schlappa *et al.*, 2018). The spin dynamics in the intermediate state (see the upper panel of Fig. 50) , defined by the competition between the spin hoping rate (inverse exchange constant, J) and the lifetime $1/\Gamma$ of the core-excited state. The simulations (Schlappa *et al.*, 2018) show the decrease of intensity of magnetic excitations in O K RIXS upon decreasing the core-hole lifetime. Moreover, the four-spinon excitations decrease faster than the two-
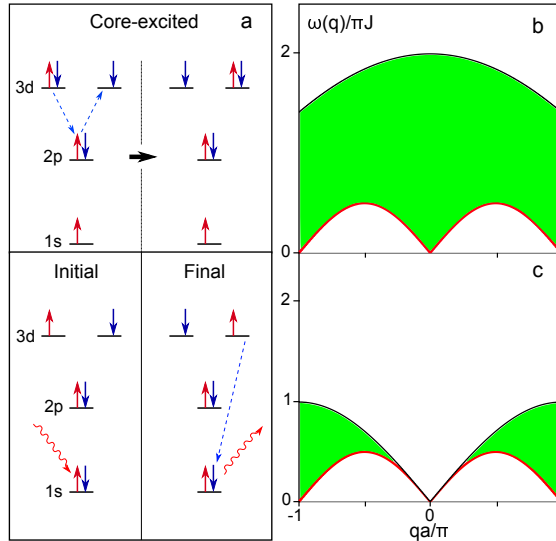
FIG. 50 a) Sketch of double spin-flip RIXS process in -Cu-O-Cu- chain. b) The two $(\omega_{2s}(q))$- and four $(\omega_{4s}(q))$-spinon continua: $(1/2)|\sin(qa)| \leq \omega_{2s}/(q)\pi J \leq \sin(qa/2)$, $(1/2)|\sin(qa)| \leq \omega_{4s}(q)/\pi J \leq \sqrt{2(1+\cos(qa/2))}$ (Caux and Hagemans, 2006). The dispersion law of the single spinon $\omega_{1s}(q) = (1/2)|\sin(qa)|$ is depicted by red line.

spinon ones. One can expect that direct time-resolved XFEL studies will facilitate studying such a spin dynamics at the femtosecond timescale.

## XIV. NONLINEAR PHENOMENA IN STRONG FIELD OF XFEL PULSES

### A. Stimulated RIXS, four-wave mixing, pulse compression, superfluorescence, suppression of the Auger decay channel

In previous sections we highlighted the current state of RIXS and RAS studies based on long-pulse synchrotron X-ray sources. For more than a decade new XFEL and HHG sources (Duris *et al.*, 2020; Johnson *et al.*, 2018) of short (down to attoseconds), coherent and intense (up to gigawatt) X-ray pulses have been operating, making it possible to investigate ultrafast electronic and nuclear dynamics as well as high energy-density systems (Humphries *et al.*, 2020). Intense XFEL radiation allows to study such nonlinear RIXS-related processes (Kowalewski *et al.*, 2017; Rossbach *et al.*, 2019; Young *et al.*, 2018) as stimulated RIXS (Kimberg and Rohringer, 2013, 2016; Kimberg *et al.*, 2016; Sun *et al.*, 2009a,b, 2010a; Weninger *et al.*, 2013) and X-ray lasing (Miao *et al.*, 2012; Rohringer *et al.*, 2012), two-
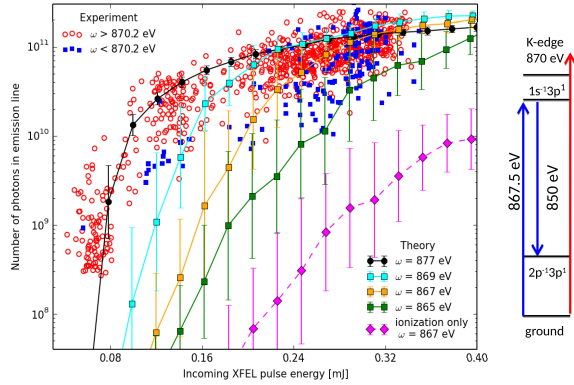
FIG. 51 Pump energy dependence of the SRIXS signal from Ne: measured number of photons in the emission line as a function of the incoming pulse energy for $\omega >870$ eV (average $\overline{\omega}$=876 eV) and $\omega < 870$ eV (average $\overline{\omega} = 868$ eV) along with the theory results. Adapted from Weninger *et al.*, 2013; Weninger and Rohringer, 2013.

photon RIXS (Hopersky *et al.*, 2018; Sun *et al.*, 2010b), X-ray pulse compression (Kumar *et al.*, 2020; Li *et al.*, 2020b; Sun *et al.*, 2009a,b, 2010a), four-wave mixing (Bencivenga *et al.*, 2015; Mukamel, 2005; Sun *et al.*, 2009a,b, 2010a; Tanaka and Mukamel, 2002) and nonlinear wave mixing of X-ray and near-infrared beams (Glover *et al.*, 2012). Special attention was paid to the competition between stimulated X-ray emission and Auger decay (Liu *et al.*, 2010; Rohringer and Santra, 2008; Sun *et al.*, 2018).

Soft X-ray lasing was first observed in neon vapor (Rohringer *et al.*, 2012) at the Linac Coherent Light Source (LCLS) and later extended to the hard X-ray range by lasing in a Cu foil of thickness 20 mm (Yoneda *et al.*, 2015), performed at SPring-8 Angstrom Compact free electron Laser (SACLA) facility. First demonstration of stimulated RIXS (SRIXS) was performed by resonant excitation of a dense neon gas target with femtosecond, high-intensity X-ray pulses from the LCLS (see Fig. 51). As compared to the spontaneous RIXS process, signal enhancement of 7-9 orders of magnitude was achieved. Later stimulated X-Ray emission was observed in 5M solution of $MnCl_2$ complex (Kroll *et al.*, 2018) (Fig. 52). That the stimulated X-Ray emission regime was reached was proven by the observation of exponential grow of the number of photons with increase of the pump pulse energy and by the narrowing of the line shape of the SRIXS (Kroll *et al.*, 2018). Seeded amplified K$\beta$ X-ray emission with a signal enhancement of more than $10^5$ was recently observed in a $NaMnO_4$ solution using two colors of XFEL pulses(Kroll *et al.*, 2020).

Recently a very unusual manifestation of the recoil effect in SRIXS was observed, namely
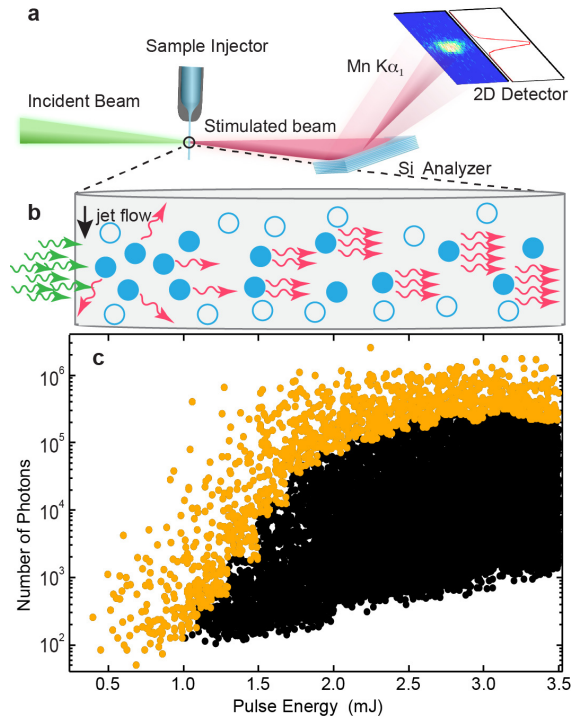
FIG. 52 (a) Experimental setup of the stimulated X-Ray emission from 5M solution of $MnCl_2$ complex: the incoming XFEL pulses are focused onto the liquid jet. (b) Sketch of the stimulated X-ray emission: the arrows represent incoming (green) and emitted (red) photons, while the circles indicate the excited (filled) and nonexcited (open) Mn ions, respectively. (c) Detected number of photons in the Mn $K_{\alpha_1}$ region (5 eV integration window) as a function of the nominal incoming XFEL pulse energy for the 5M $MnCl_2$ solution. The actual pulse energy on target is $\sim 20\%$ of the nominal pulse energy shown in the figure. The 50 strongest shots in each 0.1 mJ interval are shown in orange, all other shots in black. From Kroll *et al.*, 2018.

the recoilless stimulated RIXS (Eichmann *et al.*, 2020). The random distribution of momenta of spontaneously emitted photons gives a broad velocity distribution of the atoms in the course of RIXS. The situation is qualitatively different in stimulated RIXS where the recoil momentum from the absorbing photon is almost exactly compensated by the recoil momentum of the SRIXS photon, emitted in the forward direction. This results in a narrow recoilless peak in the broad velocity distribution due to the recoil from spontaneous photons. This effect has close analogy with Doppler-free two-photon absorption peak in a standing wave (Popova *et al.*, 1970) and with laser cooling (Kazantsev *et al.*, 1990).

The stimulated elastic scattering into the forward direction of the incident narrow bandwidth XFEL pulses was evidenced by the characteristic disappearance of both charge and

magnetic diffraction contrast at the Co $L_3$ resonance scattering (778 eV) of the Co/Pd multilayer worm domain sample (Wu *et al.*, 2016).

A two-color all X-ray pump-probe experiment with sub-70 fs temporal resolution selectively probes the response of orbital and charge degree of freedom in the prototypical functional oxide magnetite after photoexcitation (Pontius *et al.*, 2018). It was found that the electronic order was quenched on a time scale of $\sim 30$ fs and hence most likely faster than what is to be expected for any lattice dynamics. One of the main applications of XFELs is related to a unique opportunity to study the dynamics of quantum systems in real time using time-resolved RIXS (Beye *et al.*, 2013) (see Sec. XIV.E, Sec.).

## B. Second Harmonic generation

High pulse intensities of XFEL create room for studies of nonlinear effects such as second-harmonic generation (SHG) in the X-ray energy range. SHG is a nonlinear optical process of sum frequency generation which produces new photons with twice the frequency. SHG has traditionally been studied as an even-order nonlinear optical effect allowed in the media without inversion symmetry and is one of the best-understood nonlinear effects in optics (Boyd, 2010). Pioneering studies by Shwartz *et al.* (2014) and Yudovich and Shwartz (2015) gave recently experimental evidence for "off-resonant" SHG in diamond in the hard X-ray region with a pump frequency of 7.3 keV and the SHG efficiency $5.8 \times 10^{-11}$. One should mention also theoretical studies of the X-ray SHG in solids (Nazarkin *et al.*, 2003) and gas phase (Liu *et al.*, 2019a), where this process is also allowed due to inversion symmetry.

## C. Superfluorescence and superradiance

There is a fundamental collective process - superfluorescence (SF) (Bonifacio and Lugiato, 1975) in which short pump pulse excites the initially incoherent ensemble of $N$ atoms. SF starts from spontaneous emission which couples the radiation phases of different atoms building up a macroscopic dipole. This gives rise to a SF pulse delayed by the time $\tau_D \propto (\ln N)/N$ needed for the individual dipoles to become phase-locked. The intrinsic property of SF are the scaling law for the intensity of the coherent process ($\propto N^2$) and the Burnham-Chiao ringing (Burnham and Chiao, 1969; Sun *et al.*, 2010a). One should distinguish SF
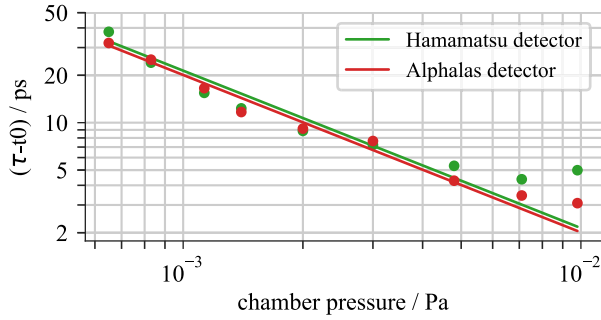
FIG. 53 Higher number densities lead to larger peaks with shorter delays, a clear hallmark of superfluorescence. From Harries *et al.*, 2018.

from superradiance (SR) of Dicke (Dicke, 1954), where a macroscopic dipole moment is created in advance by the collective excitation process. The time delay $\tau_D$ is unique for SF, yet absent in SR and amplified spontaneous emission (ASE).

The SF was observed in XUV region in the course of the propagation of partially coherent XFEL SACLA pulses of wavelength 24.3 nm through a dense helium gas (Harries *et al.*, 2018). Intense, highly directional emission on the $2p \rightarrow 1s$ transition (30.4 nm / 40.79 eV) in pumped He$^+$ ions was observed and interpreted as yoked SF (Brownell *et al.*, 1995).

The SF was detected by measuring its fingerprint as the decrease of the delay time $\tau_D$ with increase of the pressure (see Fig. 53). Combined experimental (the CAMP end station of the FLASH facility) and theoretical study of XUV SF was done in xenon gas pumped by the photons of 73 and 92 eV, tuned below and on the giant $4d$ resonance, respectively (Mercadier *et al.*, 2019). Population inversion is achieved by Auger pumping via the rapid Auger decay following the photoionization of the $4d$ shell of Xe. It was speculated that the emission at 65.18 and 68.14 nm could stem from SF, based on the measured line broadening and emission yield (Mercadier *et al.*, 2019). However, no other proof that this is SF was presented.

The SR in crystals at the Mössbauer transition of nuclei was predicted in Refs. (Afanas'ev and Kagan, 1965; Hannon and Trammell, 1989). A speedup of decay in comparison with the natural decay was observed in the $^{57}$FeBO$_3$ crystal (14.4 keV $^{57}$F nuclear transition) (van Bürck *et al.*, 1987) at the Bragg condition. Chumakov *et al.*, 2018 used resonant diffraction of X-rays from the SACLA XFEL (the Mössbauer 14.4 keV nuclear transition of $^{57}$Fe nuclei) to investigate SR decay in $^{57}$FeBO$_3$.
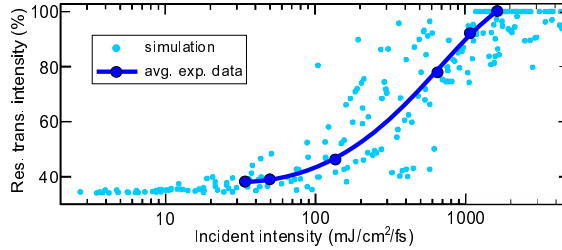
FIG. 54 Experimentally observed change in the transmitted intensity as a function of incident intensity (solid blue circles and line). Each data point is an average over multiple shots. The open blue circles correspond to the simulated shot-by-shot response. Adapted from Chen *et al.*, 2018.

### D. Self-induced X-Ray transparency

Another milestone phenomenon related to the resonant pulse propagation is the effect of self-induced transparency well known in optical laser spectroscopy (Allen and Eberly, 1987). In fact, there are two effects named self-induced transparency. The first one is the self-induced transparency by McCall and Hahn (McCall and Hahn, 1967), which takes place for $n\pi$-pulses shorter than the inverse homogeneous broadening of the spectral transition. This effect was used successfully for compression and enhancement of the optical pulses (Allen and Eberly, 1987) and analyzed theoretically for intense X-ray pulses (Li *et al.*, 2020b; Sun *et al.*, 2010a). The second one is caused by the saturation of the spectral transition when the absorption probability $\sigma_{abs} \propto \rho_{11} - \rho_{00} \to 0$ because the populations of the excited $\rho_{11}$ and ground $\rho_{00}$ states become equal for high intensity of the pump pulse (McCall and Hahn, 1967). The self-induced transparency caused by the saturation effect was recently observed in X-ray range (Chen *et al.*, 2018) in the Co/Pd multilayer sample using 2.5 fs and 25 fs self-amplified spontaneous emission (SASE) pulses at LCLS with the photon energy around Co $L_3$ resonance of 778 eV (Fig. 54).

### E. Time-resolved RIXS studies of magnetic excitations

Investigation of the dynamics of magnetic correlations in doped Mott insulators sheds light on our understanding of the pseudogap, non-Fermi liquids and high-temperature superconductivity. Recently time-resolved (tr) magnetic RIXS (tr-RIXS) at XFELs was used to directly determine the magnetic dynamics after photo-doping the Mott insulator $Sr_2IrO_4$ (Cao *et al.*, 2019; Dean *et al.*, 2016). Pump laser pulses with an energy of 620 meV (2 $\mu$m)
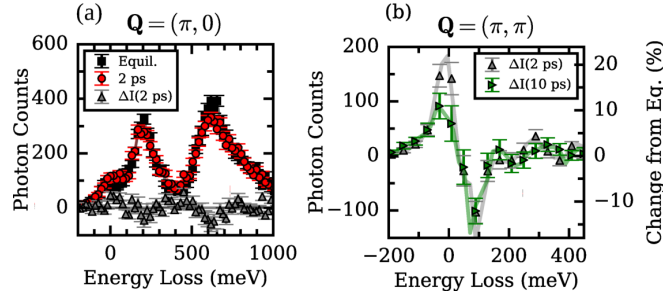
FIG. 55 (a) tr-RIXS spectra showing magnetic excitations (0-200 meV) and orbital excitations (∼600 meV) in the equilibrium state 50 ps before photo-excitation (labeled Equil.) and 2 ps after photo-excitation. (b) Intensity difference spectra, $\Delta I$, between the equilibrium state and the 2 ps transient state and between the equilibrium state and 10 ps. This shows a depletion of approximately 20% of the magnetic spectral weight around ∼100 meV and additional spectral intensity appearing at very low energy. Adapted by permission from Springer Nature Customer Service Centre GmbH: Dean *et al.*, 2016.

drive carriers from the lower Hubbard band (LHB) to the upper Hubbard band (UHB). The incident X-ray pulses excite an Ir $2p$ core electron into the $5d$ valence band, to couple to the spin degree of freedom. Through the resonant magnetic X-ray scattering mechanism, photons scattered around 90° were measured as a function of momentum transfer, $\mathbf{Q}$, energy loss, E, and time delay, t. The chosen pump level 6 mJ cm$^{-2}$ corresponds to what was required to destroy 3D magnetic order. Orbital excitations $J_{\text{eff}} = 1/2 \rightarrow 3/2$ appear in the RIXS spectra around 600 meV. Figure 55a shows the experimental RIXS spectra at equilibrium (50 ps before the pump) and in the transient state after pumping. The low-energy excitation spectrum features a dispersing spin-wave below 200 meV and an orbital excitation around 600 meV.

Despite the almost- complete destruction of the magnetic Bragg peak in the transient state, magnons are still observed at both $\mathbf{Q}$ points. One can see that the magnon at $(\pi, 0)$ is identical before and after the pump. At $(\pi, \pi)$, however, there is an appreciable change. This indicates that the high-energy ∼200 meV correlations at $(\pi, 0)$ are more robust than the lower-energy spin wave at $(\pi, \pi) \lesssim 100$ meV. The possible reason for this is that the higher- energy magnons recover to their equilibrium configuration faster than 2 ps, because a higher-energy excitation can decay into lower-energy multi-particle excitations in a greater number of different ways than can the lower-energy magnons. Current stage of time-resolved

RIXS in pumped Mott Insulators can be found in Refs. (Chen *et al.*, 2019; Wang *et al.*, 2020).

Mitrano *et al.* exploited tr-RIXS to characterize photoinduced decoherence of charge excitations in stripe-ordered $La_{2-x}Ba_xCuO_4$ (Mitrano *et al.*, 2019a,b), where transient superconductivity had been observed earlier(Nicoletti *et al.*, 2014).

## F. Dynamics of liquid-liquid phase transitions revealed by ultrashort optical pump and XFEL probe pulses

Unique properties of XFELs allow to study the melting dynamics and, more generally, liquid-liquid phase transitions, as it was demonstrated recently for crystalline silicon (Beye *et al.*, 2010). Silicon is one representative out of a whole class of so-called tetrahedral network formers, spanning from the IV- and III-V semiconductors like silicon, germanium, indium-antimonide to silica, carbon and water. These materials commonly share a phase diagram with many stable phases, including the ability to form glasses and different liquid phases. Many predictions about the existence of a liquid-liquid phase transition have been made in theory (Ganesh and Widom, 2009). However, it is rather difficult experimentally to access directly the relevant temperatures and pressures, because the phases of interest are metastable on a picosecond time scale.

The optical excitation of electrons in a crystalline silicon from the valence to the conduction band by a 3.1 eV femtosecond pump laser pulse, generates enough energy in the form of "hot electrons". Due to electron-phonon coupling the excited electrons lose their energy to the lattice (Beye *et al.*, 2009), the temperature and pressure in the sample increases and the sample melts into a liquid state. The electronic structure of the liquid phase was characterized by X-ray emission, induced by the time-delayed soft X-ray pulse from FLASH (Ganesh and Widom, 2009). It was found that the molten silicon is semimetallic with a pseudogap in the density of states around the Fermi level, which is characteristic for the low-density liquid (LDL) with a density similar to the crystal. Silicon stays in this phase for the first four picoseconds after laser excitation because the transition to the metallic without a band gap high-density liquid (HDL) phase takes time around 1.5 ps.
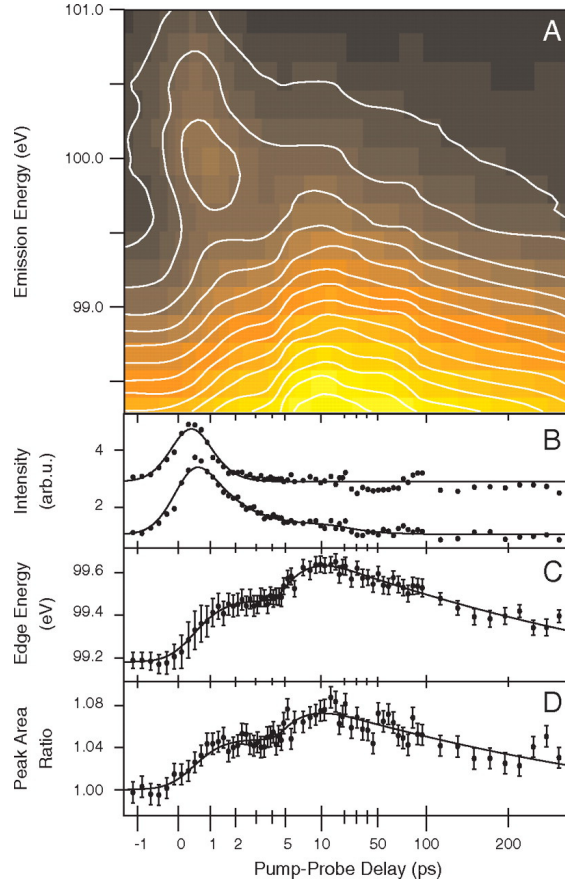
FIG. 56 Two distinct phase transitions are visible in the electronic structure of silicon. (A) In the false color map of the band gap region (higher intensities are brighter) with smooth white lines of equal intensity, the transient occupation of the conduction band and the transitions to the LDL phase in the first ps and to the HDL phase around 6 ps are obvious. (B) Hot electrons appear in time with laser excitation in the conduction band. Highly excited electrons decay faster than thermalized electrons trapped at the conduction band bottom. (C) The phase transitions shift the valence band edge. The transition to the LDL phase starts with the electronic excitation. The plateau between 2 and 4 ps followed by a step is the footprint of the first-order phase transition to the HDL state. (D) The structure of stronger bound states changes alongside, prominently represented by the changing ratio of the $L_1$ and $L_2$ peaks in the X-ray emission. From Beye *et al.*, 2010.

## G. Time-resolved UV pump RIXS probe spectroscopy to monitor reaction paths in chemical processes in solution

The development of time-resolved techniques based on use of XFEL and HHG sources enables investigations of ultra-fast processes including both spectroscopic probes and scattering (Kraus *et al.*, 2018; Schoenlein *et al.*, 2019; Wernet, 2019). The ability of time-resolved RIXS, involving a photon-in and photon-out probe, to deeply penetrate a condensed phase sample can be used to investigate photoinduced reactions in solution, with element selectivity and chemical sensitivity. In this subsection, we will focus on time-resolved RIXS measurements, although other important and related techniques include valence-to-core X-ray emission (Gallo and Glatzel, 2014), X-ray absorption and photo-electron spectroscopy.

Laser pump X-ray probe RIXS spectroscopy, supported by spectral fingerprints from static experiments or advanced quantum chemical calculations (Norell *et al.*, 2018; Wernet *et al.*, 2015), allows to investigate photo-induced processes by probing short-lived intermediates and population dynamics of different chemical species. Time-resolved Fe L-edge RIXS has been employed to study the photodissociation of ironpentacarbonyl $Fe(CO)_5$ in solution (Wernet *et al.*, 2015) using LCLS (Emma *et al.*, 2010). The removal of CO generates a $Fe(CO)_4$ species (Fig. 57), which subsequently may be involved in solvent association. Theoretical analysis of the transient RIXS signal allowed for detailed insight into the excited state dynamics, in which decreasing ligand coordination, when going from $Fe(CO)_5$ to $Fe(CO)_4$, causes changes in the frontier-orbital interactions. A valence hole localized on the metal and a concomitant decrease in the $d_\pi - d_\sigma^*$ splitting are manifested in the Fe $L_3$-RIXS spectra at time delays of 0–700 fs (Fig. 57c, middle) as a new low-energy XAS resonance at 706.5 eV and a red shift in the energy transfer of the main RIXS feature relative to that of $Fe(CO)_5$. Subsequently restored $2p \rightarrow$LUMO and $d_\pi \rightarrow d_\sigma^*$ transition energies, comparable to $Fe(CO)_5$, at late delays of 0.7–3.5 ps (Fig. 57c, bottom) was explained by reformation of a fifth Fe-C bond indicative of solvent association. The transient RIXS signal could be explained by assuming branching involving inter system crossing into a chemically inert triplet $Fe(CO)_4$ species and a reactive singlet $Fe(CO)_4$ pathway leading to solvent association (Wernet *et al.*, 2015). In further theoretical analysis of ultra-high energy-resolution or ultra-high time-resolution (Kunnus *et al.*, 2016a), the possibility to probe the initial steps in the excited state dynamics in future experiments with improved settings has been proposed.
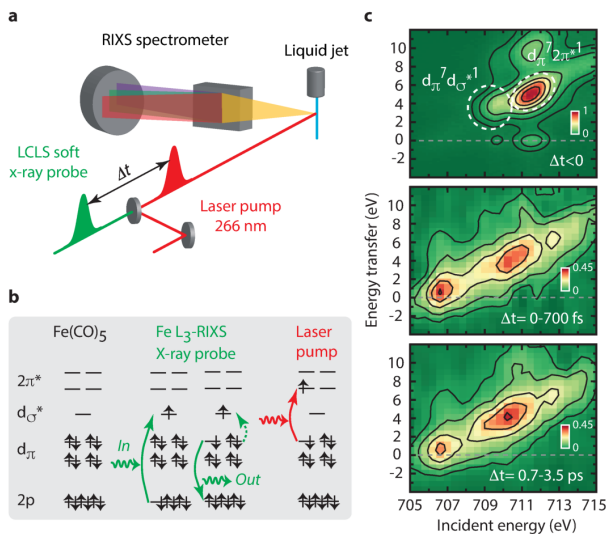
FIG. 57 Schemes and results of the time-resolved RIXS experiment on $Fe(CO)_5$ in ethanolic solution. a) Optical-laser pump and soft X-ray probe setup with pump–probe time delay $\Delta t$. b) RIXS and valence transitions in $Fe(CO)_5$. c) RIXS intensities measured at Fe $L_3$ edge. c) Top: ground-state $Fe(CO)_5$ (probed before pump). Middle and bottom: Intensities for transient species at delay intervals $\Delta t = $ 0-700 fs and 0.7-3.5 ps, respectively. From Wernet *et al.*, 2015.

In particular, search for anti-stokes RIXS features were identified as a means to identify valence-excited states of the same multiplicity as the ground state.

Time-resolved RIXS spectroscopy has also been employed to study coupled electron-nuclear dynamics involving charge-transfer excitations in ironhexacyanide in aqueous solution using Fe L-edge RIXS (Jay *et al.*, 2018) complemented by theoretical simulations to determine the spectral finger print of possible reaction intermediates (Norell *et al.*, 2018), which could help identifying a short-lived quartet state suggested to mediate the repopulation of the electronic ground state. As a natural probe of changes in chemical bonding, N K-edge RIXS has been used to investigate electron dynamics leading to excited state proton transfer in 2-thiopyridone in aqueous solution (Eckert *et al.*, 2017). However, further studies at high time-resolution and improved statistics are required to resolve the relation to measurements with IR and N K-edge and S K-edge XA probes.

## XV. SUMMARY

In this review, we survey resonant inelastic x-ray and resonant Auger scattering. We focus both on the basic processes in these akin X-ray processes and on the information about electron-nuclear dynamics in free molecules, liquids and solids that can extracted from RIXS and RAS experiments. During last decade we have witnessed a significant increase in brightness of tunable synchrotron radiation light sources and a tremendous improvement in spectral resolution of spectrometers. Energy transfers in the range of a few meV give access to detailed measurements of collective excitations in correlated materials and collective dynamics in non-crystalline materials.

Both RIXS and RAS can be considered as some kind of pump-probe experiments. The concept of scattering duration (Gel'mukhanov *et al.*, 1999) controlled by the detuning brings effective "time resolution" in these processes even when continuous wave X-rays are used. Sometimes the lifetime of the core-excited state serves the role of a delay time between the absorption and decay processes (Brühwiler *et al.*, 2002; Céolin *et al.*, 2019). The effective "time-resolution" in these measurements introduces nonequilbrium dynamics in X-ray spectroscopy. This type of implicitly time resolved measurements has been performed to study down to femtosecond electron-nuclear (Gel'mukhanov and Ågren, 1999) and charge-transfer dynamics (Brühwiler *et al.*, 2002). The ultrafast electronic wave packet dynamics (attosecond and below) (Schweigert and Mukamel, 2007) is the challenge for actually time-resolved pump-probe X-ray spectroscopy. For example the tunneling through the effective barrier in the case of shape resonances (Stöhr, 1992) or the set of problems related to relaxation of the electron cloud on the created core-hole (Calegari *et al.*, 2014).

X-ray free-electron lasers being new, large-scale research facilities, allow us to film electron-nuclear dynamics and chemical reactions in real time varying the time delay between pump and probe pulses. The goal is a deeper understanding of ultrafast phenomena in atomic physics, chemistry, materials science and structural biology (Khalil and Mukamel, 2020). One of the main applications is the extension of RIXS into the time domain making use *e.g.* of stimulated RIXS or RIXS probe of a laser pumped system. The combination of XFELs and synchronized optical lasers enables pump–probe measurements of previously inaccessible processes in short-lived and extreme states of matter generated by optical lasers (Chen *et al.*, 2019; Liu *et al.*, 2021a,b; Picón *et al.*, 2016; Wang *et al.*, 2020; Wernet, 2019;

Wernet *et al.*, 2015) (See Secs. XIV.E, XIV.F, XIV.G). Pumping the ground state vibrational levels with an IR field strongly changes and elongates the vibrational progression in XAS and in quasi-elastic RIXS channel of isolated molecules and liquids. This IR pump X-ray-probe spectroscopy opens new opportunities to reach the high energy part of inter- and intramolecular potentials and to study, for example, the influence of hydrogen bonding on the long range part of the OH potential in various molecular liquids.

Ultra short and highly intense X-ray pulses generated at the XFELs make it possible to study the effects of nonlinearity on X-ray optics and narrowing of X-ray pulses (Sun *et al.*, 2010a). With X-ray flashes of unprecedented brightness and shortness, the XFELs allow direct observation of single molecules and atoms. For example, the high flux of XFEL can be used to observe recently predicted recoil-induced dissociation (Liu *et al.*, 2019b). Seeded XFELs (Callegari *et al.*, 2021), open possibilities to perform phase sensitive X-ray pump-probe measurements, of which we evidenced only the initial steps. For example, symmetry-forbidden RIXS induced by coherent mixing of core-excited states of opposite parity (Liu *et al.*, 2008). Special attention should be paid to study stimulated X-ray emission and RIXS (Kroll *et al.*, 2020), and four wave mixing (Tanaka and Mukamel, 2002). The next goal is the physics of phase transitions shedding light on most extreme and exotic forms of matter.

Strong attosecond XFEL fields, in which the phase of each oscillation is locked to the pulse envelope, offer new tools to control and manipulate by the currents and flow of spin in solids and to create and explore new phases of materials. There is an example of shaping matter with intense light in which the electron motion is dominated by the laser field, but the electron is still bound to the atomic core, this is the so-called Kramers–Henneberger atom (Henneberger, 1968; Matthews *et al.*, 2018).

Many applications like the measurement of element specific spatial correlation functions and pump-probe spectroscopy need high longitudinal coherence of X-ray radiation. Although SASE-based XFEL light has a high transverse coherence, its longitudinal coherence remains low. Longitudinal coherence can be obtained using a multi-stage cascade seeding scheme (Petrillo *et al.*, 2020). Another leading candidate for obtaining longitudinal coherence cavity-based XFELs (Kim *et al.*, 2008; Shvyd'ko, 2019) is capable of generating fully coherent X-ray beams of high brilliance and stability, like in classical lasers.

Regarding the experimental and theoretical studies of liquids, despite much progress in the field, it is not difficult to infer that controversies in studies of these complex systems will

remain. This refers both to ambient properties as well as the regions of phase transitions. Here the role of new pump-probe tools and refinement of theoretical methods is crucial.

Our hope is that this review will introduce increased understanding of resonant X-ray scattering and helps physicists and physical chemists to realize new applications of the techniques and how their research field can benefit from the burgeoning field of synchrotron radiation and XFEL based research. With the current steady progress in instrumentation, new sources of brilliant and short X-ray pulses combined with the increasing theoretical expertise, the use of resonant x-ray scattering techniques is becoming increasingly prevalent.

## LIST OF SYMBOLS AND ABBREVIATIONS

| | |
|---|---|
| $\lvert 0 \rangle$ | Ground state |
| $\alpha$ | Fine structure constant |
| $\omega, \omega'$ | Frequency of incident and scattered photons |
| $E$ | Energy of Auger electron |
| $\mathbf{k}, \mathbf{k}'$ | Momentum of incident and scattered photons |
| $\mathbf{q}$ | Transferred momentum $\mathbf{k}' - \mathbf{k}$ |
| $\mathbf{e}, \mathbf{e}'$ | Polarization vector of incident and scattered photons |
| $\mathbf{p}$ | Momentum of electron |
| $\varepsilon_\nu$ | Vibrational energy |
| $\mathbf{d}_{ij}$ | Transition dipole moment |
| $R_{fi}/\mathcal{R}_{fi}$ | Anisotropy parameter |
| $M$ | Nuclear mass |
| $H$ | Hamiltonian |
| $F$ | Scattering amplitude |
| $\sigma(\omega', \omega)$ | RIXS cross section |
| $\sigma(E, \omega)$ | RAS cross section |
| $\Omega$ | Detuning of $\omega$ from resonance |
| $\Gamma$ | Lifetime broadening of core-excited state |
| $\mathbf{G}$ | Reciprocal lattice vector |

| | |
|---|---|
| $\theta$ | Angle between $\mathbf{e}$ and $\mathbf{e}'$ |
| $\chi$ | Angle between $\mathbf{e}$ and $\mathbf{k}'$ |
| $\Theta$ | Angle between $\mathbf{k}$ and $\mathbf{k}'$ |
| $\mathbf{s}$ | Spin operator $\boldsymbol{\sigma}/2$ |
| $\boldsymbol{\sigma}$ | Vector of Pauli matrices |
| $r_\circ$ | Classical electron radius |
| $R$ | Interatomic distance |
| $\mathcal{D}$ | Doppler shift |
| $\mathbf{w}$ | Angular velocity |
| 1D | One-dimensional |
| ASE | Amplified spontaneous emission |
| BO | Born-Oppenheimer (approximation) |
| CI | Configuration interaction |
| CT | Charge transfer |
| FC | Franck-Condon (factor) |
| HB | Hydrogen bond |
| HDL | High-density liquid |
| HHG | High-harmonic generation |
| HF | Hartree-Fock |
| JT | Jahn-Teller (effect) |
| IR | Infrared |
| KH | Kramers-Heisenberg (equation) |
| LVI | Life-time vibrational interference |
| MD | Molecular dynamics |
| MO | Molecular orbital |
| NIXS | Non-resonant inelastic X-ray scattering |
| PEC | Potential energy curve |
| RAS | Resonant Auger scattering |
| RIXS | Resonant inelastic X-ray scattering |

| | |
|---|---|
| SACLA | SPring-8 Angstrom Compact free electron LAser |
| SASE | Self-amplified spontaneous emission |
| SF | Superfluorescence |
| SHG | Second harmonic generation |
| SR | Superradiance |
| SRIXS | Stimulated RIXS |
| TM | Transition metal |
| TOF | Time-of-flight mass spectroscopy |
| tr-RIXS | Time-resolved RIXS |
| VC | vibronic coupling |
| VSA | Vibrational scattering anisotropy |
| XAS | X-ray absorption spectroscopy |
| XPS | X-ray photoelectron spectroscopy |
| XES | X-ray emission spectroscopy |
| XFEL | X-ray Free-Electron Laser |
| YDSE | Young's double-slit experiment |

## ACKNOWLEDGMENTS

# REFERENCES

Achkar, A J, R. Sutarto, X. Mao, F. He, A. Frano, S. Blanco-Canosa, M. Le Tacon, G. Ghiringhelli, L. Braicovich, M. Minola, M. Moretti Sala, C. Mazzoli, R. Liang, D. A. Bonn, W. N. Hardy, B. Keimer, G. A. Sawatzky, and D. G. Hawthorn (2012), "Distinct charge orders in the planes and chains of ortho-III-ordered $YBa_2Cu_3O_{6+\delta}$ superconductors identified by resonant elastic x-ray scattering," Phys. Rev. Lett. **109**, 167001.

Adachi, J, N. Kosugi, and A. Yagishita (2005), "Symmetry-resolved soft x-ray absorption spectroscopy: Its application to simple molecules," J. Phys. B: At. Mol. Opt. Phys. **38**, R127.

Afanas'ev, A M, and Yu. Kagan (1965), "Radiation of a system of excited nuclei in a crystal," JETP Lett. **2**, 81–83.

Aidas, K, K. V. Mikkelsen, B. Mennucci, and J. Kongsted (2011), "Fluorescence and phosphorescence of acetone in neat liquid and aqueous solution studied by QM/MM and PCM approaches," Int. J. Quantum Chem. **111**, 1511–1520.

Allen, L, and J. H. Eberly (1987), *Optical Resonance and Two-level Atoms* (Dover Publications Inc, New York).

Amann, J, W. Berg, V. Blank, F.-J. Decker, Y. Ding, P. Emma, Y. Feng, J. Frisch, D. Fritz, J. Hastings, Z. Huang, J. Krzywinski, R. Lindberg, H. Loos, A. Lutman, H.-D. Nuhn, D. Ratner, J. Rzepiela, D. Shu, Yu. Shvyd'ko, S. Spampinati, S. Stoupin, S. Terentyev, E. Trakhtenberg, D. Walz, J. Welch, J. Wu, A. Zholents, and D. Zhu (2012), "Demonstration of self-seeding in a hard-x-ray free-electron laser," Nat. Photonics **6**, 693–698.

Amann-Winkel, K, R. Böhmer, F. Fujara, C. Gainaru, B. Geil, and T. Loerting (2016), "Colloquium: Water's controversial glass transitions," Rev. Mod. Phys. **88**, 011002.

Ament, L J P, G. Ghiringhelli, M. Moretti Sala, L. Braicovich, and J. van den Brink (2009), "Theoretical demonstration of how the dispersion of magnetic excitations in cuprate compounds can be determined using resonant inelastic x-ray scattering," Phys. Rev. Lett. **103**, 117003.

Ament, L J P, M. van Veenendaal, T. P. Devereaux, J. P. Hill, and J. van den Brink (2011), "Resonant inelastic x-ray scattering studies of elementary excitations," Rev. Mod. Phys. **83**, 705.

Anderson, P W (1961), "Localized Magnetic States in Metals," Phys. Rev. **124**, 41.

Argenti, L, T D Thomas, E Plésiat, X-J Liu, C Miron, T Lischke, G Prümper, K Sakai, T Ouchi, R Püttner, V Sekushin, T Tanaka, M Hoshino, H Tanaka, P Decleva, K Ueda, and F Martín

(2012), "Double-slit experiment with a polyatomic molecule: vibrationally resolved C1s photo-electron spectra of acetylene," New J. Phys. **14**, 033012.

Auer, B M, and J. L. Skinner (2008), "IR and Raman spectra of liquid water: Theory and interpretation," J. Chem. Phys. **128**, 224511.

Baba, M, I. Hanazaki, and U. Nagashima (1985), "The $S_1(n, \pi^*)$ states of acetaldehyde and acetone in supersonic nozzle beam: Methyl internal rotation and C=O out-of-plane wagging," J. Chem. Phys. **82**, 3938–3947.

Baev, A, F. Gel'mukhanov, P. Sałek, H. Ågren, K. Ueda, A. de Fanis, K. Okada, and S. Sorensen (2002), "Doppler interference in dissociative resonant photoemission," Phys. Rev. A **66**, 022509.

Bagger, A, T. Haarman, A. P. Molin, P. G. Moses, H. Ishii, N. Hiraoka, Y.-H. Wu, K.-D. Tsuei, I. Chorkendorff, and F. de Groot (2017), "1s2p resonant inelastic x-ray scattering combined dipole and quadrupole analysis method," J. Synchrotron Radiat. **24**, 296–301.

Bakker, H J, and J. L. Skinner (2010), "Vibrational spectroscopy as a probe of structure and dynamics in liquid water," Chem. Rev **110**, 1498–1517.

Bao, Z, R. F. Fink, O. Travnikova, D. Céolin, S. Svensson, and M. N. Piancastelli (2008), "Detailed theoretical and experimental description of normal Auger decay in $O_2$," J. Phys. B: At. Mol. Opt. Phys. **41**, 125101.

Barletta, Paolo, Sergei V. Shirin, Nikolai F. Zobov, Oleg L. Polyansky, Jonathan Tennyson, Edward F. Valeev, and Attila G. Császár (2006), "CVRQD ab initio ground-state adiabatic potential energy surfaces for the water molecule," J. Chem. Phys. **125** (20), 204307.

Bednorz, J G, and K. A. Müller (1986), "Possible high $T_C$ superconductivity in the Ba-La-Cu-O system," Z. Phys. B. **64**, 189–193.

Bencivenga, F, R. Cucini, F. Capotondi, A. Battistoni, R. Mincigrucci, E. Giangrisostomi, A. Gessini, M. Manfredda, I. P. Nikolov, E. Pedersoli, E. Principi, C. Svetina, P. Parisse, F. Casolari, M. B. Danailov, M. Kiskinova, and C. Masciovecchio (2015), "Four-wave mixing experiments with extreme ultraviolet transient gratings," Nature **520**, 205–208.

Benkert, A, F. Meyer, D. Hauschild, M. Blum, W. Yang, R. G. Wilks, M. Bär, F. Reinert, C. Heske, and L. Weinhardt (2016), "Isotope effects in the resonant inelastic soft x-ray scattering maps of gas-phase methanol," J. Phys. Chem. A **120**, 2260–2267.

Bertie, J E, and Z. Lan (1996), "Infrared intensities of liquids XX: The intensity of the oh stretching band of liquid water revisited, and the best current values of the optical constants of $H_2O$ (l) at

25°C between 15,000 and 1 cm$^{-1}$," Appl. Spectrosc. **50**, 1047–1057.

Beye, M, F. Hennies, M. Deppe, E. Suljoti, M. Nagasono, W. Wurth, and A. Föhlisch (2009), "Dynamics of electron-phonon scattering: Crystal- and angular-momentum transfer probed by resonant inelastic x-ray scattering," Phys. Rev. Lett. **103**, 237401.

Beye, M, F. Sorgenfrei, W. F. Schlotter, W. Wurth, and A. Föhlisch (2010), "The liquid-liquid phase transition in silicon revealed by snapshots of valence electrons," Proc. Natl. Acad. Sci. U.S.A. **107**, 16772–16776.

Beye, M, Ph. Wernet, C. Schüßler-Langeheine, and A. Föhlisch (2013), "Time resolved resonant inelastic x-ray scattering: A supreme tool to understand dynamics in solids and molecules," J. Electron Spectros. Relat. Phenomena **188**, 172–182.

Bisogni, V, K. Wohlfeld, S. Nishimoto, C. Monney, J. Trinckauf, K. Zhou, R. Kraus, K. Koepernik, C. Sekar, V. Strocov, B. Büchner, T. Schmitt, J. van den Brink, and J. Geck (2015), "Orbital control of effective dimensionality: From spin-orbital fractionalization to confinement in the anisotropic ladder system $CaCu_2O_3$," Phys. Rev. Lett. **114**, 096402.

Björneholm, O (2001), "Direct and indirect methods for studying the energetics and dynamics of the Auger Doppler effect in femtosecond ultra-fast dissociation," J. Chem. Phys. **115**, 4139.

Björneholm, O, M. Bässler, A. Ausmees, I. Hjelte, R. Feifel, H. Wang, C. Miron, M. N. Piancastelli, S. Svensson, S. L. Sorensen, F. Gel'mukhanov, and H. Ågren (2000), "Doppler splitting of in-flight Auger decay of dissociating oxygen molecules: The localization of delocalized core holes," Phys. Rev. Lett. **84**, 2826–2829.

Björneholm, O, S. Sundin, S. Svensson, R. R. T. Marinho, A. Naves de Brito, F. Gel'mukhanov, and H. Ågren (1997), "Femtosecond dissociation of core-excited HCl monitored by frequency detuning," Phys. Rev. Lett. **79**, 3150–3153.

Błachucki, W, J. Szlachetko, J. Hoszowska, J.-Cl. Dousse, Y. Kayser, M. Nachtegaal, and J. Sá (2014), "High energy resolution off-resonant spectroscopy for x-ray absorption spectra free of self-absorption effects," Phys. Rev. Lett. **112**, 173003.

Blackburn, E, J. Chang, A. H. Said, B. M. Leu, R. Liang, D. A. Bonn, W. N. Hardy, E. M. Forgan, and S. M. Hayden (2013), "Inelastic x-ray study of phonon broadening and charge-density wave formation in ortho-II-ordered $YBa_2Cu_3O_{6.54}$," Phys. Rev. B **88**, 054506.

Blanco-Canosa, S, A. Frano, T. Loew, Y. Lu, J. Porras, G. Ghiringhelli, M. Minola, C. Mazzoli, L. Braicovich, E. Schierle, E. Weschke, M. Le Tacon, and B. Keimer (2013), "Momentum-

dependent charge correlations in $YBa_2Cu_3O_{6+\delta}$ superconductors probed by resonant x-ray scattering: Evidence for three competing phases," Phys. Rev. Lett. **7**, 187001.

Blum, M, M. Odelius, L. Weinhardt, S. Pookpanratana, M. Bär, Y. Zhang, O. Fuchs, W. Yang, E. Umbach, and C. Heske (2012), "Ultra-fast proton dynamics in aqueous amino acid solutions studied by resonant inelastic soft x-ray scattering," J. Phys. Chem. B **116**, 13757–13764.

Blume, M (1985), "Magnetic scattering of x-rays," J. Appl. Phys. **57**, 3615–3618.

Bohr, N (1983), "Discussion with Einstein on epistemological problems in atomic physics," in *Quantum Theory and Measurement*, edited by J. A. Wheeler and W. H. Zurek (Princeton University Press, Princeton) pp. 9–49.

Bokarev, S I, and O. Kühn (2020), "Theoretical x-ray spectroscopy of transition metal compounds," WIREs Comput. Mol. Sci. **10**, e1433.

Bonifacio, R, and L. A. Lugiato (1975), "Cooperative radiation processes in two-level systems: super fluorescence." Phys. Rev. A **11**, 1507–1521.

Boyd, R W (2010), *Nonlinear Optics* (Academic Press, Elsevier, Singapore).

Braicovich, L, M. Minola, G. Dellea, M. L. Tacon, M. M. Sala, C. Morawe, J.-C. Peffen, R. Supruangnet, F. Yakhou, G. Ghiringhelli, and N. B. Brookes (2014), "The simultaneous measurement of energy and linear polarization of the scattered radiation in resonant inelastic soft x-ray scattering," Rev. Sci. Instrum **85**, 115104.

Brena, B, D. Nordlund, M. Odelius, H. Ogasawara, A. Nilsson, and L. G. M. Pettersson (2004), "Ultrafast molecular dissociation of water in ice," Phys. Rev. Lett. **93**, 148302.

van den Brink, J (2016), "Resonant inelastic x-ray scattering on elementary excitations," in *Quantum Materials: Experiments and Theory*, Modeling and Simulation, Vol. 6, edited by Eva Pavarini, Erik Koch, Jeroen van den Brink, and George Sawatzky, Chap. 12 (Forschungszentrum Jülich, Jülich) pp. 12.1–12.31.

Brookes, N B, F. Yakhou-Harris, K. Kummer, A. Fondacaro, J. C. Cezara, D. Betto, E. Velez-Forta, A. Amorese, G. Ghiringhelli, L. Braicovich, R. Barretta, G Berruyer, F. Cianciosi, L. Eybert, P. Marion, P. van der Linden, and L. Zhang (2018), "The beamline ID32 at the ESRF for soft x-ray high energy resolution resonant inelastic X-ray scattering and polarisation dependent X-ray absorption spectroscopy," Nucl. Instrum. Methods. Phys. Res. B **903**, 175–192.

Brownell, J H, X. Lu, and S. R. Hartmann (1995), "Yoked Superfluorescence," Phys. Rev. Lett. **75**, 3265–3268.

Brühwiler, P A, O. Karis, and N. Mårtensson (2002), "Charge-transfer dynamics studied using resonant core spectroscopies," Rev. Mod. Phys. **74**, 703–740.

van Bürck, U, R. L. Mössbauer, E. Gerdau, R. Rüffer, R. Hollatz, G. V. Smirnov, and J. P. Hannon (1987), "Nuclear Bragg scattering of synchrotron radiation with strong speedup of coherent decay, measured on antiferromagnetic $^{57}FeBO_3$," Phys. Rev. Lett. **59**, 355–358.

Burnham, D C, and R. Y. Chiao (1969), "Coherent resonance fluorescence excited by short light pulses," Phys. Rev. **188**, 667–675.

Calegari, F, D. Ayuso, A. Trabattoni, L. Belshaw, S. De Camillis, S. Anumula, F. Frassetto, L. Poletto, A. Palacios, P. Decleva, J. B. Greenwood, F. Martín, and M. Nisoli (2014), "Ultrafast electron dynamics in phenylalanine initiated by attosecond pulses," Science **346** (6207), 336–339.

Callegari, C, A.N. Grum-Grzhimailo, K.L. Ishikawa, K.C. Prince, G. Sansone, and K. Ueda (2021), "Atomic, molecular and optical physics applications of longitudinally coherent and narrow bandwidth Free-Electron Lasers," Phys. Rep. **000**, 00.

Canton, S E, E. Pleśiat, J. D. Bozek, B. S. Rude, P. Decleva, and F. Martin (2011), "Direct observation of Young's double-slit interferences in vibrationally resolved photoionization of diatomic molecules," Proc. Natl. Acad. Sci. U. S. A **108**, 7302–7306.

Cao, Y, D. G. Mazzone, D. Meyers, J. P. Hill, X. Liu, S. Wall, and M. P. M. Dean (2019), "Ultrafast dynamics of spin and orbital correlations in quantum materials: an energy- and momentum-resolved perspective," Phil. Trans. R. Soc. A **377**, 20170480.

Carleer, M, A. Jenouvrier, A.-C. Vandaele, P. F. Bernath, M. F. Mérienne, R. Colin, N. F. Zobov, Oleg L. Polyansky, Jonathan Tennyson, and V. A. Savin (1999), "The near infrared, visible, and near ultraviolet overtone spectrum of water," J. Chem. Phys. **111** (6), 2444–2450.

Carlisle, J A, E. L. Shirley, E. A. Hudson, L. J. Terminello, T. A. Callcott, J. J. Jia, D. L. Ederer, R. C. C. Perera, and F. J. Himpse (1995), "Probing the graphite band structure with resonant soft-x-ray fluorescence," Phys. Rev. Lett. **74**, 1234.

Carlisle, J A, E. L. Shirley, L. J. Terminello, J. J. Jia, T. A. Callcott, D. L. Ederer, R. C. C. Perera, and F. J. Himpsel (1999), "Band-structure and core-hole effects in resonant inelastic soft-x-ray scattering: Experiment and theory," Phys. Rev. B **59**, 7433.

Carniato, S, R. Guillemin, W. C. Stolte, L. Journel, R. Taïeb, D. W. Lindle, and M. Simon (2009), "Experimental and theoretical investigation of molecular field effects by polarization-resolved resonant inelastic x-ray scattering," Phys. Rev. A **80**, 032513.

Carniato, S, P. Selles, L. Journel, R. Guillemin, W. C. Stolte, L. El Khoury, T. Marin, F. Gel'mukhanov, D. W. Lindle, and M. Simon (2012), "Thomson-resonant interference effects in elastic x-ray scattering near the Cl K edge of HCl," J. Chem. Phys. **137**, 094311.

Carra, P, M. Fabrizio, and B. T. Thole (1995), "High resolution x-ray resonant Raman scattering," Phys. Rev. Lett. **74**, 3700–3703.

Caupin, F, and M. A. Anisimov (2019), "Thermodynamics of supercooled and stretched water: Unifying two-structure description and liquid-vapor spinodal," J. Chem. Phys. **151**, 034503.

Caux, J-S, and R. Hagemans (2006), "The four-spinon dynamical structure factor of the Heisenberg chain," J. Stat. Mech. **2006**, 12013.

Céolin, D, J.-C. Liu, V. Vaz da Cruz, H. Ågren, L. Journel, R. Guillemin, T. Marchenko, R. K. Kushawaha, M. N. Piancastelli, R. Püttner, M. Simon, and F. Gel'mukhanov (2019), "Recoil-induced ultrafast molecular rotation probed by dynamical rotational Doppler effect," Proc. Natl. Acad. Sci. U.S.A. **116**, 4877–4882.

Cesar, A, F. Gel'mukhanov, Y. Luo, H. Ågren, P. Skytt, P. Glans, J. Guo, K. Gunnelin, and J. Nordgren (1997), "Resonant x-ray scattering beyond the Born-Oppenheimer approximation: Symmetry breaking in the oxygen resonant x-ray emission spectrum of carbon dioxide," J. Chem. Phys. **106**, 3439.

Chainani, A, A. Yamamoto, R. Eguchi M. Matsunami, M. Taguchi, Y. Takata, S. Shin H. Takagi, Y. Nishino, M. Yabashi, K. Tamasaku, and T. Ishikawa (2013), "Quantifying covalency and metallicity in correlated compounds undergoing metal-insulator transition," Phys. Rev. B **87**, 045108.

Chaix, L, G. Ghiringhelli, Y. Y. Peng, M. Hashimoto, B. Moritz, K. Kummer, N. B. Brookes, Y. He, S. Chen, S. Ishida, Y. Yoshida, H. Eisaki, M. Salluzzo, L. Braicovich, Z.-X. Shen, T. P. Devereaux, and W.-S. Lee (2017), "Dispersive charge density wave excitations in $Bi_2Sr_2CaCu_2O_{8+\delta}$," Nat. Phys. **13**, 952.

Chandler, D (2016), "Metastability and no criticality," Nature **531**, E1–E2.

Chang, J, E. Blackburn, A. T. Holmes, N. B. Christensen, J. Larsen, J. Mesot, R. Liang, D. A. Bonn, W. N. Hardy, A. Watenphul, M. v. Zimmermann, E. M. Forgan, and S. M. Hayden (2012), "Direct observation of competition between superconductivity and charge density wave order in $YBa_2Cu_3O_{6.67}$," Nat. Phys. **8**, 871.

Chen, C-C, M. van Veenendaal, T. P. Devereaux, and K. Wohlfeld (2015), "Fractionalization, entanglement, and separation: Understanding the collective excitations in a spin-orbital chain," Phys. Rev. B **91**, 165102.

Chen, W, X. Wu, and R. Car (2010), "X-ray absorption signatures of the molecular environment in water and ice," Phys. Rev. Lett. **105**, 017802.

Chen, Y, Y. Wang, C. Jia, B. Moritz, A. M. Shvaika, J. K. Freericks, and T. P. Devereaux (2019), "Theory for time-resolved resonant inelastic x-ray scattering," Phys. Rev. B **99**, 104306.

Chen, Z, D. J. Higley, M. Beye, M. Hantschmann, V. Mehta, O. Hellwig, A. Mitra, S. Bonetti, M. Bucher, S. Carron, T. Chase, E. Jal, R. Kukreja, T. Liu, A. H. Reid, G. L. Dakovski, A. Föhlisch, W. F. Schlotter, H. A. Dürr, and J. Stöhr (2018), "Ultrafast self-induced x-ray transparency and loss of magnetic diffraction," Phys. Rev. Lett. **121**, 137403.

Chiuzbăian, G S, T. Schmitt, M. Matsubara, A. Kotani, G. Ghiringhelli, C. Dallera, A. Tagliaferri, L. Braicovich, V. Scagnoli, N. B. Brookes, U. Staub, and L. Patthey (2008), "Combining M- and L-edge resonant inelastic x-ray scattering for studies of 3d transition metal compounds," Phys. Rev. B **78**, 245102.

Chubar, O, G. Geloni, V. Kocharyan, A. Madsen, E. Saldin, S. Serkez, Y. Shvyd'ko, and J. Sutter (2016), "Ultra-high-resolution inelastic x-ray scattering at high-repetition-rate self-seeded x-ray free-electron lasers," J. Synchrotron Radiat. **23**, 410–424.

Chumakov, A I, A. Q. R. Baron, I. Sergueev, C. Strohm, O. Leupold, Y. Shvyd'ko, G. V. Smirnov, R. Rüffer, Y. Inubushi, M. Yabashi, K. Tono, T. Kudo, and T. Ishikawa (2018), "Superradiance of an ensemble of nuclei excited by a free electron laser," Nat. Phys. **14**, 261–264.

Clark, G N I, G. L. Hura, J. Teixeira, A. K. Soper, and T. Head-Gordon (2010), "Small-angle scattering and the structure of ambient liquid water," Proc. Natl. Acad. Sci. U.S.A. **107**, 14003–14007.

Cohen, H D, and U. Fano (1966), "Interference in the photo-ionization of molecules," Phys. Rev. **150**, 30.

Coheur, P-F, S. Fally, M. Carleer, C. Clerbaux, R. Colin, A. Jenouvrier, M.-F. Mérienne, C. Hermans, and A. C. Vandaele (2002), "New water vapor line parameters in the 26000-13000 $cm^{-1}$ region," J. Quant. Spectrosc. Radiat. Transfer **74**, 493–510.

Comin, R, and A. Damascelli (2016), "Studies of charge order in cuprates," Annu. Rev. Condens. Matter Phys. **7**, 36–405.

Comin, R, R. Sutarto, E. H. da Silva Neto, L. Chauviere, R. Liang, W. N. Hardy, D. A. Bonn, F. He, G. A. Sawatzky, and A. Damascelli (2015), "Broken translational and rotational symmetry via charge stripe order in underdoped $YBa_2Cu_3O_{6+y}$," Science **347**, 1335.

Couto, R C, M. Guarise, A. Nicolaou, N. Jaouen, G. S. S. Chiuzbăian, J. Lüning, V. Ekholm, J.-E. Rubensson, C. Såthe, F. Hennies, F. F. Guimarães, H. Ågren, F. Gel'mukhanov, L. Journel, M. Simon, and V. Kimberg (2016a), "Coupled electron-nuclear dynamics in resonant $1\sigma \rightarrow 2\pi$ x-ray Raman scattering of CO molecules," Phys. Rev. A **93**, 032510.

Couto, R C, M. Guarise, A. Nicolaou, N. Jaouen, G. S. S. Chiuzbăian, J. Lüning, V. Ekholm, J.-E. Rubensson, C. Såthe, F. Hennies, V. Kimberg, F. F. Guimarães, H. Ågren, F. Gel'mukhanov, L. Journel, and M. Simon (2016b), "Anomalously strong two-electron one-photon x-ray decay transitions in CO caused by avoided crossing," Sci. Rep. **6**, 20947.

Couto, R C, V. Vaz da Cruz, E. Ertan, S. Eckert, M. Fondell, M. Dantz, B. Kennedy, T. Schmitt, A. Pietzsch, F. F. Guimarães, H. Ågren, F. Gel'mukhanov, M. Odelius, V. Kimberg, and A. Föhlisch (2017), "Selective gating to vibrational modes through resonant x-ray scattering," Nat. Commun. **8**, 14165.

Császár, A G, T. E. Mátyusa, Szidarovszky, L. Lodi, N. F. Zobov, S. V. Shirin, O. L. Polyansky, and J. Tennyson (2010), "First-principles prediction and partial characterization of the vibrational states of water up to dissociation," J. Quant. Spectrosc. Radiat. Transfer **111**, 1043–1064.

Das, L, F. Forte, R. Fittipaldi, C. G. . Fatuzzo, V. Granata, O. Ivashko, M. Horio, F. Schindler, Y. Dantz, M. Tseng, D. E. McNally, H. M. Rønnow, W. Wan, N. B. Christensen, J. Pelliciari, P. Olalde-Velasco, N. Kikugawa, T. Neupert, A. Vecchione, T. Schmitt, M. Cuoco, and J. Chang (2018), "Spin-orbital excitations in $Ca_2RuO_4$ revealed by resonant inelastic x-ray scattering," Phys. Rev. X **8**, 011048.

Das, S C, R. J. Green, J. Podder, T. Z. Regier, G. S. Chang, and A. Moewes (2013), "Band gap tuning in ZnO through Ni doping via spray pyrolysis," J. Phys. Chem. C **117(24)**, 12745–12753.

Dean, M P M, Y. Cao, X. Liu, S. Wall, D. Zhu, R. Mankowsky, V. Thampy, X. M. Chen, J. G. Vale, D. Casa, Jungho Kim, A. H. Said, P. Juhas, R. Alonso-Mori, J. M. Glownia, A. Robert, J. Robinson, M. Sikorski, S. Song, M. Kozina, H. Lemke, L. Patthey, S. Owada, T. Katayama, M. Yabashi, Yoshikazu Tanaka, T. Togashi, J. Liu, C. Rayan Serrao, B. J. Kim, L. Huber, C.-L. Chang, D. F. McMorrow, M. Först, and J. P. Hill (2016), "Ultrafast energy- and momentum-resolved dynamics of magnetic correlations in the photo-doped Mott insulator $Sr_2IrO_4$," Nat.

Mater. **15**, 601–605.

Demekhin, Ph V, I. D. Petrov, V. L. Sukhorukov, W. Kielich, A. Knie, H. Schmoranzer, and A. Ehresmann (2010a), "Strong interference effects in the angularly resolved Auger decay and fluorescence emission spectra of the core-excited NO molecule," J. Phys. B: At. Mol. Opt. Phys. **43**, 165103.

Demekhin, Ph V, I. D. Petrov, V. L. Sukhorukov, W. Kielich, A. Knie, H. Schmoranzer, and A. Ehresmann (2010b), "Symmetry forbidden electronic state interference observed in angularly resolved $NO^+$ ($A^1\Pi$) deexcitation spectra of the $N^*O$ ($2\sigma^{-1}2\pi^2$) resonance," Phys. Rev. Lett. **104**, 243001.

Demekhin, Ph V, I. D. Petrov, T. Tanaka, M. Hoshino, H. Tanaka, K. Ueda, W. Kielich, and A. Ehresmann (2010c), "Large impact of the weak direct photoionization on the angularly resolved $CO^+(A^2\Pi)$ de-excitation spectra of the $CO^*(1\sigma^{-1}2\pi)$ resonance," J. Phys. B: At. Mol. Opt. Phys. **43**, 065102.

Dicke, R H (1954), "Coherence in spontaneous radiation processes," Phys. Rev. **93**, 99.

Dirac, P A M (1927), "The quantum theory of the emission and absorption of radiation," Proceedings of The Royal Society A: Mathematical, Physical and Engineering Sciences **114**, 243–265.

Domcke, W, and L. S. Cederbaum (1978), "Electronic recoil effects in high-energy photoelectron spectroscopy," J. Electron Spectros. Relat. Phenomena **13**, 161–173.

Doniach, S, and E. H. Sondheimer (1998), *Green's functions for solid state physicists* (Imperial College Press, London).

Dressel, M (2018), "Advances in organic conductors and superconductors," Crystals **8**, 332.

Duris, J, S. Li, T. Driver, E. G. Champenois, J. P. MacArthur, A. A. Lutman, Z. Zhang, P. Rosenberger, J. W. Aldrich, R. Coffee, G. Coslovich, F. J. Decker, J. M. Glownia, G. Hartmann, W. Helml, J. Kamalov, A.and Knurr, J. Krzywinski, M. F. Lin, J. P. Marangos, M. Nantel, A. Natan, J. T. O'Neal, N. Shivaram, P. Walter, A. L. Wang, J. J. Welch, T. J.A. Wolf, J. Z. Xu, M. F. Kling, P. H. Bucksbaum, A. Zholents, Z. Huang, J. P. Cryan, and A. Marinelli (2020), "Tunable isolated attosecond X-ray pulses with gigawatt peak power from a free-electron laser," Nat. Photonics **14** (1), 30–36, 1906.10649.

Eckert, S, J. Norell, P. S. Miedema, M. Beye, M. Fondell, W. Quevedo, B. Kennedy, M. Hantschmann, A. Pietzsch, B. E. Van Kuiken, M. Ross, M. P. Minitti, S. P. Moeller, W. F. Schlotter, M. Khalil, M. Odelius, and A. Föhlisch (2017), "Ultrafast independent N-H and N-C

bond deformation investigated with resonant inelastic x-ray scattering," Angew. Chem. Int. Ed **56**, 6088–6092.

Eckert, S, V. Vaz da Cruz, F. Gel'mukhanov, E. Ertan, N. Ignatova, R. C. Couto S. Polyutov, M. Fondell, M. Dantz, B. Kennedy, T. Schmitt, A. Pietzsch, M. Odelius, and A. Föhlisch (2018), "One-dimensional cuts through multidimensional potential-energy surfaces by tunable x-rays," Phys. Rev. A **97**, 053410.

Efetov, K B, and A. I. Larkin (1976), "Correlation functions in one-dimensional systems with a strong interaction," Sov. Phys.-JETP **42**, 390–396.

Eichmann, U, H. Rottke, S. Meise, J.-E. Rubensson, J. Söderström, M. Agåker, C. Såthe, M. Meyer, T. M. Baumann, R. Boll, A. De Fanis, P. Grychtol, M. Ilchen, T. Mazza, J. Montano, V. Music, Y. Ovcharenko, D. E. Rivas, S. Serkez, R. Wagner, and S. Eisebitt (2020), "Photon-recoil imaging: Expanding the view of nonlinear x-ray physics," Science **369**, 1630–1633.

Ekholm, V, G. S. Chiuzbăian, C. Såthe, A. Nicolaou, M. Guarise, M. Simon, N. Jaouen, J. M. Lüning, C. F. Hague, F. K. H. Gel'mukhanov, M. Odelius, O. Björneholm, and J.-E. Rubensson (2020), "Core-hole localization and ultra-fast dissociation in $SF_6$," J. Phys. B: At. Mol. Opt. Phys. **53**, 185101.

Elfimov, I S, V. I. Anisimov, and G. A. Sawatzky (1999), "Orbital ordering, Jahn-Teller distortion, and anomalous x-ray scattering in manganates," Phys. Rev. Lett. **82**, 4264–4267.

Elnaggar, H, R.-P. Wang, S. Lafuerza, E. Paris, Y. Tseng, D. McNally, A. Komarek, M. Haverkort, M. Sikora, T. Schmitt, and F. M. F. de Groot (2019), "Magnetic contrast at spin-flip excitations: An advanced x-ray spectroscopy tool to study magnetic-ordering," ACS Appl. Mater. Interfaces **11**, 36213–36220.

Elnaggar, H, R.P. Wang, M. Ghiasi, M. Yañez, M. U. Delgado-Jaime, M. H. Hamed, A. Juhin, S. S. Dhesi, and F. de Groot (2020), "Probing the local distortion of Fe sites in $Fe_3O_4$ thin films using enhanced symmetry selection in XMLD," Phys. Rev. Mater. **4**, 024415.

Emma, P, R. Akre, J. Arthur, R. Bionta, C. Bostedt, J. Bozek, A. Brachmann, P. Bucksbaum, R. Coffee, F.-J. Decker, Y. Ding, D. Dowell, S. Edstrom, A. Fisher, J. Frisch, S. Gilevich, J. Hastings, G. Hays, Ph. Hering, Z. Huang, R. Iverson, H. Loos, M. Messerschmidt, A. Miahnahri, S. Moeller, H.-D. Nuhn, G. Pile, D. Ratner, J. Rzepiela, D. Schultz, T. Smith, P. Stefan, H. Tompkins, J. Turner, J. Welch, W. White, J. Wu, G. Yocky, and J. Galayda (2010), "First lasing and operation of an ångstrom-wavelength free-electron laser," Nat. Photonics **4**, 641–647.

English, N J, P. G. Kusalik, and J. S. Tse (2013), "Density equalisation in supercooled high- and low-density water mixtures," J. Chem. Phys. **139**, 084508.

English, N J, and J. S. Tse (2011), "Density fluctuations in liquid water," Phys. Rev. Lett. **106**, 037801.

Ertan, E, M. Lundberg, L. K. Sørensen, and M. Odelius (2020), "Setting the stage for theoretical x-ray spectra of the $H_2S$ molecule with multi-configurational quantum chemical calculations of the energy landscape," J. Chem. Phys. **152**, 094305.

Ertan, E, V. Savchenko, N. Ignatova, V. Vaz da Cruz, R. C. Couto, S. Eckert, M. Fondell, M. Dantz, B. Kennedy, T. Schmitt, A. Pietzsch, A. Föhlisch, F. Gel'mukhanov, M. Odelius, and V. Kimberg (2018), "Ultrafast dissociation features in RIXS spectra of the water molecule," Phys. Chem. Chem. Phys. **20**, 14384–14397.

Fabrizio, M, M. Altarelli, and M. Benfatto (1998), "X-ray resonant scattering as a direct probe of orbital ordering in transition-metal oxides," Phys. Rev. Lett. **80**, 3400–3403.

Faddeev, L D, and L. A. Takhtajan (1981), "What is the spin of a spin wave?" Phys. Lett. A **81**, 375.

Fatale, S, C. G. Fatuzzo, P. Babkevich, N. E. Shaik, J. Pelliciari, X. Lu, D. E. McNally, T. Schmitt, A. Kikkawa, Y. Taguchi, Y. Tokura, B. Normand, H. M. Rønnow, and M. Grioni (2017), "Electronic and magnetic excitations in the half-stuffed Cu-O planes of $Ba_2Cu_3O_4Cl_2$ measured by resonant inelastic x-ray scattering," Phys. Rev. B **96**, 115149.

Feifel, R, F. Burmeister, P. Sałek, M. N. Piancastelli, M. Bässler, S. L. Sorensen, C. Miron, H. Wang, I. Hjelte, O. Björneholm, A. Naves de Brito, F. Kh. Gel'mukhanov, H. Ågren, and S. Svensson (2000), "Observation of a continuum-continuum interference hole in ultrafast dissociating core-excited molecules," Phys. Rev. Lett. **85**, 3133.

Feifel, R, F. Gel'mukhanov, A. Baev, H. Ågren, M. N. Piancastelli, M. Bässler, C. Miron, S. L. Sorensen, A. Naves de Brito, O. Björneholm, L. Karlsson, and S. Svensson (2002), "Interference quenching of $\nu'' = 1$ vibrational line in resonant photoemission of $N_2$: A possibility to obtain geometrical information on the core-excited state," Phys. Rev. Lett. **89**, 103002.

Feifel, R, Y. Velkov, V. Carravetta, C. Angeli, R. Cimiraglia, P. Sałek, F. Gel'mukhanov, S. L. Sorensen, M. N. Piancastelli, A. De Fanis, K. Okada, M. Kitajima, T. Tanaka, H. Tanaka, and K. Ueda (2008), "X-ray absorption and resonant Auger spectroscopy of $O_2$ in the vicinity of the $O\ 1s \rightarrow \sigma^*$ resonance: Experiment and theory," J. Chem. Phys. **128**, 064304.

Felicíssimo, V C, F. F. Guimarães, and F. Gel'mukhanov (2005), "Enhancement of the recoil effect in x-ray photoelectron spectra of molecules driven by a strong IR field," Phys.Rev.A **72**, 023414.

Fischer, H E, A. C. Barnes, and P. S. Salmon (2006), "Neutron and x-ray diffraction studies of liquids and glasses," Rep. Prog. Phys. **69**, 233–299.

Forsberg, J, Johan Gråsjö, B. Brena, J. Nordgren, Laurent-C. Duda, and J.-E. Rubensson (2009), "Angular anisotropy of resonant inelastic soft x-ray scattering from liquid water," Phys. Rev. B **79**, 132203.

Fuchs, O, M. Zharnikov, L. Weinhardt, M. Blum, M. Weigand, Y. Zubavichus, M. Bär, F. Maier J. D. Denlinger, C. Heske, M. Grunze, and E. Umbach (2008), "Isotope and temperature effects in liquid water probed by x-ray absorption and resonant x-ray emission spectroscopy," Phys. Rev. Lett. **100**, 027801.

Gallo, E, and P. Glatzel (2014), "Valence to core x-ray emission spectroscopy," Adv. Mater. **26** (46), 7730–7746.

Ganesh, P, and M. Widom (2009), "Liquid-liquid transition in supercooled silicon determined by first-principles simulation," Phys. Rev. Lett. **102**, 075701.

Gao, X, D. Casa, J. Kim, T. Gog, C. Li, and C. Burns (2016), "Toroidal silicon polarization analyzer for resonant inelastic x-ray scattering," Rev. Sci. Instrum. **87**, 083107.

Gavrilyuk, S, Y.-P. Sun, S. Levin, H. Ågren, and F. Gel'mukhanov (2010), "Recoil splitting of x-ray-induced optical fluorescence," Phys. Rev. A **81**, 035401.

Gel'mukhanov, F, and H. Ågren (1994), "Resonant inelastic x-ray scattering with symmetry-selective excitation," Phys. Rev. A **49**, 4378.

Gel'mukhanov, F, and H. Ågren (1996a), "Raman, non-Raman, and anti-Raman dispersion in resonant x-ray scattering spectra of molecules," Phys. Rev. A **54**, 3960–3970.

Gel'mukhanov, F, and H. Ågren (1996b), "X-ray resonant scattering involving dissociative states," Phys. Rev. A **54**, 379.

Gel'mukhanov, F, and H. Ågren (1998a), "Channel interference in x-ray raman scattering: parity selection rules, dephasing and localization of core holes," J. Electron Spectros. Relat. Phenomena **93**, 31–37.

Gel'mukhanov, F, and H. Ågren (1998b), "Spectral features of resonant radiative x-ray Raman scattering in polymers and solids," Phys. Rev. B **57**, 2780–2792.

Gel'mukhanov, F, and H. Ågren (1999), "Resonant x-ray Raman scattering," Phys. Rep. **312**, 87.

Gel'mukhanov, F, H. Ågren, M. Neeb, J.-E. Rubensson, and A. Bringer (1996a), "Integral properties of channel interference in resonant x-ray scattering," Phys. Lett. A **211**, 101–108.

Gel'mukhanov, F, H. Ågren, and P. Sałek (1998a), "Doppler effects in resonant x-ray Raman scattering," Phys. Rev. A **57**, 2511–2526.

Gel'mukhanov, F, H. Ågren, S. Svensson, H. Aksela, and S. Aksela (1996b), "Theory of Auger spectra for molecular-field-split core levels," Phys. Rev. A **53**, 1379–1387.

Gel'mukhanov, F, V. Kimberg, X.-J. Liu, G. Prümper, T. Tanaka, M. Hoshino, H. Tanaka, and K. Ueda (2007), "Young's double-slit experiment using two-center core-level photoemission: Photoelectron recoil effects," J. Electron Spectros. Relat. Phenomena **265**, 156–158.

Gel'mukhanov, F, T. Privalov, and H. Ågren (1998b), "Channel interference in x-ray raman scattering: parity selection rules, dephasing and localization of core holes," J. Chem. Phys. **109**, 5060.

Gel'mukhanov, F, T. Privalov, and H. Ågren (1998c), "Soft and hard x-ray Raman scattering by oriented symmetrical molecules: Selection rules, interference, and dephasing mechanisms," J. Chem. Phys. **109**, 5060.

Gel'mukhanov, F, T. Privalov, and H. Ågren (2000), "Temperature dependence and Debye-Waller factors for resonant X-ray Raman scattering in solids," Phys. Rev. B **62**, 13996–14005.

Gel'mukhanov, F, P. Sałek, T. Privalov, and H. Ågren (1999), "Duration of x-ray raman scattering," Phys. Rev. A **59**, 380.

Gel'mukhanov, F Kh, and H. Ågren (1996c), "X-Ray Raman scattering involving electronic continuum resonances," J. Phys. B: At. Mol. Opt. Phys. **29**, 2751–2762.

Gel'mukhanov, F Kh, and L. N. Mazalov (1977), "Polarisation of the x-ray fluorescence of molecules," Opt. Spectrosc. (USSR) **42**, 371–374.

Gel'mukhanov, F Kh, L. N. Mazalov, and A. V. Kondratenko (1977a), "A theory of vibrational structure in the x-ray spectra of molecules," Chem. Phys. Lett. **46**, 133–137.

Gel'mukhanov, F Kh, L. N. Mazalov, and N. A. Shklyaeva (1976), "An interference effect in x-ray fluorescence spectra," Sov. Phys. JETP **42**, 1001–1005.

Gel'mukhanov, F Kh, L. N. Mazalov, and N. A. Shklyaeva (1977b), "Some features of x-ray fluorescence in metals near the absorption threshold," Sov. Phys. JETP **44**, 504.

Gel'mukhanov, F Kh, T. I. Privalov, and H. Ågren (1997a), "Collapse of vibrational structure in spectra of resonant x-ray Raman scattering," Phys. Rev. A **56**, 256.

Gel'mukhanov, F Kh, T. I. Privalov, and H. Ågren (1997b), "Restoration of selection rules in nonadiabatic resonant inelastic x-ray scattering," Sov. Phys. JETP **85**, 20–26.

Ghiringhelli, G, M. Le Tacon, M. Minola, S. Blanco-Canosa, C. Mazzoli, N. B. Brookes, G. M. De Luca, A. Frano, D. G. Hawthorn, F. He, T. Loew, M. M. Sala, D. C Peets, M. Salluzzo, E. Schierle, R. Sutarto, G. A. Sawatzky, E. Weschke, B. Keimer, and L. Braicovich (2012), "Long-range incommensurate charge fluctuations in $(Y,Nd)Ba_2Cu_3O_{6+x}$," Science **337**, 821.

Ghiringhelli, G, M. Matsubara, C. Dallera, F. Fracassi, R. Gusmeroli, A. Piazzalunga, A. Tagliaferri, N. B. Brookes, A. Kotani, and L. Braicovich (2005), "NiO as a test case for high resolution resonant inelastic soft x-ray scattering," J. Phys.: Condens. Matter **17(35)**, 5397.

Ghiringhelli, G, M. Matsubara, C. Dallera, F. Fracassi, A. Tagliaferri, N. B. Brookes, A. Kotani, and L. Braicovich (2006), "Resonant inelastic x-ray scattering of MnO: $L_{2,3}$ edge measurements and assessment of their interpretation," Phys. Rev. B **73(3)**, 035111.

Giamarchi, T (2016), "One-dimensional physics in the 21st century," Comptes Rendus Physique **17**, 322–331.

Giamarchi, T, and Oxford University Press (2004), *Quantum Physics in One Dimension*, International Series of Monogr (Clarendon Press).

Glans, P, K. Gunnelin, P. Skytt, J.-H. Guo, N. Wassdahl, J. Nordgren, F. Kh. Gel'mukhanov H. Ågren, T. Warwick, and Eli Rotenberg (1996a), "Resonant x-ray emission spectroscopy of molecular oxygen," Phys. Rev. Lett. **76**, 2448.

Glans, P, P. Skytt, K. Gunnelin, J.-H. Guo, and J. Nordgren (1996b), "Selectively excited x-ray emission spectra of $N_2$," J. Electron Spectros. Relat. Phenomena **82**, 193.

Glans, P, P. Skytt, K. Gunnelin, J.-H. Guo, and J. Nordgren (1996c), "Selectively excited X-ray emission spectra of $N_2$," J. Electron Spectros. Relat. Phenomena **82**, 193–201.

Glatzel, P, and U. Bergmann (2005), "High resolution 1s core hole x-ray spectroscopy in 3d transition metal complexes - electronic and structural information," Coord. Chem. Rev. **249**, 65–95.

Glatzel, P, F. M. F. de Groot, O. Manoilova, D. Grandjean, B. M. Weckhuysen, U. Bergmann, and R. Barrea (2005), "Range-extended EXAFS at the L edge of rare earths using high-energy-resolution fluorescence detection: A study of La in LaOCl," Phys. Rev. B **72**, 014117.

Glatzel, P, L. Jacquamet, U. Bergmann, F. M. F. de Groot, and S. P. Cramer (2002), "Site-selective exafs in mixed-valence compounds using high-resolution fluorescence detection: A study of iron in prussian blue," Inorg. Chem. **41**, 3121–3127.

Glatzel, P, M. Sikora, and M. Fernández-Garćia (2009), "Resonant x-ray spectroscopy to study K absorption pre-edges in 3d transition metal compounds," Eur. Phys. J. Special Topics **169**, 207–214.

Glover, T E, D. M. Fritz, M. Cammarata, T. K. Allison, Sinisa Coh, J. M. Feldkamp, H. Lemke, D. Zhu, Y. Feng, R. N. Coffee, M. Fuchs, S. Ghimire, J. Chen, S. Shwartz, D. A. Reis, S. E. Harris, and J. B. Hastings (2012), "X-ray and optical wave mixing," Nature **488**, 603–608.

Grechko, M, P. Maksyutenko, N. F. Zobov, S. V. Shirin, O. L. Polyansky, T. R. Rizzo, and Oleg V. Boyarkin (2008), "Collisionally assisted spectroscopy of water from 27000 to 34000 $cm^{-1}$," J. Phys. Chem. A **112**, 10539–10545.

Grechko, Maxim, Oleg V. Boyarkin, Thomas R. Rizzo, Pavlo Maksyutenko, Nikolay F. Zobov, Sergei V. Shirin, Lorenzo Lodi, Jonathan Tennyson, Attila G. Császár, and Oleg L. Polyansky (2009), "State-selective spectroscopy of water up to its first dissociation limit," J. Chem. Phys. **131**, 221105.

Green, R J, D. A. Zatsepin, A. Hunt, E. Z. Kurmaev, N. V. Gavrilov, and A. Moewes (2013), "The formation of Ti-O tetrahedra and band gap reduction in $SiO_2$ via pulsed ion implantation," J. Appl. Phys. **113(10)**, 103704.

de Groot, F (2001), "High-resolution x-ray emission and x-ray absorption spectroscopy," Chem. Rev. **101**, 1779–1808.

de Groot, F (2005), "Multiplet effects in X-ray spectroscopy," Coord. Chem. Rev **249**, 31–63.

de Groot, F, J. Fuggle, B. Thole, and G. Sawatzky (1990), "2p x-ray absorption of 3d transition-metal compounds: An atomic multiplet description including the crystal field," Phys. Rev. B **42**, 5459.

de Groot, F M F, and A. Kotani (2008), *Core Level Spectroscopy of Solids* (CRC Press, Taylor & Francis Group).

de Groot, F M F, P. Kuiper, and G. A. Sawatzky (1998), "Local spin-flip spectral distribution obtained by resonant x-ray Raman scattering," Phys. Rev. B **57**, 14584–14587.

Guillemin, R, S. Carniato, W. C. Stolte, L. Journel, R. Taïeb, D. W. Lindle, and M. Simon (2008), "Linear dichroism in resonant inelastic x-ray scattering to molecular spin-orbit states," Phys. Rev. Lett. **101**, 133003.

Gunnarsson, O, and K. Schönhammer (1983), "Electron spectroscopies for Ce compounds in the impurity model," Phys. Rev. B **28**, 4315.

Gunnelin, K, P. Glans, P. Skytt, J.-H. Guo, and J. Nordgren (1998), "Assigning x-ray absorption spectra by means of soft-x-ray emission spectroscopy," Phys. Rev. A **57**, 864.

Guo, J, P. Skytt, N. Wassdahl, J. Nordgren, Y. Liu, O. Vahtras, and H. Ågren (1995), "Resonant and non-resonant x-ray scattering from $C_{70}$," Chem. Phys. Lett. **235**, 152–159.

Haldane, F D M (1981), "Luttinger liquid theory of one-dimensional quantum fluids. I. Properties of the Luttinger model and their extension to the general 1D interacting spinless Fermi gas," J. Phys. C: Solid State Phys. **14**, 2585–2609.

Hämäläinen, K, and S. Manninen (2001), "Resonant and non-resonant inelastic x-ray scattering," J. Phys.: Condens. Matter **13**, 7539–7555.

Hämäläinen, K, D. P. Siddons, J. B. Hastings, and L. E. Berman (1991), "Elimination of the inner-shell lifetime broadening in x-ray-absorption spectroscopy," Phys. Rev. Lett. **67**, 2850–2853.

Hancock, J N, R. Viennois, D. van der Marel, H. M. Rønnow, M. Guarise, P.-H. Lin, M. Grioni, M. Moretti Sala, G. Ghiringhelli, V. N. Strocov, J. Schlappa, and T. Schmitt (2010), "Evidence for core-hole-mediated inelastic x-ray scattering from metallic $Fe_{1.087}Te$," Phys. Rev. B **82**, 020513(R).

Hannon, J P, and G. T. Trammell (1989), "Coherent excitations of nuclei in crystals by synchrotron radiation pulses," Physica B **159**, 161–167.

Harada, Y, J. Miyawaki, H. Niwa, K. Yamazoe, L. G. M. Pettersson, and A. Nilsson (2017), "Probing the OH Stretch in Different Local Environments in Liquid Water," J. Phys. Chem. Lett. **8** (22), 5487–5491.

Harada, Y, T. Tokushima, Y. Horikawa, O. Takahashi, M. Kobayashi H. Niwa, M. Oshima, Y. Senba, H. Ohashi, K. T. Wikfeldt, A. Nilsson, L. G. M. Pettersson, and S. Shin (2013), "Selective probing of the OH or OD stretch vibration in liquid water using resonant inelastic soft-x-ray scattering," Phys. Rev. Lett. **111**, 193001.

Harada, Y, T. Tokushima, Y. Takata, T. Takeuchi, Y. Kitajima, S. Tanaka, Y. Kayanuma, and S. Shin (2004), "Dynamical Symmetry Breaking under Core Excitation in Graphite: Polarization Correlation in Soft X-Ray Recombination Emission," Phys. Rev. A **93**, 017401.

Hariki, A, R.-P. Wang, A. Sotnikov, K. Tomiyasu, D. Betto, N. B. Brookes, Y. Uemura, M. Ghiasi, F. M. F. de Groot, and J. Kuneš (2020a), "Damping of spinful excitons in lacoo₃ by thermal fluctuations: Theory and experiment," Phys. Rev. B **101**, 245162.

Hariki, A, M. Winder, T. Uozumi, and J. Kuneš (2020b), "LDA + DMFT approach to resonant inelastic x-ray scattering in correlated materials," Phys. Rev. B **101**, 115130.

Harries, J R, H. Iwayama, S. Kuma, M. Iizawa, N. Suzuki, Y. Azuma, I. Inoue, S. Owada, T. Togashi, K. Tono, M. Yabashi, and E. Shigemasa (2018), "Superfluorescence, free-induction decay, and four-wave mixing: Propagation of free-electron laser pulses through a dense sample of helium ions," Phys. Rev. Lett. **121**, 263201.

Haverkort, M W (2010), "Theory of resonant inelastic x-ray scattering by collective magnetic excitations," Phys. Rev. Lett. **105**, 167404.

Haverkort, M W, M. Zwierzycki, and O. K. Andersen (2012), "Multiplet Ligand-field Theory using Wannier Orbitals," Phys. Rev. B **85**, 165113.

Head-Gordon, T, and M.E. Johnson (2006), "Tetrahedral structure or chains for liquid water," Proc. Natl. Acad. Sci. U.S.A. **103**, 7973.

Henneberger, WC (1968), "Perturbation method for atoms in intense light beams," Phys. Rev. Lett. **21**, 838–841.

Hennies, F, S. Polyutov, I. Minkov, A. Pietzsch, H. Ågren M. Nagasono, L. Triguero, M.-N. Piancastelli, W. Wurth, F. Gel'mukhanov, and A. Föhlisch (2007), "Dynamic interpretation of resonant x-ray Raman scattering: Ethylene and benzene," Phys. Rev. A **76**, 032505.

Hennies, F, S. Polyutov, I. Minkov, A. Pietzsch, M. Nagasono, F. Gel'mukhanov, L. Triguero, M.-N. Piancastelli, W. Wurth, H. Ågren, and A. Föhlisch (2005), "Nonadiabatic effects in resonant inelastic x-ray scattering," Phys. Rev. Lett. **95**, 163002.

Hermanns, M, I. Kimchi, and J. Knolle (2018), "Physics of the Kitaev model: Fractionalization, dynamic correlations, and material connections," Annu. Rev. Condens. Matter Phys. **9**, 17–33.

Hikosaka, Y, Y. Velkov, E. Shigemasa, T. Kaneyasu, Y. Tamenori, J. Liu, and F. Gel'mukhanov (2008), "X-ray absorption measured in the resonant Auger scattering mode," Phys. Rev. Lett. **101**, 073001.

Hopersky, A N, A. M. Nadolinsky, and S. A. Novikov (2018), "Resonant inelastic scattering of two x-ray photons by a many-electron atom," Phys. Rev. A **98**, 063424.

Huang, X-C, X.-J. Kong, T.-J. Li, Z.-R. Ma, H.-C. Wang, G.-C. Liu, Z.-S. Wang, W.-B. Li, and L.-F. Zhu (2021), "Controlling core-hole lifetime through an x-ray planar cavity," arXiv:2101.11225v1.

Humphries, O S, R.S. Marjoribanks, Q. van den Berg, E.C. Galtier, M.F. Kasim, H.J. Lee, A.J.F. Miscampbell, B. Nagler, R. Royle, J.S. Wark, and S.M. S Vinko (2020), "Mapping

the Electronic Structure of Warm Dense Nickel via Resonant Inelastic X-ray Scattering," arXiv:2001.05813v1[physics.plas-ph].

Hunault, M OJY, Y. Harada, J. Miyawaki, J. Wang, A. Meijerink, F. M. F. de Groot, and van Schooneveld M. M. (2018), "Direct observation of $Cr^{3+}$ 3d states in ruby: Toward experimental mechanistic evidence of metal chemistry," J. Phys. Chem. A **122**, 4399–4413.

Iga, F, M. Tsubota, M. Sawada, H. B. Huang, S. Kura, M. Takemura, K. Yaji, M. Nagira, A. Kimura, T. Jo, T. Takabatake, H. Namatame, and M. Taniguchi (2004), "Determination of the orbital polarization in $YTiO_3$ by using soft x-ray linear dichroism," Phys. Rev. Lett. **93**, 257207.

Ignatova, N, V. Vaz da Cruz, R. C. Couto, E. Ertan, M. Odelius, H. Ågren, F. F. Guimarães, A. Zimin, S. P. Polyutov, F. Gel'mukhanov, and V. Kimberg (2017a), "Infrared-pump–x-ray-probe spectroscopy of vibrationally excited molecules," Phys. Rev. A **95** (4), 042502.

Ignatova, N, V. Vaz da Cruz, R.C. Couto, E. Ertan, A. Zimin, F. F. Guimarães, S. Polyutov, H. Ågren, V. Kimberg, M. Odelius, and F. Gel'mukhanov (2017b), "Gradual collapse of nuclear wave functions regulated by frequency tuned X-ray scattering," Sci. Rep. **7**, 43891.

Ishihara, S (2017), "Resonant X-ray Scattering and Orbital Degree of Freedom in Correlated Electron Systems," in *Resonant X-ray Scattering in Correlated Systems, Eds. Y. Murakami and S. Ishihara* (Springer-Verlag, Heidelberg) pp. 1–46.

Ishii, K (2017), "Resonant Inelastic X-ray Scattering in Strongly Correlated Copper Oxides," in *Resonant X-ray Scattering in Correlated Systems, Eds. Y. Murakami and S. Ishihara* (Springer-Verlag, Heidelberg) pp. 197–241.

Ishii, K, I. Jarrige, M. Yoshida, K. Ikeuchi, T. Inami, Y. Murakami, and J. Mizuki (2013), "Instrumental upgrades of the RIXS spectrometer at BL11XU at SPring-8," J. Electron Spectros. Relat. Phenomena **188**, 127–132.

Ishikawa, T (2018), "Accelerator-based x-ray sources: synchrotron radiation, x-ray free electron lasers and beyond," Phil. Trans. R. Soc. A **377**, 0231.

Ismail, I, M. Simon, and Francis Penent (2020), *MOSARIX: PROGRESS REPORT* (Sorbonne Université; CNRS).

Jackeli, G, and G. Khaliullin (2009), "Mott insulators in the strong spin-orbit coupling limit: From Heisenberg to a quantum compass and Kitaev models," Phys. Rev. Lett. **102**, 017205.

Jaeschke, EJ, S. Khan, J. R. Schneider, and J. B. Hastings (2020), *Synchrotron Light Sources and Free-Electron Lasers: Accelerator Physics, Instrumentation and Science Applications*, 2nd ed.,

edited by E.J. Jaeschke and S. Khan and J.R. Schneider and J.B. Hastings (Springer International Publishing).

Jang, H, W.S. Lee, H. Nojiri, S. Matsuzawa, H. Yasumura, L. Nie, A.V. Maharaj, S. Gerber, Y.J. Liu, A. Mehta, D.A. Bonn, R. Liang, W.N. Hardy, C.A. Burns, Z. Islam, S. Song, J. Hastings, T.P. Devereaux, Z.X. Shen, S.A. Kivelson, C.C. Kao, D. Zhu, and J.S. Lee (2016), "Ideal charge-density-wave order in the high-field state of superconducting YBCO," Proc. Natl. Acad. Sci. U.S.A. **113**, 14645–14650.

Jarrige, I, V. Bisogni, w. Leonhardt, and J. Dvorak (2018), "Paving the way to ultra-high-resolution resonant inelastic x-ray scattering with the SIX Beamline at NSLS-II," Synchrotron Radiat. News **31**, 7.

Jay, R M, J. Norell, S. Eckert, M. Hantschmann, M. Beye, B. Kennedy, W. Quevedo, W. F. Schlotter, G. L. Dakovski, M. P. Minitti, M. C. Hoffmann, A. Mitra, S. P. Moeller, D. Nordlund, W. Zhang, H. W. Liang, Kr. Kunnus, K. Kubiček, S. A. Techert, M. Lundberg, Ph. Wernet, and K. Gaffney (2018), "Disentangling Transient Charge Density and Metal-Ligand Covalency in Photoexcited Ferricyanide with Femtosecond Resonant Inelastic Soft X-ray Scattering," J. Phys. Chem. Lett. **9**, 3538–3543.

Jérome, D, and H. J. Schulz (1982), "Organic conductors and superconductors," Adv. Phys. **31**, 299–490.

Jeyachandran, Y L, F. Meyer, S. Nagarajan, A. Benkert, M. Bär, M. Blum, W. Yang, F. Reinert, C. Heske, L. Weinhardt, and M. Zharnikov (2014), "Ion-solvation-induced molecular reorganization in liquid water probed by resonant inelastic soft x-ray scattering," J. Phys. Chem. Lett. **5**, 4143–4148.

Johnson, A S, D. R. Austin, D.A. Wood, C. Brahms, A. Gregory, K. B. Holzner, S. Jarosch, E. W. Larsen, S. Parker, C. S. Strüber, P. Ye, J. W. G. Tisch, and J. P. Marangos (2018), "High-flux soft x-ray harmonic generation from ionization-shaped few-cycle laser pulses," Sci. Adv. **4** (5), 10.1126/sciadv.aar3761.

Jonker, G H (1966), "Magnetic and semiconducting properties of perovskites containing manganese and cobalt," J. Appl. Phys. **37**, 1424.

Josefsson, I, K. Kunnus, S. Schreck, A. Föhlisch, F. de Groot, Ph. Wernet, and M. Odelius (2012), "Ab initio calculations of x-ray spectra: Atomic multiplet and molecular orbital effects in a multi-configurational scf approach to the L-edge spectra of transition metal complexes," J. Phys. Chem.

Lett. **3**, 3565–3570.

Juhin, A, C. Brouder, and F. de Groot (2014), "Angular dependence of resonant inelastic x-ray scattering: a spherical tensor expansion," Cent. Eur. J. Phys. **12(5)**, 323–340.

Kanász-Nagy, M, Y. Shi, I. Klich, and E. A. Demler (2016), "Resonant inelastic x-ray scattering as a probe of band structure effects in cuprates," Phys. Rev. B **94**, 165127.

Kane, P P (1992), "Inelastic scattering of x-rays and gamma rays by inner shell electrons," Phys. Rep **218**, 67.

Kassi, S, P. Macko, O. Naumenko, and A. Campargue (2005), "The absorption spectrum of water near 750 nm by CW-CRDS: contribution to the search of water dimer absorption," Phys. Chem. Chem. Phys. **7**, 2460–2467.

Kazantsev, AP, G.I. Surdutovich, and Yakovlev V.P. (1990), *Mechanical action of light on atoms* (World Scientific).

Khalil, M, and S. Mukamel (2020), "Ultrafast spectroscopy and diffraction from xuv to x-ray," J. Chem. Phys. **153**, 100401.

Khaliullin, G, and V. Oudovenko (1997), "Spin and orbital excitation spectrum in the Kugel-Khomskii model," Phys. Rev. B **56**, R14243–14246.

Kikas, A, T. Käämbre, A. Saar, K. Kooser, E. Nõmmiste, I. Martinson, V. Kimberg, S. Polyutov, and F. Gel'mukhanov (2004), "Resonant inelastic x-ray scattering at the F 1s photoabsorption edge in LiF: Interplay of excitonic and conduction states, and Stokes' doubling," Phys. Rev. B **70**, 085102.

Kim, B J, H. Koh, E. Rotenberg, S.-J. Oh, H. Eisaki, N. Motoyama, S. Uchida, T. Tohyama, S. Mekawa, Z.-X. Shen, and C. Kim (2006), "Distinct spinon and holon dispersions in photoemission spectral functions from one-dimensional $SrCuO_2$," Nat. Phys. **2**, 397–401.

Kim, C, A. Y. Matsuura, Z.-X. Shen, N. Motoyama, H. Eisaki, S. Uchida, T. Tohyama, and S. Maekawa (1996), "Observation of spin-charge separation in one-dimensional $SrCuO_2$," Phys. Rev. Lett. **77**, 4054–4057.

Kim, C, A. Y. Matsuura, Z.-X. Shen, N. Motoyama, H. Eisaki, S. Uchida, T. Tohyama, and S. Maekawa (1997), "Separation of spin and charge excitations in one-dimensional $SrCuO_2$," Phys. Rev. B **56**, 15589–15595.

Kim, J, D. Casa, A. Said, R. Krakora, B. J. Kim, E. Kasman, X. Huang, and T. Gog (2018), "Quartz-based flat-crystal resonant inelastic x-ray scattering spectrometer with sub-10 meV en-

ergy resolution," Sci. Rep. **8**, 1958.

Kim, J, D. Casa, M. H. Upton, T. Gog, Y.-J. Kim, J. F. Mitchell, M. van Veenendaal, M. Daghofer, J. van den Brink, G. Khaliullin, and B. J. Kim (2012), "Magnetic excitation spectra of $Sr_2IrO_4$ probed by resonant inelastic x-ray scattering: Establishing links to cuprate superconductors," Phys. Rev. Lett. **108**, 177003.

Kim, K-J, Y. Shvyd'ko, and S. Reiche (2008), "A proposal for an x-ray free-electron laser oscillator with an energy-recovery linac," Phys. Rev. Lett. **100**, 244802.

Kim, KH, K. Amann-Winkel, N. Giovambattista, A. Späh, F. Perakis, H. Pathak, M. L. Parada, C. Yang, D. Mariedahl, T. Eklund, T. J. Lane, S. You, S. Jeong, M. Weston, J. H. Lee, I. Eom, M. Kim, J. Park, S. H. Chun, P. H. Poole, and A. Nilsson (2020), "Experimental observation of the liquid-liquid transition in bulk supercooled water under pressure," Science **370**, 978–982.

Kim, KH, A. Späh, H. Pathak, F. Perakis, D. Mariedahl, K. Amann-Winkel, J. A. Sellberg, J. H. Lee, S. Kim, J. Park, K.H. Nam, T. Katayama, and A. Nilsson (2017), "Maxima in the thermodynamic response and correlation functions of deeply supercooled water," Science **358**, 1589–1593.

Kimberg, V, T. Gejo, M. Oura, T. Tokushima, Y. Horikawa, H. Arai, S. Shin, and N. Kosugi (2012), "Rydberg-valence mixing and interchannel coupling in resonant oxygen 1s inelastic x-ray scattering of $O_2$," Phys. Rev. A **85**, 032503.

Kimberg, V, and C. Miron (2014), "Molecular potentials and wave function mapping by high-resolution electron spectroscopy and ab initio calculations," J. Electron Spectros. Relat. Phenomena **195**, 301.

Kimberg, V, and N. Rohringer (2013), "Amplified x-ray emission from core-ionized diatomic molecules," Phys. Rev. Lett. **110**, 043901.

Kimberg, V, and N. Rohringer (2016), "Stochastic stimulated electronic x-ray Raman spectroscopy," Struct. Dyn. **3**, 034101.

Kimberg, V, A. Sanchez-Gonzalez, L. Mercadier, C. Weninger, A. Lutman, D. Ratner, R. Coffee, M. Bucher, M. Mucke, M. Agåker, C. Såthe, C. Bostedt, J. Nordgren, J.-E. Rubensson, and N. Rohringer (2016), "Stimulated x-ray Raman scattering - a critical assessment of the building block of nonlinear x-ray spectroscopy," Faraday Discuss **194**, 305.

Kitaev, A (2006), "Anyons in an exactly solved model and beyond," Ann. Physics **321**, 2–111.

Kitajima, M, K. Ueda, A. De Fanis, T. Furuta, H. Shindo, H. Tanaka, K. Okada, R. Feifel, S. L. Sorensen, F. Gel'mukhanov, A. Baev, and H. Ågren (2003), "Doppler effect in resonant photoe-

mission from $SF_6$: Correlation between Doppler profile and Auger emission anisotropy," Phys. Rev. Lett. **91**, 213003.

Kjellsson, L, V. Ekholm, M. Agåker, C. Såthe, A. Pietzsch, H. O. Karlsson, N. Jaouen, A. Nicolau, M. Guarise, C. Hague, J. Lüning, S. G. Chiuzbăian, and J. E. Rubensson (2021), "Resonant inelastic x-ray scattering at the $N_2$ $\pi^*$ resonance: Lifetime-vibrational interference, radiative electron rearrangement, and wave-function imaging," Phys. Rev. A **103**, 022812.

Kotani, A, and S. Shin (2001), "Resonant inelastic x-ray scattering spectra for electrons in solids," Rev. Mod. Phys. **73**, 203–245.

Köuppel, H, W. Domcke, and L. S. Cederbaum (2007), "Multimode molecular dynamics beyond the Born-Oppenheimer approximation," in *Advances in Chemical Physics LVII*, edited by I. Prigogin and S.A. Rice (Wiley & Sons, Inc p) pp. 59–246.

Kowalewski, M, B. P. Fingerhut, K. E. Dorfman, K. Bennett, and S. Mukamel (2017), "Simulating coherent multidimensional spectroscopy of nonadiabatic molecular processes: From the infrared to the x-ray regime," Chem. Rev. **117**, 12165–12226.

Kramers, H A, and W. Heisenberg (1925), "Über die streuung von strahlung durch atome," Z. Phys. **31**, 681–708.

Kraus, P M, M. Zürch, S. K. Cushing, D. M. Neumark, and S. R. Leone (2018), "The ultrafast x-ray spectroscopic revolution in chemical dynamics," Nat. Rev. Chem. , 82–94.

Kringle, L, W.A. Thornley, B.D. Kay, and G.A. Kimmel (2020), "Reversible structural transformations in supercooled liquid water from 135 to 245 K," Science **369**, 1490–1492.

Kroll, T, C. Weninger, R. Alonso-Mori, D. Sokaras, D. Zhu, L. Mercadier, V. P. Majety, A. Marinelli, A. Lutman, M. W. Guetg, F.-J. Decker, S. Boutet, A. Aquila, J. Koglin, J. Koralek, D. P. DePonte, J. Kern, F. D. Fuller, E. Pastor, T. Fransson, Y. Zhang, J. Yano, V. K. Yachandra, N. Rohringer, and U. Bergmann (2018), "Stimulated x-ray emission spectroscopy in transition metal complexes," Phys. Rev. Lett. **120**, 133203.

Kroll, T, C. Weninger, F. D. Fuller, M. W. Guetg, A. Benediktovich, Y. Zhang, A. Marinelli, R. Alonso-Mori, A. Aquila, M. Liang, J. Koglin, J. Koralek, D. Sokaras, D. Zhu, J. Kern, J. Yano V. K. Yachandra, N. Rohringer, A. Lutman, and U. Bergmann (2020), "Observation of Seeded Mn $K\beta$ Stimulated X-Ray Emission Using Two-Color X-ray Free-Electron Laser Pulses," Phys. Rev. Lett. **125**, 037404.

Kugel', K I, and D. I. Khomskii (1982), "The Jahn-Teller effect and magnetism: transition metal compounds," Sov. Phys. Usp. **25**, 231.

Kühne, T D, and R. Z. Khaliullin (2013), "Electronic signature of the instantaneous asymmetry in the first coordination shell of liquid water," Nat. Commun. **4**, 1450.

Kukk, E, T. D. Thomas, D. Céolin, S. Granroth, O. Travnikova, M. Berholts, T. Marchenko, R. Guillemin, L. Journel, I. Ismail, R. Püttner, M. N. Piancastelli, K. Ueda, and M. Simon (2018), "Energy transfer into molecular vibrations and rotations by recoil in inner-shell photoemission," Phys. Rev. Lett. **121**, 073002.

Kumar, M P, G. Cesare, Di Fraia Michele, Matteo Moioli, Dominik Ertel, Hamed Ahmadi, Oksana Plekan, Paola Finetti, Enrico Allaria, Luca Giannessi, Giovanni De Ninno, Carlo Spezzani, Giuseppe Penco, Simone Spampinati, Alexander Demidovich, Miltcho B. Danailov, Roberto Borghes, George Kourousias, Carlos Eduardo Sanches Dos Reis, Fulvio Billé, Alberto A. Lutman, Richard J. Squibb, Raimund Feifel, Paolo Carpeggiani, Maurizio Reduzzi, Tommaso Mazza, Michael Meyer, Samuel Bengtsson, Neven Ibrakovic, Emma Rose Simpson, Johan Mauritsson, T. Csizmadia, Mathieu Dumergue, Sergei Kühn, Harshitha Nandiga Gopalakrishna, Daehyun You, Kiyoshi Ueda, Marie Labeye, Jens Egebjerg Bæhøj, Kenneth J. Schafer, Elena V. Gryzlova, Alexei N. Grum-Grzhimailo, Kevin C. Prince, Carlo Callegari, and Giuseppe Sansone (2020), "Attosecond pulse shaping using a seeded free-electron laser," Nature **578**, 386–391.

Kumar, Umesh, Alberto Nocera, Elbio Dagotto, and Steve Johnston (2018), "Multi-spinon and antiholon excitations probed by resonant inelastic x-ray scattering on doped one- dimensional antiferromagnets," New J. Phys. **20**, 1073019.

Kunnus, K, I. Josefsson, I. Rajkovic, S. Schreck, W. Quevedo, M. Beye, S. Grübel, M. Scholz, D. Nordlund, W. Zhang, R. W. Hartsock, K. J Gaffney, W. F. Schlotter, J. J. Turner, B. Kennedy, F. Hennies, S. Techert, Ph. Wernet, M. Odelius, and A. Föhlisch (2016a), "Anti-Stokes resonant x-ray Raman scattering for atom specific and excited state selective dynamics," New J. Phys. **18**, 103011.

Kunnus, K, W. Zhang, M. G. Delcey, R. V. Pinjari, P. S. Miedema, S. Schreck, W. Quevedo, H. Schröder, A. Föhlisch, K. J. Gaffney, M. Lundberg, M. Odelius, and P. Wernet (2016b), "Viewing the Valence Electronic Structure of Ferric and Ferrous Hexacyanide in Solution from the Fe and Cyanide Perspectives," J. Phys. Chem. B **120**, 7182–7194.

Lange, K M, and E. F. Aziz (2013), "Electronic structure of ions and molecules in solution: a view from modern soft x-ray spectroscopies," Chem. Soc. Rev. **42**, 6840.

Lange, K M, R. Könnecke, M. Soldatov, R. Golnak, J.-E. Rubensson, A. Soldatov, and E. F. Aziz (2011), "On the Origin of the Hydrogen-Bond-Network Nature of Water: X-Ray Absorption and Emission Spectra of Water-Acetonitrile Mixtures," Angew. Chem. Int. Ed **50**, 10621–10625.

Le Tacon, M, A. Bosak, S. M. Souliou, G. Dellea, T. Loew, R. Heid, K-P. Bohnen, G. Ghiringhelli, M. Krisch, and B. Keimer (2014), "Inelastic x-ray scattering in $YBa_2Cu_3O_{6.6}$ reveals giant phonon anomalies and elastic central peak due to charge-density-wave formation," Nat. Phys. **10**, 52.

Li, J, A. Nag, J. Pelliciari, H. Robarts, A. Walters, M. Garcia-Fernandez, H. Eisaki, D. Song, H. Ding, S. Johnston, R. Comin, and K.-J. Zhou (2020a), "Multiorbital charge-density wave excitations and concomitant phonon anomalies in $Bi_2Sr_2LaCuO_{6+\delta}$," Proc. Natl. Acad. Sci. U.S.A. **117**, 16219.

Li, K, M. Labeye, P.J. Ho, M. B. Gaarde, and L. Young (2020b), "Resonant propagation of x-rays from the linear to the nonlinear regime," Phys. Rev. A **102**, 053113.

Lieb, E H, and F. Y. Wu (1968), "Absence of Mott transition in an exact solution of the short-range, one-band model in one dimension," Phys. Rev. Lett. **20**, 1445–1448.

Limmer, D T, and D. Chandler (2013), "The putative liquid-liquid transition is a liquid-solid transition in atomistic models of water II," J. Chem. Phys. **138**, 214504.

Lindblad, A, J. Söderström, C. Nicolas, E. Robert, and C. Miron (2013), "A multi purpose source chamber at the PLEIADES beamline at SOLEIL for spectroscopic studies of isolated species: Cold molecules, clusters, and nanoparticles," Rev. Sci. Instrum **84**, 113105.

Lindle, D W, P. L. Cowan, T. Jach, R. E. LaVilla, R. D. Deslattes, and R. C. C. Perera (1991), "Polarized x-ray emission studies of methyl chloride and the chlorofluoromethanes," Phys. Rev. A **43**, 2353.

Lindle, D W, P. L. Cowan, R. E. LaVilla, T. Jach, R. D. Deslattes, B. Karlin, J. A. Sheehy, T. J. Gil, and P. W. Langhoff (1998), "Polarization of molecular x-ray fluorescence," Phys. Rev. Lett. **60**, 1010.

Liu, J-C, C. Miron, H. Ågren, S. Polyutov, and F. Gel'mukhanov (2019a), "Resonant x-ray second-harmonic generation in atomic gases," Phys. Rev. A **100**, 063403.

Liu, J-C, C. Nicolas, Y.-P. Sun., R. Flammini, P. O'Keeffe, L. Avaldi, P. Morin, V. Kimberg, N. Kosugi, F. Gel'mukhanov, and C. Miron (2011a), "Multimode Resonant Auger Scattering

from the Ethene Molecule," J. Phys. Chem. B **115**, 5103–5112.

Liu, J-C, C. Nicolas, Y.-P. Sun, R. Flammini, P. O'Keeffe, L. Avaldi, P. Morin, V. Kimberg, N. Kosugi, F. Gel'mukhanov, and C. Miron (2011b), "Multimode resonant Auger scattering from the ethene molecule," J. Phys. Chem. B **115**, 5103.

Liu, J-C, V. Savchenko, V. Kimberg, F. Gel'mukhanov, and M. Odelius (2021a), "High-resolution x-ray spectra of carbon monoxide reveal ultrafast dynamics induced by long UV pulse," New J. Phys. **00**, 0000.

Liu, J-C, V. Savchenko, V. Kimberg, M. Odelius, and F. Gel'mukhanov (2021b), "Polarization-sensitive IR-pump-x-ray-probe spectroscopy," Phys. Rev. A **00**, 0000.

Liu, J-C, Y.-P. Sun, C.-K. Wang, H. Ågren, and F. Gel'mukhanov (2010), "Auger effect in the presence of strong x-ray pulses," Phys. Rev. A **81**, 043412.

Liu, J-C, V. Vaz da Cruz, S. Polyutov, A. Föhlisch, and F. Gel'mukhanov (2019b), "Recoil-induced dissociation in hard-x-ray photoionization," Phys. Rev. A **100**, 053408.

Liu, J-C, Y. Velkov, Z. Rinkevicius, H. Ågren, and F. Gel'mukhanov (2008), "Symmetry-forbidden x-ray raman scattering induced by strong infrared-laser pulse," Phys. Rev. A **77**, 043405.

Liu, X-J, N. A. Cherepkov, S. K. Semenov, V. Kimberg, F. Gel'mukhanov, G. Prümper, T. Lischke, T. Tanaka, M. Hoshino, H. Tanaka, and K. Ueda (2006), "Young's double-slit experiment using core-level photoemission from $N_2$: revisiting Cohen-Fano's two-centre interference phenomenon," J. Phys. B: At. Mol. Opt. Phys. **39**, 4801.

Liu, X-J, Q. Miao, F. Gel'mukhanov, M. Patanen, O. Travnikova, C. Nicolas, H. Ågren, K. Ueda, and C. Miron (2015), "Einstein-Bohr recoiling double-slit gedanken experiment performed at the molecular level," Nat. Photonics **9**, 120.

Liu, X-J, C. Nicolas, and C. Miron (2013), "Design of a lens table for a double toroidal electron spectrometer," Rev. Sci. Instrum. **84**, 033105.

Liu, X J, G. Prümper, E. Kukk, R. Sankari, M. Hoshino, C. Makochekanwa, M. Kitajima, H. Tanaka, H. Yoshida, Y. Tamenori, and K. Ueda (2005), "Site-selective ion production of the core-excited $CH_3F$ molecule probed by Auger-electron-ion coincidence measurements," Phys. Rev. A **72**, 042704.

Ljungberg, M P, I. Zhovtobriukh, O. Takahashi, and L. G. M. Pettersson (2017), "Core-hole-induced dynamical effects in the x-ray emission spectrum of liquid methanol," J. Chem. Phys. **146**, 134506.

Lucchese, R R, J. Söderström, T. Tanaka, M. Hoshino, M. Kitajima, H. Tanaka, A. De Fanis, J.-E. Rubensson, and K. Ueda (2007), "Vibrationally resolved partial cross sections and asymmetry parameters for nitrogen K-shell photoionization of the $N_2O$ molecule," Phys. Rev. A **76**, 012506.

Lundberg, M, and Ph. Wernet (2019), "Resonant inelastic x-ray scattering (RIXS) studies in chemistry: Present and future," in *Synchrotron Light Sources and Free-Electron Lasers: Accelerator Physics, Instrumentation and Science Applications*, edited by E. Jaeschke, S. Khan, J. R. Schneider, and J. B. Hastings (Springer International Publishing, Cham, Schweiz) pp. 1–52.

Lüning, J, J.-E. Rubensson, C. Ellmers, S. Eisebitt, and W. Eberhardt (1997), "Site- and symmetry-projected band structure measured by resonant inelastic soft x-ray scattering," Phys. Rev. B **56**, 13147.

Luo, Y, H. Ågren, F. Gel'mukhanov, J. Guo, P. Skytt, N. Wassdahl, and J. Nordgren (1995), "Symmetry-selective resonant inelastic x-ray scattering of $C_{60}$," Phys. Rev. B **52**, 14479.

Luo, Y, O. Vahtras, F. Gel'mukhanov, and H. Ågren (1997), "Theory of natural circular dichroism in x-ray raman scattering from molecules," Phys. Rev. A **55**, 2716.

Luttinger, J M (1963), "An exactly soluble model of a many-fermion system," J. Math. Phys. **4**, 1154–1162.

Maganas, D, P. Kristiansen, L.-C. Duda, A. Knop-Gericke, S. DeBeer, R. Schlögl, and F. Neese (2014), "Combined experimental and ab initio multireference configuration interaction study of the resonant inelastic x-ray scattering spectrum of $CO_2$," J. Phys. Chem. C **118**, 20163–20175.

Magnuson, M, S. Butorin, J. H. Guo, and J. Nordgren (2002a), "Electronic structure investigation of CoO by means of soft x-ray scattering," Phys. Rev. B **65(20)**, 205106.

Magnuson, M, S. M. Butorin, A. Agui, and J. Nordgren (2002b), "Resonant soft x-ray Raman scattering of NiO," J. Phys.: Condens. Matter **14(13)**, 3669.

Magnuson, M, L.-C. Duda, S. M. Butorin, P. Kuiper, and J. Nordgren (2006), "Large magnetic circular dichroism in resonant inelastic x-ray scattering at the Mn L-edge of Mn-Zn ferrite," Phys. Rev. B **74**, 172409.

Magnuson, M, J.-E. Rubensson, A. Föhlisch, N. Wassdahl, A. Nilsson, and N. Mårtensson (2003), "X-ray fluorescence spectra of metals excited below threshold," Phys. Rev. B **68**, 045119.

Marchenko, T, S. Carniato, L. Journel, R. Guillemin, E. Kawerk, M. Žitnik, M. Kavčič, K. Bučar, R. Bohinc, M. Petric, V. V. da Cruz, F. Gel'mukhanov, and M. Simon (2015), "Electron dynamics in the core-excited $CS_2$ molecule revealed through resonant inelastic x-ray scattering

spectroscopy," Phys. Rev. X **5**, 031021.

Marchenko, T, G. Goldsztejn, K. Jänkälä, O. Travnikova, L. Journel, R. Guillemin, N. Sisourat, D. Céolin, M. Žitnik, M. Kavčič, K. Bučar, A. Mihelič, B. Cunha de Miranda, I. Ismail, A. F. Lago, F. Gel'mukhanov, R. Püttner, M. N. Piancastelli, and M. Simon (2017), "Potential energy surface reconstruction and lifetime determination of molecular double-core-hole states in the hard x-ray regime," Phys. Rev. Lett. **119**, 133001.

Marchenko, T, L. Journel, T. Marin, R. Guillemin, S. Carniato, M. Žitnik, M. Kavčič, K. Bučar, A. Mihelič, J. Hoszowska, W. Cao, and M. Simon (2011), "Resonant inelastic x-ray scattering at the limit of subfemtosecond natural lifetime," J. Chem. Phys. **134**, 144308.

Matthews, M, F. Morales, A. Patas, A. Lindinger, J. Gateau, N. Berti, S. Hermelin, J. Kasparian, M. Richter, T. Bredtmann, O. Smirnova, J.-P. Wolf, and Ivanov M. (2018), "Amplification of intense light fields by nearly free electrons," Nat. Phys. **14**, 695–700.

Mattis, D C, and E. H. Lieb (1965), "Exact solution of a many-fermion system and its associated boson field," J. Math. Phys. **6**, 304–312.

Mayer, R, D. W. Lindle, S. H. Southworth, and P. L. Cowan (1991), "Direct determination of molecular orbital symmetry of $H_2S$ using polarized x-ray emission," Phys. Rev. A **43**, 235.

McCall, S L, and E. L. Hahn (1967), "Self-induced transparency by pulsed coherent light," Phys. Rev. Lett. **18**, 908.

Men'shikov, LI, P.L. Menshikov, and P.O. Fedichev (2020), "Effects of action at a distance in water," Phys. - Usp. **440–486**, 63.

Mercadier, L, A. Benediktovitch, C. Weninger, M. A. Blessenohl, S. Bernitt, H. Bekker, S. Dobrodey, A. Sanchez-Gonzalez, B. Erk, C. Bomme, R. Boll, Z. Yin, V. P. Majety, R. Steinbrügge, M. A. Khalal, F. Penent, J. Palaudoux, P. Lablanquie, A. Rudenko, D. Rolles, J. R. Crespo López-Urrutia, and N. Rohringer (2019), "Evidence of Extreme Ultraviolet Superfluorescence in Xenon," Phys. Rev. Lett. **123**, 023201.

Miao, Q, J.-C. Liu, H. Ågren, J.-E Rubensson, and F. Gel'mukhanov (2012), "Dissociative x-ray lasing," Phys. Rev. Lett. **109**, 233905.

Miao, Q, O. Travnikova, F. Gel'mukhanov, V. Kimberg, Y.-P. Sun, T. D. Thomas, C. Nicolas, M. Patanen, and C. Miron (2015), "Rotational Doppler effect: A probe for molecular orbital anisotropy, rotational Doppler effect: A probe for molecular orbitals anisotropy," J. Phys. Chem. Lett. **6**, 1568–1572.

Miedema, P S, M. Beye, R. Könnecke, G. Schiwietz, and A. Föhlisch (2014), "The angular- and crystal-momentum transfer through electron-phonon coupling in silicon and silicon- carbide: similarities and differences," New J. Phys. **16**, 093056.

Millot, M, S. Hamel, J. Ryan Rygg, P. M. Celliers, G. W. Collins, F. Coppari, D. E. Fratanduono, R. Jeanloz, D. C. Swift, and J. H. Eggert (2018), "Experimental evidence for superionic water ice using shock compression," Nat. Phys. **14**, 297–302.

Mills, D, J. A. Sheehy, T. A. Ferrett, S. H. Southworth, R. Mayer, D. W. Lindle, and P. W. Langhoff (1997), "Nondipole resonant x-ray Raman spectroscopy: Polarized inelastic scattering at the K edge of $Cl_2$," Phys. Rev. Lett. **79**, 383.

Miron, C, V. Kimberg, P. Morin, C. Nicolas, N. Kosugi, S. Gavrilyuk, and F. Gel'mukhanov (2010), "Vibrational scattering anisotropy generated by multichannel quantum interference," Phys. Rev. Lett. **105**, 093002.

Miron, C, Q. Miao, C. Nicolas, J. D. Bozek, W. Andrałojć, M. Patanen, G. Simões, O. Travnikova, H. Å gren, and F. Gel'mukhanov (2014), "Site-selective photoemission from delocalized valence shells induced by molecular rotation," Nat. Commun. **5**, 3816.

Miron, C, C. Nicolas, O. Travnikova, P. Morin, Y.-P. Sun, F. Gel'mukhanov, N. Kosugi, and V. Kimberg (2012), "Imaging molecular potentials using ultrahigh-resolution resonant photoemission," Nat. Phys. **8**, 135.

Mitrano, Matteo, Sangjun Lee, Ali A. Husain, Luca Delacretaz, Minhui Zhu, Gilberto de la Peña Munoz, Stella X.-L. Sun, Young Il Joe, Alexander H. Reid, Scott F. Wandel, Giacomo Coslovich, William Schlotter, Tim van Driel, John Schneeloch, G. D. Gu, Sean Hartnoll, Nigel Goldenfeld, and Peter Abbamonte (2019a), "Ultrafast time-resolved x-ray scattering reveals diffusive charge order dynamics in $La_{2-x}Ba_xCuO_4$," Sci. Adv. **5**, eaax3346.

Mitrano, Matteo, Sangjun Lee, Ali A. Husain, Minhui Zhu, Gilberto de la Peña Munoz, Stella X.-L. Sun, Young Il Joe, Alexander H. Reid, Scott F. Wandel, Giacomo Coslovich, William Schlotter, Tim van Driel, John Schneeloch, G. D. Gu, Nigel Goldenfeld, and Peter Abbamonte (2019b), "Evidence for photoinduced sliding of the charge-order condensate in $La_{1.875}Ba_{0.125}CuO_4$," Phys. Rev. B **100**, 205125.

Miyawaki, J, S. Suga, H. Fujiwara, M. Urasaki, H. Ikeno, H. Niwa, H. Kiuchi, and Y. Harada (2017), "Dzyaloshinskii-moriya interaction in $\alpha Fe_2O_3$ measured by magnetic circular dichroism in resonant inelastic soft x-ray scattering," Phys. Rev. B **96**, 214420.

Mizokawa, T, D. I. Khomskii, and G. A. Sawatzky (1999), "Interplay between orbital ordering and lattice distortions in $LaMnO_3$, $YVO_3$, and $YTiO_3$," Phys. Rev. B **60**, 7309.

Morin, P, and I. Nenner (1986), "Atomic autoionization following very fast dissociation of core-excited HBr," Phys. Rev. Lett. **56**, 1913.

Mukamel, S (2005), "Multiple core-hole coherence in x-ray four-wave- mixing spectroscopies," Phys. Rev. B **72**, 235110.

Murakami, Y, J. P. Hill, D. Gibbs, M. Blume, I. Koyama, M. Tanaka, H. Kawata, T. Arima, Y. Tokura, K. Hirota, and Y. Endoh (1998a), "Resonant x-ray scattering from orbital ordering in $LaMnO_3$," Phys. Rev. Lett. **81**, 582–585.

Murakami, Y, H. Kawada, H. Kawata, M. Tanaka, T. Arima, Y. Moritomo, and Y. Tokura (1998b), "Direct observation of charge and orbital ordering in $La_{0.5}Sr_{1.5}MnO_4$," Phys. Rev. Lett. **80**, 1932–1935.

Murakami, Y, H. Nakao, T. Matsumura, and H. Ohsumi (2007), "Mechanism of resonant x-ray scattering to observe the orbital ordering," J. Magn. Magn. Mater. **310**, 723–729.

Nag, A, H. C. Robarts, F. Wenzel, J. Li, H. Elnaggar, R.-P. Wang, A. C. Walters, M. García-Fernández, F. M. F. de Groot, M. W. Haverkort, and K.-J. Zhou (2020), "Many-body physics of single and double spin-flip excitations in nio," Phys. Rev. Lett. **124**, 067202.

Nagasaka, Masanari, Hayato Yuzawa, and Nobuhiro Kosugi (2020), "Soft x-ray absorption spectroscopy of liquids for understanding chemical processes in solution," Analytical Sciences **36** (1), 10.2116/analsci.19R005.

Nandi, S, C. Nicolas, A. N. Artemyev, N. M. Novikovskiy, C. Miron, J. D. Bozek, and Ph. V. Demekhin (2017), "Electronic-state interference in the C 1s excitation and decay of methyl chloride studied by angularly resolved Auger spectroscopy," Phys.Rev. A **96**, 052501.

Naus, H, W. Ubachs, P.F. Levelt, O.L. Polyansky, N.F. Zobov, and J. Tennyson (2001), "Cavity-ring-down spectroscopy on water vapor in the range 555-604 nm," J. Mol. Spectrosc. **205**, 117–121.

Nazarkin, A, S. Podorov, I. Uschmann, E. Förster, and R. Sauerbrey (2003), "Nonlinear optics in the angstrom regime: Hard-x-ray frequency doubling in perfect crystals," Phys. Rev. A **67**, 041804R.

Neeb, M, J.-E. Rubensson, M. Biermann, and W. Eberhardt (1994), "Coherent excitation of vibrational wave functions observed in core hole decay spectra of $O_2$, N2 and CO," J. Electron Spectros. Relat. Phenomena **67**, 261.

Nicoletti, D, E. Casandruc, Y. Laplace, V. Khanna, C. R. Hunt, S. Kaiser, S. S. Dhesi, G. D. Gu, J. P. Hill, and A. Cavalleri (2014), "Optically induced superconductivity in striped $La_{2-x}Ba_xCuO_4$ by polarization-selective excitation in the near infrared," Phys. Rev. B **90**.

Nilsson, A, and L. G. M. Pettersson (2011), "Perspective on the structure of liquid water," Chem. Phys. **389**, 1–34.

Nilsson, A, and L. G. M. Pettersson (2015), "The structural origin of anomalous properties of liquid water," Nat. Commun. **6**, 8998.

Nilsson, A, T. Tokushima, Y. Horikawa, Y. Harada, M. P. Ljungberg, S. Shin, and L. G. M. Pettersson (2013), "Resonant inelastic x-ray scattering of liquid water," J. Electron Spectros. Relat. Phenomena **188**, 84–100.

Nishizawa, K, N. Kurahashi, K. Sekiguchi, T. Mizuno, Y. Ogi, T. Horio, M. Oura, N. Kosugia, and T. Suzuki (2011), "High-resolution soft x-ray photoelectron spectroscopy of liquid water," Phys. Chem. Chem. Phys. **13**, 413–417.

Niskanen, J, M. Fondell, C. J. Sahle, S. Eckert, R. M. Jay, K. Gilmore, A. Pietzsch, M. Dantz, X. Lu, D. E. McNally, T. Schmitt, V. Vaz da Cruz, V. Kimberg, F. Gel'mukhanov, and A. Föhlisch (2019), "Compatibility of quantitative x-ray spectroscopy with continuous distribution models of water at ambient conditions," Proc. Natl. Acad. Sci. U.S.A. **116**, 4058.

Nordgren, Joseph, and Jan-Erik Rubensson (2013), "Resonant soft x-ray emission for studies of molecules and solids," J. Electron Spectros. Relat. Phenomena **188**, 3 – 9.

Norell, J, R. M. Jay, M. Hantschmann, S. Eckert, M. Guo, K. J. Gaffney, Ph. Wernet, M. Lundberg, A. Föhlisch, and M. Odelius (2018), "Fingerprints of electronic, spin and structural dynamics from resonant inelastic soft x-ray scattering in transient photo-chemical species," Phys. Chem. Chem. Phys. **20**, 7243–7253.

Norman, P, and A. Dreuw (2018), "Simulating x-ray spectroscopies and calculating core-excited states of molecules," Chem. Rev. **118**, 7208–7248.

Noziéres, P, and E. Abrahams (1974), "Threshold singularities of the x-ray Raman scattering in metals," Phys. Rev. B **10**, 3099.

Odelius, M (2009a), "Information content in O[1s] K-edge x-ray emission spectroscopy of liquid water," J. Phys. Chem. A **113**, 8176–8181.

Odelius, M (2009b), "Molecular dynamics simulations of fine structure in oxygen K- edge x-ray emission spectra of liquid water and ice," Phys. Rev. B **79**, 144204.

Odelius, M, H. Ogasawara, D. Nordlund, O. Fuchs, L. Weinhardt, F. Maier, E. Umbach, C. Heske, Y. Zubavichus, M. Grunze, J. D. Denlinger, L. G. M. Pettersson, and A. Nilsson (2005), "Ultrafast core hole induced dynamics in water probed by x-ray emission spectroscopy," Phys. Rev. Lett. **94**, 227401.

Olalde-Velasco, P, J. Jiménez-Mier, J. D. Denlinger, Z. Hussain, and W. L. Yang (2011), "Direct probe of Mott-Hubbard to charge-transfer insulator transition and electronic structure evolution in transition-metal systems," Phys. Rev. B **83**, 241102(R).

Palmer, J C, R. Car, and P. G. Debenedetti (2013), "The liquid-liquid transition in supercooled ST2 water: a comparison between umbrella sampling and well–empered metadynamics," Faraday Discuss **167**, 77.

Palmer, J C, P. H. Poole, F. Sciortino, and P. G. Debenedetti (2018), "Advances in computational studies of the liquid-liquid transition in water and water-like models," Chem.Rev **118**, 9129–9151.

Pellegrini, C, A. Marinelli, and S. Reiche (2016), "The physics of x-ray free-electron lasers," Rev. Mod. Phys. **88**, 015006.

Perakis, F, L. De Marco, A. Shalit, F. Tang, Z. R. Kann, T. D. Künne, R. Torre, M. Bonn, and Y. Nagata (2016), "Vibrational spectroscopy and dynamics of water," Chem. Rev. **116**, 7590–7607.

Petrillo, V, M. Opromolla, A. Bacci, F. Broggi, I. Drebot, G. Ghiringhelli, E. Puppin, M.R. Conti, A. R. Rossi, M. Ruijter, S. Samsam, A. Tagliaferri, G. Rossi, and L . Serafini (2020), "Coherent, high repetition rate tender x-ray free-electron laser seeded by an extreme ultra-violet free-electron laser oscillator," New J. Phys. **22**, 073058.

Piancastelli, M-N, T. Marchenko, R. Guillemin, L. Journel, O. Travnikova, I. Ismail, and M. Simon (2020), "Hard x-ray spectroscopy and dynamics of isolated atoms and molecules: A review," Rep. Prog. Phys. **83**, 016401.

Picón, A, C. S. Lehmann, C. Bostedt, A. Rudenko, A. Marinelli, T. Osipov, D. Rolles, N. Berrah, C. Bomme, M. Bucher, G. Doumy, B. Erk, K. R. Ferguson, T. Gorkhover, P. J. Ho, E. P. Kanter, B. B. Krässig, J. Krzywinski, A. A. Lutman, A. M. March, D. Moonshiram, D. Ray, L. Young, S. T. Pratt, and S. H. Southworth (2016), "Hetero-site-specific x-ray pump-probe spectroscopy for femtosecond intramolecular dynamics," Nat. Commun. **11652**, 11652.

Pietzsch, A, F. Hennies, P. S. Miedema, B. Kennedy, J. Schlappa, T. Schmitt, V. N. Strocov, and A. Föhlisch (2015), "Snapshots of the fluctuating hydrogen bond network in liquid water on the

sub-femtosecond timescale with vibrational resonant inelastic x-ray scattering," Phys. Rev. Lett. **114**, 088302.

Pietzsch, A, Y.-P. Sun, F. Hennies, Z. Rinkevicius, H. O. Karlsson, T. Schmitt, V. N. Strocov, J. Andersson, B. Kennedy, J. Schlappa, A. Föhlisch, J.-E. Rubensson, and F. Gel'mukhanov (2011), "Spatial Quantum Beats in Vibrational Resonant Inelastic Soft X-Ray Scattering at Dissociating States in Oxygen," Phys. Rev. Lett. **106**, 153004.

Pinjari, R V, M. G. Delcey, M. Guo, M. Odelius, and M. Lundberg (2014), "Restricted active space calculations of L-edge X-ray absorption spectra: From molecular orbitals to multiplet states," J. Chem. Phys. **141**, 124116.

Polyansky, Oleg L, Roman I. Ovsyannikov, Aleksandra A. Kyuberis, Lorenzo Lodi, Jonathan Tennyson, and Nikolai F. Zobov (2013), "Calculation of rotation-vibration energy levels of the water molecule with near-experimental accuracy based on an ab initio potential energy surface," J. Phys. Chem. A **117**, 9633–9643.

Pontius, N, M. Beye, C. Trabant, R. Mitzner, F. Sorgenfrei, T. Kachel, M. Wöstmann, S. Roling, H. Zacharias, R. Ivanov, R. Treusch, M. Buchholz, P. Metcalf, C. Schüßler-Langeheine, and A. Föhlisch (2018), "Probing the non-equilibrium transient state in magnetite by a jitter-free two-color x-ray pump and x-ray probe experiment," Struct. Dyn. **5**, 054501.

Popova, TY a, A. K. Popov, S. G. Raurtian, and R. I. Sokolovskii (1970), "Nonlinear interference effects in emission, absorption, and generation spectra," Sov. Phys. JETP **30**, 466–472.

Privalov, T, F. Gel'mukhanov, and H. Ågren (1999), "Role of electron-phonon interaction in resonant x-ray Raman scattering by polymers and solids," Phys. Rev. B **59**, 9243.

Privalov, T, F. Gel'mukhanov, and H. Ågren (2001), "X-ray Raman scattering from molecules and solids in the framework of the Mahan-Noziéres-De Dominicis model," Phys. Rev. B **64**, 165116.

Puglisi, A, P. Selles, N. Sisourat, and S. Carniato (2020), "L-edge photoelectron spectra of silicon hydride cations: Imprint of molecular-field and spin-orbit effects," Phys. Rev. A **102**, 042801.

Revelli, A, M. Moretti Sala, G. Monaco, P. Becker, L. Bohatý, M. Hermanns, T. C. Koethe, T. Fröhlich, P. Warzanowski, T. Lorenz, S. V. Streltsov, P. H. M. van Loosdrecht, D. I. Khomskii, J. van den Brink, and M. Grüninger (2019), "Resonant inelastic x-ray incarnation of Young's double-slit experiment," Sci. Adv. **5**, eaav4020.

Robin, M, I. Ishii, R. McLaren, and A. Hitchcock (1988), "Fluorination effects on the inner-shell spectra of unsaturated molecules," J. Electron Spectros. Relat. Phenomena **47**, 53.

Rohringer, N, D. Ryan, R. A. London, M. Purvis, F. Albert, J. Dunn, J. D. Bozek, C. Bostedt, A. Graf, R. Hill, S. P. Hau-Riege, and J. J. Rocca (2012), "Atomic inner-shell x-ray laser at 1.46 nanometres pumped by an x-ray free-electron laser," Nature **481**, 488.

Rohringer, N, and R. Santra (2008), "Resonant Auger effect at high x-ray intensity," Phys. Rev. A **77**, 053404.

Röntgen, W K (1892), "Ueber die constitution des flüssigen wassers," Annalen der Physik **45**, 91–97.

Rosenqvist, L, K. Wiesner, A. Naves de Brito, M. Bässler, R. Feifel, I. Hjelte, C. Miron, H. Wang, M. N. Piancastelli, S. Svensson, O. Björneholm, and S. L. Sorensen (2001), "Femtosecond dissociation of ozone studied by the Auger Doppler effect," J. Chem. Phys. **115**, 3614.

Rossbach, J, J. R. Schneider, and W. Wurth (2019), "10 years of pioneering x-ray science at the free-electron laser FLASH at DESY," Phys. Rep. **808**, 1–74.

Rossi, M, R. Arpaia, R. Fumagalli, M. Moretti Sala, D. Betto, K. Kummer, G. M. De Luca, J. van den Brink, M. Salluzzo, N. B. Brookes, L. Braicovich, and G. Ghiringhelli (2019a), "Experimental determination of momentum-resolved electron-phonon coupling," Phys. Rev. Lett. **123**, 027001.

Rossi, M, C. Henriquet, J. Jacobs, C. Donnerer, S. Boseggia, A. Al-Zein, R. Fumagalli, Yi. Yao, E. C. Vale, J. G.and Hunter, R. S. Perry, I. Kantor, G. Garbarino, W. Crichton, G. Monaco, D. F. McMorrow, M. Krisch, and M. M. Sala (2019b), "Resonant inelastic x-ray scattering of magnetic excitations under pressure," J. Synchrotron Radiat. **26**, 1725–1732.

Rubensson, J-E (2000), "RIXS dynamics for beginners," J. Electron Spectros. Relat. Phenomena **110-111**, 135–151.

Rueff, J-P, and A. Shukla (2010), "Inelastic x-ray scattering by electronic excitations under high pressure," Rev. Mod. Phys. **82**, 847–896.

Russo, J, and H. Tanaka (2014), "Understanding water's anomalies with locally favoured structures," Nat. Commun. **5**, 3556.

Safonova, O V, M. Tromp, J. A. van Bokhoven, F. M. F. de Groot, J. Evans, and P. Glatzel (2006), "Identification of CO adsorption sites in supported Pt catalysts using high-energy-resolution fluorescence detection x-ray spectroscopy," J. Phys. Chem. B **110**, 16162–16164.

Sala, M M, K. Martel, C. Henriquet, A. Al Zein, L. Simonelli, Ch. J. Sahle, H. Gonzalez, M.-C. Lagier, C. Ponchut, S. Huotari, R. Verbeni, M. Krisch, and G. Monaco (2018), "A high-energy-resolution resonant inelastic x-ray scattering spectrometer at ID20 of the European Synchrotron

Radiation Facility," J. Synchrotron Radiat. **25**, 580–591.

Salamon, M B, and M. Jaime (2001), "The physics of manganites: Structure and transport," Rev. Mod. Phys. **73**, 583–628.

Sałek, P, V. Carravetta, F. Gel'mukhanov, H. Ågren, B. Schimmelpfennig, M.-N Piancastelli, S. Sorensen, R. Feifel, I. Hjelte, M. Bässler, S. Svensson, O. Bjöorneholm, and A. Naves de Britto (2001), "Dynamical suppression of atomic peaks in resonant dissociative photoemission," Chem. Phys. Lett. **343**, 332.

Sałek, P, F. Gel'mukhanov, and H. Ågren (1999), "Wave-packet dynamics of resonant x-ray Raman scattering: Excitation near the Cl $L_{II,III}$ edge of HCl," Phys. Rev. A **59**, 1147.

Såthe, C, F. F. Guimarães, J.-E. Rubensson, J. Nordgren, A. Agui, J. Guo, U. Ekström, P. Norman, F. Gel'mukhanov, and H. Ågren (2006), "Resonant $L_{II,III}$ x-ray Raman scattering from HCl," Phys. Rev. A **74**, 062512.

Savchenko, V, I. E. Brumboiu, V. Kimberg, M. Odelius, P. Krasnov, J.-C. Liu, J.-E. Rubensson, O. Björneholm, C. Såthe, J. Gråsjö, M. Dong, A. Pietzsch, A. Föhlisch, T. Schmitt, D. McNally, X. Lu, S. Polyutov, P. Norman, M. Iannuzzi, F. Gel'mukhanov, and V. Ekholm (2021), "Vibrational resonant inelastic x-ray scattering inliquid acetic acid: a ruler for molecular chain lengths," Sci. Rep. **11**, 4098.

Schinke, R (2009), *Photodissociation Dynamics* (Cambridge University Press, Cambridge).

Schlappa, J, U. Kumar, K. J. Zhou, S. Singh, M. Mourigal, V. N. Strocov, A. Revcolevschi, L. Patthey, H. M. Rønnow, S. Johnston, and T. Schmitt (2018), "Probing multi-spinon excitations outside of the two-spinon continuum in the antiferromagnetic spin chain cuprate $Sr_2CuO_3$," Nat. Commun. **9**, 5394.

Schlappa, J, K. Wohlfeld, K. J. Zhou, M. Mourigal, M. W. Haverkort, V. N. Strocov, L. Hozoi, C. Monney, S. Nishimoto, S. Singh, A. Revcolevschi, J.-S. Caux, L. Patthey, H. M. Rønnow, J. van den Brink, and T. Schmitt (2012), "Spin-orbital separation in the quasi-one-dimensional Mott insulator $Sr_2CuO_3$," Nature **485**, 82–85.

Schmitt, T, F. M. F. de Groot, and J.-E. Rubensson (2014), "Prospects of high-resolution resonant x-ray inelastic scattering studies on solid materials, liquids and gases at diffraction-limited storage rings," J. Synchrotron Radiat. **21**, 1065–1076.

Schmitt, T, V. N. Strocov, K.-J. Zhou, J. Schlappa, C. Money, U. Flechsig, and L. Patthey (2013), "High-resolution resonant inelastic x-ray scattering with soft x-rays at the ADRESS beamline of

the Swiss light source: Instrumental developments and scientific highlight," J. Electron Spectros. Relat. Phenomena **188**, 38–46.

Schoenlein, R, T. Elsaesser, K. Holldack, Z. Huang, H. Kapteyn, M. Murnane, and M. Woerner (2019), "Recent advances in ultrafast x-ray sources," Philos. Trans. A Math. Phys. Eng. Sci. **377**, 20180384.

Schreck, S, A. Pietzsch, B. Kennedy, C. Såthe, P. S. Miedema, S. Techert, V. N. Strocov, T. Schmitt, F. Hennies, J.-E. Rubensson, and A. Föhlisch (2016), "Ground state potential energy surfaces around selected atoms from resonant inelastic x-ray scattering," Sci. Rep **6**, 20054.

Schreck, S, A. Pietzsch, K. Kunnus, B. Kennedy, W. Quevedo, P. S. Miedema, P. Wernet, and A. Föhlisch (2014), "Dynamics of the OH group and electronic structure of liquid alcohols," Struct. Dyn. **1**, 054901.

Schülke, W (2007), *Electron Dynamics by Inelastic X-Ray Scattering* (Oxford University Press, Oxford).

Schweigert, I, and S. Mukamel (2007), "Probing valence electronic wave-packet dynamics by all x-ray stimulated Raman spectroscopy: A simulation study," Phys. Rev. A **76** (1), 012504.

Shi, R, and H. Tanaka (2020), "Direct evidence in the scattering function for the coexistence of two types of local structures in liquid water," J. Am. Chem. Soc. **142**, 2868–2875.

Shia, R, J. Russo, and H. Tanaka (2018), "Origin of the emergent fragile-to-strong transition in supercooled water," Proc. Natl. Acad. Sci. U.S.A. **115**, 9444–9449.

Shin, S, A. Agui, M. Watanabe, M. Fujisawa, Y. Tezuka, and T. Ishii (1996), "Observation of resonant Raman scattering at the Si $L_{2,3}$ core exciton," Phys. Rev. B **53**, 15660.

Shirley, EL (2000), "Theory and simulation of resonant inelastic x-ray scattering in s-p bonded systems: graphite, hexagonal boron nitride, diamond, and cubic boron nitride," J. Electron Spectros. Relat. Phenomena **110-111**, 305–321.

Shvyd'ko, Y (2019), "Output coupling from x-ray free-electron laser cavities with intracavity beam splitters," Phys. Rev. Accel. Beams **22**, 100703.

Shvyd'ko, Y, S. Stoupin, K. Mundboth, and J. Kim (2013), "Hard x-ray spectrographs with resolution beyond 100 $\mu$eV," Phys. Rev. A **87**, 043935.

Shwartz, S, M. Fuchs, J. B. Hastings, Y. Inubushi, T. Ishikawa, T. Katayama, D. A. Reis, T. Sato, K. Tono, M. Yabashi, S. Yudovich, and S. E. Harris (2014), "X-ray second harmonic generation," Phys. Rev. Lett. **112**, 163901.

da Silva Neto, E H, R. Comin, F. He, R. Sutarto, Y. Jiang, R. L. Greene, G. A. Sawatzky, and A. Damascelli (2015), "Charge ordering in the electron-doped superconductor $Nd_{2-x}Ce_xCuO_4$," Science **347**, 282.

Simon, M, L. Journel, R. Guillemin, W. C. Stolte, I. Minkov, F. Gel'mukhanov, P. Sałek, H. Ågren, S. Carniato, R. Taïeb, A. C. Hudson, and D. W. Lindle (2006), "Femtosecond nuclear motion of HCl probed by resonant x-ray Raman scattering in the Cl 1s region," Phys. Rev. A **73**, 020706(R).

Simon, M, R. Püttner, T. Marchenko, R. Guillemin, R. K. Kushawaha, L. Journel, G. Goldsztejn, M. N. Piancastelli, J. M. Ablett, J.-P. Rueff, and D. Céolin (2014), "Atomic Auger Doppler effects upon emission of fast photoelectrons," Nat. Commun. **5**, 4069.

Simon, M, and T. Schmitt (2013), "Progress in resonant inelastic x-ray scattering," J. Electron Spectros. Relat. Phenomena **188**, 1 – 2.

Sivia, D S (2011), *Elementary Scattering Theory: For X-ray And Neutron Users*, 1st ed. (Oxford, Oxford University Press;).

Skytt, P, P. Glans, K. Gunnelin, J. Guo, and J. Nordgren (1997), "Lifetime-vibrational interference effects in the resonantly excited x-ray-emission spectra of CO," Phys. Rev. A **55**, 146.

Skytt, P, P. Glans, J.-H. Guo, K. Gunnelin, C. Såthe, J. Nordgren, F. Kh. Gel'mukhanov, A. Cesar, and H. Ågren (1996), "Quenching of symmetry breaking in resonant inelastic x-ray scattering by detuned excitation," Phys. Rev. Lett. **77**, 5035.

Smallenburg, F, and F. Sciortino (2015), "Tuning the liquid-liquid transition by modulating the hydrogen-bond angular flexibility in a model for water," Phys. Rev. Lett. **115**, 015701.

Söderström, J, R. Stefanuik, F. Hennies, T. Schmitt, V. N. Strocov, J. Andersson, B. Kennedy, J. Schlappa, A. Föhlisch, A. Pietzsch, and J.-E. Rubensson (2020), "Resonant inelastic x-ray scattering on $CO_2$: Parity conservation in inversion-symmetric polyatomics," Phys. Rev. A **101**, 062501.

Soper, A K (2019), "Is water one liquid or two?" J. Chem. Phys. **150**, 234503.

Soper, A K, and M. A. Ricci (2000), "Structures of high-density and low-density water," Phys. Rev. Lett. **84**, 2881–2884.

Soper, A K, J. Teixeira, and T. Head-Gordon (2010), "Is ambient water inhomogeneous on the nanometer-length scale?" Proc. Natl. Acad. Sci. U.S.A. **107**, E44.

Sorensen, L, M. Kitayama, T. Tanaka, M. Hoshino, Y. Tamenory H. Tanaka, R. Sankari, M. N. Piancastelli, K. Ueda, Y. Velkov, I. Minlov, V. Carravetta, and F. Gel'mukhanov (2007), "Elec-

tronic Doppler effect in resonant Auger decay of CO molecules upon excitation near a shake-up Π resonance," Phys. Rev. A **76**, 062704.

Southworth, S H (1994), "Resonance and threshold effects in polarized x-ray emission from atoms and molecules," Nucl. Instr. Meth. Phys. Res. B **87**, 247–252.

Southworth, S H, D. W. Lindle, R. Mayer, and P. L. Cowan (1991), "Anisotropy of polarized x-ray emission from molecules," Phys. Rev. Lett. **67**, 1098.

Spielberger, L, O. Jagutzki, R. Dörner, J. Ullrich, U. Meyer, V. Mergel, M. Unverzagt, M. Damrau, T. Vogt, Kh. Khayyat I. Ali, D. Bahr, H. G. Schmidt, R. Frahm, and H. Schmidt-Böcking (1995), "Separation of Photoabsorption and Compton Scattering Contributions to He Single and Double Ionization," Phys. Rev. Lett. **74**, 4615–4618.

Stillinger, F H (1980), "Water revisited," Science **209**, 451–457.

Stöhr, J (1992), *NEXAFS Spectroscopy*, Springer Series in Surface Sciences (Springer).

Streltsov, S V, and D. I. Khomskii (2017), "Orbital physics in transition metal compounds: new trends," Phys.-Usp **60**, 1121–1146.

Suga, S, A. Sekiyama, H. Fujiwara, Y. Nakatsu, T. Miyamachi, S. Imada, P. Baltzer, S. Niitaka, H. Takagi, K. Yoshimura, M. Yabashi, K. Tamasaku, A. Higashiya, and T. Ishikawa (2009), "Do all nuclei recoil on photoemission in compounds?" New J. Phys. **11**, 073025.

Sun, Y-P, F. Hennies, A. Pietzsch, B. Kennedy, T. Schmitt, V. N. Strocov, J. Andersson, M. Berglund, J.-E. Rubensson, K. Aidas, F. Gel'mukhanov, M. Odelius, and A. Föhlisch (2011a), "Intramolecular soft modes and intermolecular interactions in liquid acetone," Phys. Rev. B **84**, 132202.

Sun, Y-P, J.-C. Liu, and F. Gel'mukhanov (2009a), "The propagation of a strong x-ray pulse followed by pulse slowdown and compression, amplified spontaneous emission and lasing without inversion," J. Phys.B: At. Mol. Opt. Phys. **42**, 201001.

Sun, Y-P, J.-C. Liu, and F. Gel'mukhanov (2009b), "Slowdown and compression of a strong x-ray free-electron pulse propagating through the Mg vapors," Euro Phys. Lett. **87**, 64002.

Sun, Y-P, J.-C. Liu, C.-K. Wang, and F. Gel'mukhanov (2010a), "Propagation of a strong x-ray pulse: Pulse compression, stimulated Raman scattering, amplified spontaneous emission, lasing without inversion, and four-wave mixing," Phys. Rev. A **81**, 013812.

Sun, Y-P, Q. Miao, A. Pietzsch, F. Hennies, T. Schmitt, V. N. Strocov, J. Andersson, B. Kennedy, J. Schlappa, A. Föhlisch, F. Gel'mukhanov, and J.-E. Rubensson (2013), "Interference between

resonant and nonresonant inelastic x-ray scattering," Phys. Rev. Lett. **110**, 223001.

Sun, Y-P, Q. Miao, A.-P. Zhou, R.-J. Liu, B. Liu, and F. Gel'mukhanov (2018), "Suppression of resonant Auger effect with chirped x-ray free-electron laser pulse," J. Phys. B: At. Mol. Opt. Phys. **51**, 035602.

Sun, Y-P, A. Pietzsch, F. Hennies, Z. Rinkevicius, H. O. Karlsson, T. Schmitt, V. N. Strocov, J. Andersson, B. Kennedy, and J. Schlappa (2011b), "Internal symmetry and selection rules in resonant inelastic soft x-ray scattering," J. Phys. B: At. Mol. Opt. Phys. **44**, 161002.

Sun, Y-P, Z. Rinkevicius, C.-K. Wang, S. Carniato, M. Simon, R. Taïeb, and F. Gel'mukhanov (2010b), "Two-photon-induced x-ray emission in Neon atoms," Phys. Rev. A **82**, 043430.

Sun, Y-P, C.-K. Wang, and F. Gel'mukhanov (2010c), "Rotational Doppler effect in x-ray photoionization," Phys. Rev. A **82**, 052506.

Sun, Z, M. Chen, L. Zheng, J. Wang, H. Shen B. Santra, L. Xu, W. Kang, M. L. Klein, and Xifan Wu (2017), "X-ray absorption of liquid water by advanced ab initio methods," Phys. Rev. B **96**, 104202.

Sundin, S, F. Kh. Gel'mukhanov, H. Ågren, S. J. Osborne, A. Kikas, O. Björneholm, A. Ausmees, and S. Svensson (1997), "Collapse of vibrational structure in the Auger resonant Raman spectrum of CO by frequency detuning," Phys. Rev. Lett. **79**, 1451.

Svanberg, S (2001), *Atomic and Molecular Spectroscopy: Basic Aspects and Practical Applications* (Springer-Verlag, Berlin).

Svensson, S, A. Ausmees, S. J. Osborne, G. Bray, F. Gel'mukhanov, H. Ågren, A.Naves de Brito, O.-P Sairanen, A. Kivimäki, E. Nõmmiste, H. Aksela, and S. Aksela (1994), "Observation of an anomalous decay ratio between the molecular field split levels in the S 2p core photoelectron and LVV Auger spectrum of $H_2S$," Phys. Rev. Lett. **72**, 3021–3024.

Takata, Y, Y. Kayanuma, S. Oshima, S. Tanaka, M. Yabashi, K. Tamasaku, Y. Nishino, M. Matsunami, R. Eguchi, A. Chainani, M. Oura, T. Takeuchi, Y. Senba, H. Ohashi, S. Shin, and T. Ishikawa (2008), "Recoil effect of photoelectrons in the Fermi edge of simple metals," Phys. Rev. Lett. **101**, 137601.

Takata, Y, Y. Kayanuma, M. Yabashi, K. Tamasaku, Y. Nishino, D. Miwa, Y. Harada, K. Horiba, S. Shin, S. Tanaka, E. Ikenaga, K. Kobayashi, Y. Senba, H. Ohashi, and T. Ishikawa (2007), "Recoil effects of photoelectrons in a solid," Phys. Rev. B **75**, 233404.

Tanaka, A, and T. Jo (1994), "Resonant 3d, 3p and 3s Photoemission in Transition Metal Oxides Predicted at 2p Threshold," J. Phys. Soc. Jpn **63**, 2788–2807.

Tanaka, S, and S. Mukamel (2002), "Coherent x-ray Raman spectroscopy: A nonlinear local probe for electronic excitations," Phys. Rev. Lett. **89**, 043001.

Thampy, V, S. Blanco-Canosa, M. Garcia-Fernandez, M. P. M. Dean, G. D. Gu, M. Först, T. Loew, B. Keimer, M. Le Tacon, S. B. Wilkins, and J. P. Hill (2013), "Comparison of charge modulations in $La_{1.875}Ba_{0.125}CuO_4$ and $YBa_2Cu_3O$," Phys. Rev. B **88**, 024505.

Thomas, T D, E. Kukk, H. Fukuzawa, K. Ueda, R. Püttner, Y. Tamenori, T. Asahina, N. Kuze, H. Kato, M. Hoshino, H. Tanaka, M. Meyer, J. Plenge, A. Wirsing, E. Serdaroglu, R. Flesch, E. Rühl, S. Gavrilyuk, F. Gel'mukhanov, A. Lindblad, and L. J. Sæthre (2009), "Photoelectron-recoil-induced rotational excitation of the $B^2\Sigma_u^+$ state in $N_2^+$," Phys. Rev. A **79**, 022506.

Thomas, T D, E. Kukk, K. Ueda, T. Ouchi, K. Sakai, T. X. Carroll, C. Nicolas, O. Travnikova, and C. Miron (2011), "Experimental observation of rotational Doppler broadening in a molecular system," Phys. Rev. Lett. **106**, 193009.

Tokushima, T, Y. Harada, O. Takahashi, Y. Senba, H. Ohashi, L.G.M. Pettersson, A. Nilsson, and S. Shin (2008), "High resolution X-ray emission spectroscopy of liquid water: The observation of two structural motifs," Chem. Phys. Lett. **460**, 387–400.

Tokushima, T, Y. Horikawa, Y. Harada, O. Takahashi, A. Hiraya, and S. Shin (2009), "Selective observation of the two oxygen atoms at different sites in the carboxyl group (-COOH) of liquid acetic acid," Phys. Chem. Chem. Phys. **11**, 1679.

Tomonaga, S-I (1950), "Remarks on Bloch's method of sound waves applied to many-fermion problems," Prog. Theor. Phys. **5**, 544–569.

Travnikova, O, J.-C. Liu, A. Lindblad, C. Nicolas, J. Söderström, V. Kimberg, F. Gel'mukhanov, and C. Miron (2010), "Circularly Polarized X Rays: Another Probe of Ultrafast Molecular Decay Dynamics," Phys. Rev. Lett. **105**, 233001.

Tulkki, J, and T. Åberg (1982), "Behaviour of Raman resonance scattering across the K x-ray absorption edge," J. Phys. B: At. Mol. Opt. Phys. **15**, L435.

Turner, J J, K. J. Thomas, J. P. Hill, M. A. Pfeifer, K. Chesnel, Y. Tomioka, Y. Tokura, and S. D. Kevan (2008), "Orbital domain dynamics in a doped manganite," New J. Phys **10**, 053023.

Ueda, K, M. Kitajima, A. De Fanis, T. Furuta, H. Shindo, H. Tanaka, K. Okada, R. Feifel, S. L. Sorensen, H. Yoshida, and Y. Senba (2003), "Anisotropic ultrafast dissociation probed by the

Doppler effect in resonant photoemission from $CF_4$," Phys. Rev. Lett. **90**, 233006.

Ueda, K, R. Püttner, N. A. Cherepkov, F. Gel'mukhanov, and M. Ehara (2009), "High resolution x-ray photoelectron spectroscopy on nitrogen molecules," Eur. Phys. J. Special Topics **169**, 95.

Ueda, K, X.-J-Liu, G. Prümper, T. Lischke, T. Tanaka, M. Hoshimo, H. Tanaka, I. Minkov, V. Kimberg, and F. Gel'mukhanov (2006), "Role of the recoil effect in two-center interference in x-ray photoionization," Chem. Phys. **329**, 329.

Ulrich, C, L. J. P. Ament, G. Ghiringhelli, L. Braicovich, M. M. Sala, N. Pezzotta, T. Schmitt, G. Khaliullin, J. van den Brink, H. Roth, T. Lorenz, and B. Keimer (2009), "Momentum Dependence of Orbital Excitations in Mott-Insulating Titanates," Phys. Rev. Lett. **103**, 107205.

Umetsu, R Y, H. Fujiwara, K. Nagai, Y. Nakatani, M. Kawada, A. Sekiyama, F. Kuroda, H. Fujii, T. Oguchi, Y. Harada, J. Miyawaki, and S. Suga (2019), "Half-metallicity of the ferrimagnet $Mn_2VAl$ revealed by resonant inelastic soft x-ray scattering in a magnetic field," Phys. Rev. B **99**, 134414.

Vaz da Cruz, V, S. Eckert, and A. Föhlisch (2021), "Td-dft simulations of k-edge resonant inelastic x-ray scattering within the restricted subspace approximation," Phys. Chem. Chem. Phys. **23**, 1835–1848.

Vaz da Cruz, V, E. Ertan, R. C. Couto, S. Eckert, M. Fondell, M. Dantz, B. Kennedy, T. Schmitt, A. Pietzsch, F. F. Guimarães, H. Ågren, F. Gel'mukhanov, M. Odelius, A. Föhlisch, and V. Kimberg (2017), "A study of the water molecule using frequency control over nuclear dynamics in resonant x-ray scattering," Phys. Chem. Chem. Phys. **19**, 19573–19589.

Vaz da Cruz, V, E. Ertan, N. Ignatova, R. C. Couto, S. Polyutov, M. Odelius, V. Kimberg, and F. Gel'mukhanov (2018), "Anomalous polarization dependence in vibrationally resolved resonant inelastic x-ray scattering of $H_2O$," Phys. Rev. A **98**, 012507.

Vaz da Cruz, V, F. Gel'mukhanov, S. Eckert, M. Iannuzzi, E. Ertan, A. Pietzsch, R. C. Couto, J. Niskanen, Mattis Fondell, M. Dantz, T. Schmitt, X. Lu, D. McNally, R. M. Jay, V. Kimberg, A. Föhlisch, and M. Odelius (2019a), "Probing hydrogen bond strength in liquid water by resonant inelastic x-ray scattering," Nat. Commun. **10**, 10.1038/s41467-019-08979-4.

Vaz da Cruz, V, N. Ignatova, R. C. Couto, D. Fedotov, D. R. Rehn, V. Savchenko, P. Norman, H. Ågren, S. Polyutov, J. Niskanen, S. Eckert, R. M. Jay, M. Fondell, T. Schmitt, A. Pietzsch, A. Föhlisch, F. Gel'mukhanov, M. Odelius, and V. Kimberg (2019b), "Nuclear dynamics in resonant inelastic x-ray scattering and x-ray absorption of methanol," J. Chem. Phys. **150**,

234301.

van Veenendaal, M (2015), *Theory of Inelastic Scattering and Absorption of X-rays* (Cambridge University Press).

Velkov, Y, Y. Hikosaka, E. Shigemasa, T. Kaneyasu, J.-C. Liu, and F. Gel'mukhanov (2009), "Limitations of x-ray absorption spectroscopy of super-high resolution measured in the resonant Auger mode," Phys. Rev. A **79**, 022508.

Voit, J (1995), "One-dimensional Fermi liquids," Rep. Prog. Phys. **58**, 977–1116.

Wang, R-P, B. Liu, R. J. Green, M. U. Delgado-Jaime, M. Ghiasi, T. Schmitt, M. M. van Schooneveld, and F. M. F. de Groot (2017), "Charge-Transfer Analysis of 2p3d Resonant Inelastic X-ray Scattering of Cobalt Sulfide and Halides," J. Phys. Chem. C **121**, 24919–24928.

Wang, Y, Y. Chen, C. Jia, B. Moritz, and T. P. Devereaux (2020), "Time-resolved resonant inelastic x-ray scattering in a pumped Mott insulator," Phys. Rev. B **101**, 165126.

Weinhardt, L, A. Benkert, F. Meyer, M. Blum, R. G. Wilks, W. Yang, M. Bär, F. Reinert, and C. Heske (2012), "Nuclear dynamics and spectator effects in resonant inelastic soft x-ray scattering of gas-phase water molecules," J. Chem. Phys. **136**, 144311.

Weinhardt, L, E. Ertan, M. Iannuzzi, M. Weigand, O. Fuchs, M. Bär, M. Blum, J. D. Denlinger, W. Yang, E. Umbach, M. Odelius, and C. Heske (2015), "Probing hydrogen bonding orbitals: resonant inelastic soft x-ray scattering of aqueous $NH_3$," Phys. Chem. Chem. Phys. **17**, 27145–27153.

Weinhardt, L, M. Weigand, M. Bär O. Fuchs, M. Blum, J. D. Denlinger, W. Yang, E. Umbach, and C. Heske (2011), "Nuclear dynamics in the core-excited state of aqueous ammonia probed by resonant inelastic soft x-ray scattering," Phys. Rev. B **84**, 104202.

Weninger, C, M. Purvis, D. Ryan, R. A. London, J. D. Bozek, C. Bostedt, A. Graf, G. Brown, J. J. Rocca, and N. Rohringer (2013), "Stimulated electronic x-ray Raman scattering," Phys. Rev. Lett. **111**, 233902.

Weninger, C, and N. Rohringer (2013), "Stimulated resonant x-ray Raman scattering with incoherent radiation," Phys. Rev. A **88**, 053421.

Wernet, Ph (2019), "Chemical interactions and dynamics with femtosecond x-ray spectroscopy and the role of x-ray free-electron lasers," Phil. Trans. R. Soc. A **377**, 20170464.

Wernet, Ph, K. Kunnus, I. Josefsson, I. Rajkovic, W. Quevedo, M. Beye, S. Schreck, S. Grübel, M. Scholz, D. Nordlund, W. Zhang, R. W. Hartsock, W. F. Schlotter, J. J. Turner, B. Kennedy,

F. Hennies, F. M. F. de Groot, K. J. Gaffney, S. Techert, M. Odelius, and A. Föhlisch (2015), "Orbital-specific mapping of the ligand exchange dynamics of $Fe(CO)_5$ in solution," Nature **520**, 78–81.

Wernet, Ph, D. Nordlund, U. Bergmann, M. Cavalleri, M. Odelius, H. Ogasawara, L. Å. Näslund, T. K. Hirsch, L. Ojamäe, P. Glatzel, L. G. M. Pettersson, and A. Nilsson (2004), "The structure of the first coordination shell in liquid water," Science **304**, 995–999.

Wohlfeld, K, M. Daghofer, S. Nishimoto, G. Khaliullin, and J. van den Brink (2011), "Intrinsic coupling of orbital excitations to spin fluctuations in Mott insulators," Phys. Rev. Lett. **107**, 147201.

Woicik, J C, J. M. Ablett, N. F. Quackenbush, A. K. Rumaiz, C. Weiland, T. C. Droubay, and S. A. Chambers (2018), "Experimental assignment of many-electron excitations in the photoionization of NiO," Phys. Rev. B **97**, 245142.

Woicik, J C, C. Weiland, A. K. Rumaiz, M. T. Brumbach, J. M. Ablett, E. L. Shirley, J. J. Kas, and J.J. Rehr (2020), "Core hole processes in x-ray absorption and photoemission by resonant auger-electron spectroscopy and first-principles theory," Phys. Rev. B **101**, 245105.

Wold, A, and R. Arnott (1959), "Preparation and crystallographic properties of the systems $LaMn_{1-x}Ni_xO_{3+\lambda}$JA-1106," J. Phys. Chem. Solids **9**, 176.

Wollenweber, L, T. R. Preston, A. Descamps, V. Cerantola, A. Comley, J. H. Eggert, L. B. Fletcher, G. Geloni, D. O. Gericke, S. H. Glenzer, S. Göde, J. Hastings, O. S. Humphries, A. Jenei, O. Karnbach, Z. Konopkova, R. Loetzsch, B. Marx-Glowna, E. E. McBride, D. McGonegle, G. Monaco, B. K. Ofori-Okai, C. A. J. Palmer, C. Plückthun, R. Redmer, C. Strohm, I. Thorpe, T. Tschentscher, I. Uschmann, J. S. Wark, T. G. White, K. Appel, G. Gregori, and U. Zastrau (2021), "High-resolution inelastic x-ray scattering at the high energy density scientific instrument at the European X-Ray Free-Electron Laser," Rev. Sci. Instrum. **92**, 013101.

Wu, B, T. Wang, C.E. Graves, D. Zhu, W.F. Schlotter, J.J. Turner, O. Hellwig, Z. Chen, H. A. Dürr, A. Scherz, and J. Stöhr (2016), "Elimination of x-ray diffraction through stimulated x-ray transmission," Phys. Rev. Lett. **117**, 027401.

Yablonskikh, M V, Yu. M. Yarmoshenko, V. I. Grebennikov, E. Z. Kurmaev, S. M. Butorin, L.-C. Duda, J. Nordgren, S. Plogmann, and M. Neumann (2001), "Origin of magnetic circular dichroism in soft x-ray fluorescence of Heusler alloys at threshold excitation," Phys. Rev. B **63**, 235117.

Yamazoe, K, J. Miyawaki, H. Niwa, A. Nilsson, and Y. Harada (2019), "Measurements of ultrafast dissociation in resonant inelastic x-ray scattering of water," J. Chem. Phys. **150** (20), 204201.

Yang, M, and J. L. Skinner (2010), "Signatures of coherent vibrational energy transfer in IR and Raman line shapes for liquid water," Phys. Chem. Chem. Phys. **12**, 982–991.

Yavaş, H, M. Sundermann, K. Chen, A. Amorese, A. Severing, H. Gretarsson, M. W. Haverkort, and L. H. Tjeng (2019), "Direct imaging of orbitals in quantum materials," Nat. Phys. **15**, 559–562.

Yin, Z, I. Rajkovic, S. T. Veedu, S. Deinert, D. Raiser, R. Jain, H. Fukuzawa, S. Wada, W. Quevedo, B. Kennedy, S. Schreck, A. Pietzsch, P. Wernet, K. Ueda, A. Föhlisch, and S. Techert (2015), "Ionic solutions probed by resonant inelastic x-ray scattering," Z. Phys. Chem **229**, 1855–1867.

Yoneda, H, Y. Inubushi, K. Nagamine, Y. Michine, H. Ohashi, H. Yumoto, K. Yamauchi, H. Mimura, H. Kitamura, T. Katayama, T. Ishikawa, and M. Yabashi (2015), "Atomic inner-shell laser at 1.5-ångström wavelength pumped by an x-ray free-electron laser," Nature **524**, 446–449.

Young, L, K. Ueda, M. Gühr, P. H. Bucksbaum, M. Simon, S. Mukamel, N. Rohringer, K. C. Prince, C. Masciovecchio, M. Meyer, A. Rudenko, D. Rolles, C. Bostedt, M. Fuchs, D. A. Reis, R. Santra, H. Kapteyn, M. Murnane, H. Ibrahim, F. Légaré, M. Vrakking, M. Isinger, D. Kroon, M. Gisselbrecht, A. L'Huillier, H. J. Wörner, and S. R. Leone (2018), "Roadmap of ultrafast x-ray atomic and molecular physics," J. Phys. B: At. Mol. Opt. Phys. **51**, 032003.

Yudovich, S, and S. Shwartz (2015), "Second-harmonic generation of focused ultrashort x-ray pulses," J. Opt. Soc. Am. B **32**, 1894–1900.

Zaanen, J, and G. A. Sawatzky (1990), "Systematics in band gaps and optical spectra of 3d transition metal compounds," J. Solid State Chem. **88**, 8–27.

Zaanen, J, G. A. Sawatzky, and J. W. Allen (1985), "Band Gaps and Electronic Structure of Transition-Metal Compounds," Phys. Rev. Lett. **55**, 418–421.

Zhovtobriukh, I, N. A. Besley, T. Fransson, A. Nilsson, and L. G. M. Pettersson (2018), "Relationship between x-ray emission and absorption spectroscopy and the local H-bond environment in water," J. Chem. Phys. **148**, 144507.

v. Zimmermann, M, J. P. Hill, D. Gibbs, M. Blume, D. Casa, B. Keimer, Y. Murakami, Y. Tomioka, and Y. Tokura (1999), "Interplay between charge, orbital, and magnetic order in $Pr_{1-x}Ca_xMnO_3$," Phys. Rev. Lett. **83**, 4872–4875.

Zimmermann, P, N. Bouldi, M.O.J.Y. Hunault, M. Sikora, J. M. Ablett, J.-P. Rueff, B. Lebert, P. Sainctavit, F.M.F. de Groot, and A. Juhin (2018), "1s2p resonant inelastic x-ray scattering magnetic circular dichroism as a probe for the local and non-local orbitals in $CrO_2$," J. Electron Spectros. Relat. Phenomena **222**, 74–87.

Zykova, V A, Y. A. Karpegina, V. K. Malinovsky, and N. V. Surovtsev (2017), "Temperature dependence of the Landau-Placzek ratio in liquid water," Phys. Rev. E **96**, 042608.